JPRS-CST-88-009
3 MAY 1988

JPRS Report

Science & Technology

China

JPRS-CST-88-009

3 MAY 1988

SCIENCE & TECHNOLOGY

CHINA

CONTENTS

ENVIRONMENTAL QUALITY

LIFE SCIENCES

NATIONAL DEVELOPMENTS

/9986

AIRCRAFT FLIGHT DYNAMICS RESEARCH IN PAST DECADE REVIEWED

40080086 Beijing GUOJI HANGKONG [INTERNATIONAL AVIATION] in Chinese No 2, Feb 88 pp 28-31

[Article by Fan Liqin [5400 4539 2953] and Chen Qishun [7115 0796 7311]]

[Text] During the past decade, significant progress has been made in aircraft flight dyanmics research in China. Eight of the research topics have received major scientific achievement awards from the Ministry of Aviation Industry. Here, a brief review of the work done in the field of flight dynamics the past decade is presented.

Research in Aircraft Flight Quality Specifications and Flight Performance Specifications

Aircraft flight quality specifications and flight performance specifications are the basic reference for evaluation and certification of new aircraft. After more than 20 years of coordinated efforts, China has established the "Military Aircraft Quality Specifications" and the "Military Aircraft Performance Specifications" which are consistent with China's economic and technical conditions, and whose contents are comparable to the international standards of the late 70's and early 80's. It has also provided supporting documents including background materials, operations guide, computation manual and general-purpose computer programs. Thus, for the first time since China's aviation industry evolved from the old repair and imitation operations to a self-reliant productive industry, it has its own quality specifications and performance specifications.

Since their publication, the above specifications have been used in the certification of design, production, and flight tests of many aircraft models. The unique features of China's aircraft specifications are summarized below:

1. These specifications are established by studying related specifications and research achievements of other countries and by incorporating China's own experience in aircraft design and operation; they are also based on the results of theoretical research, numerical verifications, and ground and flight tests. They can be used as a guide for the design, computation and test of China's military aircraft, and as one of the basic references of flight certification.

2. In the preparation of the specifications, full advantage was taken of the latest research results from this country and abroad. For example, in the section of longitudinal quality of the Flight Quality Specifications, an in-depth study has been conducted to understand the basic principles of trajectory stability, and the results have been verified by flight tests; in the section on lateral quality, rigorous theoretical analyses have uncovered certain deficiencies with the U.S. MIL-F-8785B specification, and therefore a more appropriate lateral quality index is used; in the section on the main control system, a new index of dynamic characteristics of flight control systems is proposed; in the section on atmospheric turbulence, a mathematical model which takes into account the effects of wind shear has been proposed.

3. A computations manual and a set of computer programs have also been issued to provide a self-contained, integral set of documents.

4. Special considerations are given in the specifications to incorporate advanced technologies which are not compatible with China's existing conditions. For example, the requirements of longtitudinal damping ratio and lateral roll damping ratio of modern, high-performance aircraft cannot be satisfied without installing special stabilization equipment. Therefore, even though many aircraft in China do not have automation equipment, the "Military Aircraft Flight Quality Specifications" still impose the requirements for extensive use of automation equipment. To accommodate those aircraft without automation equipment, guidelines are provided in the background materials and opertions guide that "under these circumstances, a request can be submitted for relaxation of this requirement once an agreement is reached between the production, design, and operations organizations." Such measures are necessary to resolve the conflict between the attempt to be non-conservative and at the same time subject to practical limitations.

Controllable Flight Dynamics

From the point of view of flight dynamics, problems in controllable flight dynamics can be divided into two categories: attitude control and stability, and trajectory control and stability. THe ultimate goal is to ensure that the aircraft maintain stability under all flight conditions, and also have good static and dynamic characteristics in order to meet quality requirements.

Controllable flight dynamics is a new field which combines the two disciplines: flight dynamics and automatic control. China began its research in this field in 1980. At that time, most Chinese aircraft in service did not use stability augmentation system (SAS) or control augmentation system (CAS), but on new aircraft under development, installation of different types of SAS was being considered. Therefore, from the design point of view, there was an urgent need to analyze and assess the flight quality of aircraft equipped with SAS or CAS. In addition, China was then engaged in the development of an experimental aircraft using active control techniques and a variable-stability aircraft; it was also engaged in the research of such topics as control law design, parameter selection, and the a-plication of various control techniques. Therefore, during the Sixth 5-Year Plan, China devoted significant resources to the study of active control techniques by integrating the design experience from various

domestic aircraft equipped with SAS and by studying quality specifications of foreign aircraft with automation equipment.

At present, we have collected the computational procedures of evaluating flight quality for a variety of aircraft with SAS or CAS (including computer programs). With regard to the methods of examining flight quality, various time-domain and frequency-domain discrimination criteria have been analyzed; they include the C*, D* criteria, the numerator time constant, the beamwidth and phase sensitivity, the Ralph Smith criteria, the TRP response parameter, the Chalk pitch rate response criteria, the Neal-Smith criteria and the equivalent system approach. Finally, efforts were focused on the study of the equivalent system approach and its implementation. Today, the basic principles of the equivalent system are well understood, and the two pieces of software for implementing the approach have been used in the design of five aircraft models after being verified by ground simulation. The calculated results using these software have been shown to be in good agreement with those obtained from similar software abroad. In addition, progress has been made in the areas of control law design for electrically-driven control systems, relaxed static stability, direct lateral-force control, aerodynamic servo-elasticity, and the effect of link non-linearity on automation equipment. Most of these research activities have reached a level comparable to world standards of the late 70's and early 80's.

Atmospheric Disturbance

Atmospheric disturbance has a significant impact on the flight characteristics of an aircraft in terms of flight quality, combat performance, passenger comfort, and transport efficiency. In particular, it is a major safety consideration for low-altitude, high-speed flight of military aircraft and for cruise and take-off/landing of large aircraft. Since the 1970's, a significant amount of research has been devoted to the problem of amospheric disturbance, including the establishment of engineering models of atmospheric turbulence, particularly low-altitude, non-isotropic, non-steady turbulence model and three-dimensional wind shear model. They are used to study the dynamic response of aircraft in the presence of atmospheric disturbance (particularly three-dimensional wind shear) for different flight segments (particularly the flight segment close to ground), to explore various means of improving flight quality and increasing passenger comfort under turbulent conditions, and to design optimal control systems. In many areas, practical engineering solutions have been found: when the new U.S. specification MIL-F-8785C was established in 1980, key revisions and supplements on atmospheric disturbance were incorporated.

In China, significant progress has also been made in the research of atmospheric disturbance since 1980. The main areas of research include the following:

1. Study of disturbance model. Because of China's limited resources, in studying the complex atmospheric disturbance phenomenon, generally a detailed theoretical analysis is first carried cut. The studies use three different mathematical models for describing atmospheric turbulence: the Von Karman-Dreydon continuous turbulence model, the "1-cosine" discrete wind gust model, and the wind shear model.

2. Development of engineering methods for characterizing flight quality in the presence of atmospheric disturbance. In the case of continuous turbulent flow, a computational procedure based on its spectral component has been developed; it has been used in computations for the Y-10, the Y-7, the F-6, the F-7, the Qiang-5, and the SH-5 aircraft. In the case of discrete wind gust, a computational method based on the convolution technique has been developed. In the case of wind shear, a method has been developed which takes into account the ground effect and the effect of density variation on aircraft flight quality (including both open-loop and closed-loop conditions). These methods have been incorporated in the "Aircraft Flight Quality Computation Manual"; they are considered to be advanced methods by international standards.

3. Study of the standards for characterizing aircraft flight quality in the presence of atmospheric disturbance. The U.S. military specification MIC-F-8785C has proposed a qualitative criterion for characterizing flight quality, but at the present time there is no quantitative measure of flight quality. On the basis of articles published in foreign literature, we have proposed three primary measures of quality which can be used as standards for comparing aircraft design. They have been shown to have good results during flight tests of the SH-5, the Y-7, and the Y-10 aircraft.

4. Study of measures to improve aircraft flight quality and flight test methods in the presence of atmospheric disturbance. By combining the design and flight tests of aircraft models, research in this area has produced useful results, particularly in control/stability augmentation and pilot response.

Study of Non-Linear Characteristics

In the study of aircraft flight dynamics, many useful results can be obtained by treating the aircraft as a linear system. But strictly speaking, a truly linear system does not exist; therefore, in many cases conventional linearization techniques will lead to failure or erroneous results.

With the development of high-performance aircraft and the extensive use of automation equipment, the study of non-linear aircraft dynamics and large angle-of-attack non-linear aerodynamics has become an important topic for flight dynamicists around the world. In many developed countries equipped with large, low-speed wind tunnels and high-performance transonic wind tunnels, and aided by recent developments in wind-tunnel experimental techniques, electronic technology, ground simulation techniques and automatic control technology, outstanding achievements in non-linear flight dynamics have been reported. A good example of this reasearch is the appearance of high-performance, high-mobility aircraft operating in the transonic region at large angle of attack.

In theoretical research, a new method was proposed in the late 70's by Mehra et al for studying non-linear systems--thebranch analysis and catastrophe theoretical method (BACTM). This method is based on various disciplines used in non-linear research such as qualitative theory, differential geometry, branch analysis and catastrophe theory. It has proven to be effective in the study of aircraft stability and trailing-vortex characteristics under critical

flight conditions at large angle of attack, and in the design of flight control systems. This method may also prove effective in designing autopilot parameters within a specified range so that maximum mobility can be achieved under any flight conditions.

Research in non-linear theory in this country, which began in the early 80's, covered the following areas:

1. Study of the effect of non-linear aerodynamic derivatives under large angle-of-attack and large slip angle conditions on aircraft dynamic characteristics. The study focused on the mechanism of limit ring oscillation caused by the automation equipment and aerodynamic non-linearities, and the mechanism of lateral limit ring oscillation caused by aerodynamic hysteresis; it also established mathematical models and computational procedures. In addition, large angle-of-attack wind tunnel tests were conducted on the YF-16, the Y-10 and the F-7 aircraft to study the non-linear effects of aerodynamic forces and aerodynamic moments; analyses were also carried out to predict aircraft stall/tail spin characteristics.

2. Theoretical study of stall/tail spin characteristics. The main purpose of this study is to develop a theoretical method for predicting stall and tail spin conditions which can be applied to early designs as well as new aircraft undergoing tail-spin flight tests. The current activities of this research include: (1) establishing a set of early prediction criteria which are consistent with flight quality requirements; by using large angle-of-attack wind tunnel data and aircraft quality distribution parameters, they can predict the stall warning velocity, stall velocity, separation angle of attack, separation characteristics and tail spin sensitivity; (2) developing mathematical models and computer programs for predicting tail spin motion parameters, characteristics parameters, and the time history of these parameters. These methods have been used to perform calculations for five different domestic aircraft models; the calculated results are in good agreement with full-scale flight test results and with model free-flight data.

3. Study of aircraft flight quality in the presence of large disturbance. The focus of this study is on the fast-roll inertial coupling problem; it generally involves large-disturbance equations where the effects of longitudinal and lateral coupling, the non-linear inertial terms and the external force terms are taken into account. There are two different approaches for treating this problem. One is to seek a stationary solution of the linearized differential equations and to determine the stationary fast-roll stability boundary using analytical techniques. Specifically, we have studied the effect of gyro moment of the engine rotor on the stationary fast-roll boundary and the effect of elastic deformation on the fast-roll instability boundary; we have also generated numerical results for a practical example. The other approach is to obtain numerical solution of the non-linear differential equations of aircraft dynamics on a computer. In this respect, we have carried out large-disturbance calculations for four different aircraft models in order to study the effect of aircraft weight, flight conditions, control laws and the various parameters of automation equipment. Some preliminary but important results have been obtained.

4. Study of the effect of non-linearities in the operating and control systems on stability. In this area, we are studying the mechanisms and conditions of man-machine closed-loop oscillation or other oscillations caused by non-linearities in the operating and control systems; in particular, we hope to identify the major causes of this problem and propose a reasonable engineering model and computational procedure. At present, some encouraging results have been obtained.

Development of Test Research Methods

Test research plays a very important role in the study of flight dynamics. In particular, for modern high-performance aircraft, many technical problems cannot be solved by using theoretical methods only. Many developed countries have spent huge amounts of money to develop high-performance wind tunnels, flight simulators, large computers, and test aircraft. China has also devoted a significant amount of its resources on this issue and has made progress in the following areas:

1. Flight test research of aircraft flight quality. In the process of preparing the "Military Aircraft Flight Quality Specifications," more than 300 flight tests have been conducted on existing aircraft such as the F-6, the F-7 and the F.8. The objectives of these tests were to study longitudinal velocity stability, mobility, control characteristics, lateral modal characteristics, roll control efficiency, stationary side-slip and dynamic characteristics of the control system; some of the long-period tests such as the test on sink-float modes were conducted for the first time in this country. The flight test results provided preliminary information for China's pilots to establish 9 levels of flight quality and also provided large amounts of data for analyzing foreign specifications and revising our own.

2. Study of aircraft parameter identification. With the development of flight test equipment and computer technology, steady progress has been made in aircraft parameter identification techniques, which are playing an increasingly important role in aircraft design and in flight tests. The methods of identification have evolved from the simple formula method to the more sophisticated methods such as the output error method, the maximum-likelihood method and the pre-model estimation method; they have also extended from the time domain to the frequency domain. In the late 70's, parameter identification techniques for linear systems had reached a mature state of development. Since the 80's, the focus has shifted to the study of parameter identification of non-linear systems, identification of aeroelastic and non-stationary aerodynamic equations, identification of aircraft closed-loop systems with active control, and identification of helicopter systems.

The study of parameter identification in flight tests began in the 60's in this country. In the 70's, China began research in modern parameter identification techniques. In 1978, the Newton-Raphson technique was successfully applied to flight test data of the F-6 prototype to estimate all the static and dynamic derivatives and control derivatives in both the longtitudinal and lateral directions. Later, satisfactory results were also obtained in the flight tests of the F-8 aircraft and other aircraft. A few years ago, efforts were initiated

to study the application of the maximum-likelihood method, and a set of unique, standard computer programs were developed for aerodynamic parameter identification; they were used successfully in flight tests to study control stability of new aircraft. Recently, the concept of low-order equivalent systems was used to solve the problem of parameter identification of aircraft equipped with automatic control systems.

Today, parameter identification techniques are being used extensively in aircraft flight dynamics; specifically, they are used in the identification aerodynamic derivatives of helicopters, the estimation of aircraft polar curves and the identification of control system models.

3. Stall/tail spin test. Because of the limited number of wind tunnel facilities in this country, the model free-flight test has become an important tool for studying aircraft stall/tail spin characteristics. During the past decade, with the advancement of test instrumentation and improvement in test model materials, model tests are now capable of producing quantitative rather than just qualitative information. During the Sixty 5-Year Plan period, stall/tail spin tests for four different aircraft models were conducted to facilitate aircraft development. Through test research, it was discovered that lateral variations of the center of gravity can significantly change aircraft tail spin characteristics; when the center-of-gravity shift exceeds a certain value, its effect becomes greater than that of the rudder. In addition, test results also showed that by using existing brake chutes, it was possible to pull out of a tail spin unde mergency situations. These findings are significant in terms of achie masimum performance of existing aircraft and designing new aircraft.

Full-scale stall/tail spin tests of swept-wing aircraft were successfully conducted in the 70's; in recent years, preparation has been under way to perform tests on the new delta-wing aircraft.

4. Test research of aircraft dynamic characteristics under non-symmetric power. Through extensive theoretical research, we have proposed methods for calculating aircraft dynamic characteristics under various non-symmetric power conditions. They include the six degree-of-freedom equations of motion and the three degree-of-freedom linear and non-linear equations of motion. Large amounts of numerical computations have been carried out and semi-physical simulation tests have been conducted. Subsequently, full-scale flight tests of the Y-7 and Y-8 aircraft under non-symmetric power conditions were also conducted and measurements of important performance parameters such as decision velocity and balance field length have been made. Based on these flight test results, the proposed computational methods have been validated and a set of practical flight test methods and procedures have been established.

5. Development of test research facilities. China's major test facilities for studying flight dynamics include the longitudinal variable, stability facility for the FT-6 aircraft and the air-combat flight simulator. After 10 years of development, they are ready for acceptance and delivery. In addition to studying conventional topics in flight dynamics, these two facilities can be used for theoretical research and for studying more difficult problems.

They can also be used for studying future applications of new technologies such as the effect of non-linear control systems on flight quality, characterization of man-machine closed-loop flight quality, dynamic model of the pilot, factors which cause pilot-induced oscillations, side-lever control techniques, aircraft stall/tail spin characteristics, atmospheric turbulence, and simulation of flight control systems.

3012/9274

LATEST AEROSPACE DEVELOPMENTS REPORTED IN BRIEF

40080087 Beijing HANGKONG ZHISHI [AEROSPACE KNOWLEDGE MAGAZINE] in Chinese No 2, Feb 88 pp 2-4

[Excerpts] 1) Modified Yun-8 Could Fly by 1990

China is currently developing an air-sealed Yun-8 (Y-8) transport plane which is expected to be in service by 1990. The air-sealed Y-8 airplane is a modified version of the original Y-8 model. The Shanxi Aircraft Company, which is responsible for the major research and development of the new aircraft, has been cooperating with five domestic research and production organizations and with the U.S. Lockheed Aircraft Co to accelerate the design modification work. At the end of 1987, all the technical consultation work has been completed, and pre-manufacturing preparation is well under way. The modified Y-8 will have an air-sealed cargo bay which is 29.3 m long and has a volume of 212.15m^3. The aircraft will be equipped with advanced air-conditioning and electronics systems. At a cruising altitude of 10,000 m, the cabin temperature can be maintained between 16°C and 27.8° C. The new Y-8 airplane will have the same transport, parachute and air-drop capabilities as the original model; it will also have the same performance in terms of range, payload, endurance and reliability. It can be used as a passenger plane, a cargo plane or a combined passenger/cargo plane; it can also be used as a special-purpose aircraft for rescue or mapping missions. The passenger plane has 104 seats; the cargo plane can carry oversized cargoes 19 meters in length and 5 standard-sized cargo containers. Aviation experts believe that the Y-8 air-sealed aircraft will enhance China's competitive edge on the international market and improve the standard of China's aircraft manufacturing industry.

2) Breakthrough in Radar Technology

On 14 December, the "Hai Ying" [Sea Hawk] shipborne three-coordinate, phased-array radar, which has developed as part of the modernization effort of the Chinese Navy, successfully passed design certification in Nanjing. Experts believe that in terms of design and performance, this new radar developed by the Nanjing Shipborne Radar Research Institute has reached the same technical standard as similar radars built by other countries: it represents a major breakthrough in China's radar technology. The three-coordinate phased-array radar is an advanced product of the 80's. By using phase scan technology, it can simultaneously measure the range, azimuth, and altitude (elevation) of a

target in flight. It can also guide the shipboard missiles and guns to track and acquire the target. It is an important class of defensive equipment used by large and medium surface ships to perform aerial and ocean surveillance as well as target acquisition. At present, only a few developed countries including the United States, Italy, West Germany, and Japan can produce this type of radar. Having accepted the task of developing the radar, the Nanjing Shipborne Radar Research Institute delivered a prototype to the Navy in 1986. The unit has undergone test operations in severe weather conditions including a 12-scale typhoon. The test results showed that the radar is accurate, reliable, and has good anti-interference capability; its key technical parameters have all met design requirements.

3) Joint Space Development With West Germany

On 8 December, China's Chang Cheng Industrial Corporation, the State Science and Technology Commission and West Germany's Ministry of Research and Technology signed two agreements in Beijing to conduct micro-gravity experiments in space. According to the agreement between Chang Cheng Corporation and West Germany, a study of protein crystal growth under micro-gravity conditions in space will be conducted by West Germany in 1989 using China's retrievable satellite. This was the second agreement signed by China and West Germany within a four-month period.

The agreement signed in September 1987 specifies that in 1988 China will provide a service to launch West Germany's retrievable satellite. The agreement between the State Science and Technology Commission and West Germany specifies that the two countries will conduct more than 10 cooperative experiments in the areas of material science and life science. These two agreements were reached after a tour of China's research facilities by 16 West German aerospace scientists.

4) Sino-Swedish Joint Efforts

China has agreed to launch a scientific exploration and postal communication satellite for the Swedish government. At the end of 1987, Sweden paid the first installment fee for the launch service to the Chang Cheng Corporation, and the contract signed by the two parties officially went into effect. The contract specifies that in the fall of 1991, the Chang Cheng Corporation will launch the Swedish Space Corporation's satellite into a specified earth orbit using the "Long March 2" space launch vehicle.

5) First Shipborne Helicopter Makes Debut

On the morning of 2 December, China's first shipborne helicopter lifted off from the take-off/landing field of the Chinese Helicopter Design Research Institute. In the past, China's main obstacle in developing shipborne helicopters has been the problem of designing a high-speed ship-landing device. The Chinese Helicopter Design Research Institute, which was assigned the task of developing the helicopter, overcame this difficulty and successfully conducted the flight test.

6) Large-Scale Supersonic Wind Tunnel

At the end of 1987, China's largest (1.2m x 1.2m) transonic/supersonic wind tunnel passed technical certification in Jinyang, Sichuan Province. This facility can provide aerodynamic data for verifying the designs of various types of aircraft.

The successful development of the supersonic wind tunnel filled a gap in China's wind tunnel facilities. The uniformity of its flow field and the performance of the jet nozzles along the flexible walls have reached the standards of similar foreign-built wind tunnels. Since its completion in 1980, this wind tunnel has been used in the research and tests of many different models of aircraft, missiles and space launch vehicles; it has provided accurate aerodynamic data for design and production organizations and has played a major role in the development of China's key flight vehicles. It has also enhanced China's technical reputation in cooperative efforts and exchanges with other countries. This transonic/supersonic wind tunnel was designed and built by the Chinese Aerodynamic Research and Development Center in cooperation with many other organizations. The entire project took approximately 10 years.

3012/9274

STABILITY CRITERIA FOR NON-LINEAR GYRO SYSTEMS

40090069 Beijing ZHONGGUO KEXUE [SCIENTIA SINICA] in Chinese, Series A, No 12, (Dec) 87 pp 1268-1272

[Article by Zhang Guangshu [1728 0342 2873], Theoretical Mechanics Section, Beijing Aeronautical Engineering Institute. Received 13 Oct 86, revised 4 Mar 87]

[Abstract] On the basis of Lyapunov's stability theory, Chetaev has established stability criteria (the three KTC theorems) for gyro systems under the effects of dissipative forces. This theorem was proven only for linear systems, however, and it is not known whether it applies to non-linear systems, nor is there a general solution. This paper resolves the problem by showing that Lyapunov's theory can be equally well applied to non-linear systems (i.e., gyro systems subjected to non-linear dissipative forces and non-linear conservative forces) with multiple degrees of freedom; the results are identical to those for linear systems.

This achievement creates a broader range of applications for the KTC theorem, including rotary motion of elliptical bodies, gyro rotor configuration, and vehicle attitude stability. The attitude stability problem of the Explorer 1 and Syncom satellites, for example, previously explained with linear-system theory, can now be completely explained using the non-linear theory developed here.

Three main conclusions are: (1) If a conservative system is stable, then the system will still be stable under the effects of dissipative forces and gyro forces; (2) if a conservative system is unstable, then under the influence of completely dissipative forces it cannot undergo heightened gyro forces to make it stable; and (3) if a conservative system is stable, then when subjected to completely dissipative forces and gyro forces the system will gradually approach stability.

REFERENCES

Chetaev, N.G., Motion Stability, 1965.

Gao Weibing [7559 3634 2671], Motion Stability, Beijing Aeronautical Engineering Institute, 1984, pp 129-167, 281-364.

Kaplan, M.H., Dynamics and Control of Spacecraft, Science Publishers, 1981, pp 26-70.

Krasovskii, N.N., Some Problems in the Theory of Motion Stability, 1959, pp 80-85.

Magnus, K., Gyroscopic Theory and Applications, trade book translation, National Defense Industry Publishing House, 1983, pp 241-323.

Merkin, D.R., Gyroscopic Systems, 1956.

Wang Zhaolin [3769 3564 2651], Basic Contemporary Control Theory, National Defense Industry Publishing House, 1981, pp 214-254.

/9604

SPACE MEDICINE: GROUND LAID FOR MANNED FLIGHTS

40081058 Beijing RENMIN RIBAO (OVERSEAS EDITION) in Chinese 2 Apr 88 p 4

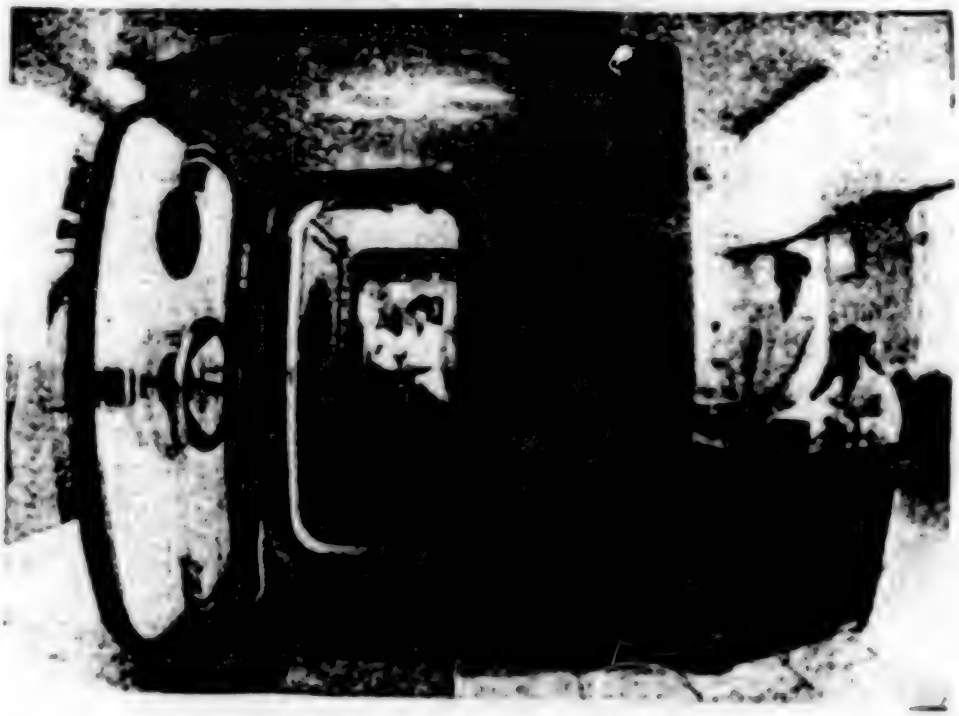

[Photograph and Caption] Achievement in space medicine engineering research has laid a solid foundation for developing Chinese manned vehicle space programs. Shown in the photograph are research technicians preparing simulation test for astronauts in a low-pressure, temperature-modified chamber.

08309
40081058

CHINESE SCIENTISTS SAY SUPERCONDUCTIVITY RESEARCH AT CRUCIAL JUNCTURE

40080079a Beijing GUANGMING RIBAO in Chinese 7 Feb 88 p 3

[Article by Chen Zhijiang [7115 1807 3068]: "Urgent Matters in the Research of Superconductivity in China"-An Interview With Professor Zhao Zhongxian [6392 1813 6343]]

[Text] Due to the competitive nature of superconductivity research and the significant accomplishment made by Chinese scientists, the famous Chinese expert on superconductivity Professor Zhao Zhongxian and his colleague Associate Professor Chen Genghua [7115 6342 5478], who are visiting Japan as a part of the Chinese S&T Accomplishments Exhibit, have become the focus of attention here. In 2 weeks, they visited six research institutes, held seven seminars and attended numerous meetings. Professor Zhao was interviewed shortly prior to his return.

Professor Zhao was impressed by the Japanese effort in superconductivity research. Superconductivity research in China, Japan, and the United States is at a crucial stage. The country that makes a breakthrough will play an active role in the coming industrial revolution. Chinese scientists must have this urgency to assess our capability and select projects to work on to bring us the ultimate victory.

Professor Zhao pointed out that all Japanese are concerned about superconductivity. If the fate of Japan was determined by semiconductors in 1960, then the fate of Japan will be determined by superconductors in the 21st century. Superconductivity research in Japan is a collaborative effort between industry and academia and is led by the government.

The Japanese have made enormous investments in superconductivity research. According to Ministry of International Trade and Industry [MITI] officials, Japan invests approximately 10 billion yen per year in superconductivity research. In the newly founded Institute of Superconductivity Engineering, the investment in equipment alone is 2 billion yen. On top of that, the operating expenses are running at 1 billion yen every year. There are numerous private industries that are spending more than 100 million yen per year in superconductivity research.

Faced with this kind of competition what should Chinese researchers do? Professor Zhao pointed out that China has a thousand people on the technical staff in superconductivity research. It is a tremendous force. However, our investment in research is limited. The most urgent matter is to concentrate our manpower and resources to work on selected projects. We should pay attention to the two following issues:

Maintain security in contacts with other countries. The Japanese are very enthusiastic about superconductivity. However, they are also very calm about it. They are constantly monitoring progress abroad to modify their own programs. In publishing their results, the Japanese manage to do it timely but without revealing any secrets. As an example, in addition to oxide superconductors, the Japanese are working on organic and non-rare-earth superconductors. However, they rarely mention anything other than what has already been published. As we were leaving Japan, they announced the successful development of a high-temperature superconductor whose critical temperature is above 100 K. Prior to this announcement, we met with the Japanese experts in many meetings. They never said a word about it.

Apply for patents. We should learn from the Japanese to aggressively and actively pursue patent applications. This does not mean that all existing Japanese patents are useful. However, it is a strategy for the future. Some patents may come in handy some day.

12553/08309

ADVANCES IN SUPERCONDUCTIVITY CLAIMED

40080095 Beijing RENMIN RIBAO in Chinese 3 Mar 88 p 1

[Text] Beijing, 2 March--Shortly after their production of non-rare earth oxide superconductor materials, the Institute of Physics of the Chinese Academy of Sciences today made another announcement disclosing the development of what is now the world's highest temperature conversion superconductor. Sources within the Institute of Physics state that this new superconducting material is composed of thallium, barium, calcium, and copper oxides. Its zero-resistance temperature is 114 K and at 117 K the material exhibits a clear diamagnetic effect. The sources pointed out that this new non-rare earth superconducting material achieves stable function and the technology may be duplicated. Scientists around the world have made the discovery of a high critical temperature superconductor their major target. Last year, the rare earth Y-Ba-Cu oxide superconductor was developed. Its zero resistance-normal stability was between 93 and 95K. This year, Chinese, Japanese, and American scientists have been working on the non-rare earth bismuth-strontium-copper oxide superconductor; its zero resistance-normal stability is 84 to 85K.

/9604

HIGHEST TRANSITION TEMPERATURE FOR SUPERCONDUCTOR ATTAINED

40080083b Beijing RENMIN RIBAO [PEOPLE'S DAILY] (Overseas Edition) in Chinese 3 Mar 88 p 4

[Article by Huang Xingzhang [7806 5281 4545] and Chen Zujia [7115 4371 3946]: "Further Important Developments in China's Superconductivity Research; Material Which Does Not Contain Rare Earths Has Stable Properties Which Can Be Replicated; New Superconductor Produced Having the Highest Transition Temperature to Date"]

[Text] Very shortly after they produced an oxide superconducting material which does not contain rare-earth elements, personnel at the Chinese Academy of Sciences' Physics Institute today announced that they have attained the highest transition temperature yet for a superconductor.

Concerned personnel of the Physics Institute said that this new superconducting material is composed of thallium, barium, calcium, copper and oxygen. It loses its resistance to electrical current at a temperature of 114 K, and demonstrates antimagnetic effects at 117 K.

These experts noted that the properties of this new non-rare-earth superconducting material appear to be both stable and reproducible. Researchers at the Physics Institute are now engaged in further studies of this material.

According to their explanation, the search for new superconductors having high critical temperatures is one of the principal goals of scientists throughout the world today. The rare-earth-containing superconductors produced last year, such as compounds of yttrium, barium, and copper oxide, generally stabilize zero resistivity at about 93 to 95 K. The superconductors being produced today by scientists in China, Japan and the United States contain the non-rare-earth elements of bismuth, strontium, and copper oxide, and in general stabilize zero resistivity at about 84 or 85 K. The new material produced at the Physics Institute clearly has a zero-resistivity temperature as high as that of previous materials.

12625/12232

ELECTRON STRUCTURE, MAGNETISM, SUPERCONDUCTIVITY OF AMORPHOUS Nb-Ni ALLOYS

40090067c Beijing WULI XUEBAO [ACTA PHYSICA SINICA] in Chinese Vol 37 No 1, Jan 88 pp 29-35

[English abstract of article by Wu Baimei [0702 2672 2653], et al., of the Department of Physics, University of Science and Technology of China, Hefei]

[Text] The electron structures of amorphous $Nb_{100-x}Ni_x$ (x = 65, 59.8, 56.4) alloys are studied by means of UV-photoelectron spectroscopy (UPS). It is found that the position of the Fermi level is located near the minimum of the density of states, which explains the double Curie-point phenomena in Nb-Ni alloys. Analyzing the electron structure of Nb-Ni alloys, it is pointed out that the hybridization of two d-bands with energies close to each other may form a new hybridizated band near E_F, and the hybridization is related to the valence difference. The charge transfer makes the band peaks shift. The density of states of T_E-T_L alloys at E_F should include contributions in two parts, i.e., those from 3d electron states, of advantage to magnetism, and those from 4d electron states, of advantage of superconductivity. Different ratios of these contributions to E_F influence the magnetism and superconductivity of the alloys. The coexistence of localized magnetic moments and superconductivity is also discussed.

9717

This article is republished
from JPRS CST-88-004 of
16 February 1988 to provide
a corrected copy.

Development of Fast Breeder Reactors in China

40080008b Beijing WULI [PHYSICS] in Chinese Vol 16 No 8, Aug 87 pp 487-493, 460

[Article by Li Shounan [2621 1108 2809], Chinese Academy of Atomic Energy: "Fusion-Fission Hybrid Reactors--The Path of China's Development of Breeder Reactors"]

[Excerpt] In 1980, in my report at the meeting to establish the China Nuclear Society, I proposed as a nuclear energy development strategy for China that in the second stage of China's nuclear energy development whether we could abandon the fast reactor and take the path of fusion-fission hybrid reactor. It was well received by the Plasma Physics Institute of the Chinese Academy of Sciences. Subsequently, a small group to carry on study of a hybrid reactor was established and in 1985 proposed the HTHR physics concept design of China's first hybrid reactor.[7] In 1984, I systematically introduced the fusion-fission hybrid reactor at such locations as the Nuclear Industry Ministry's Fast Reactor Verification Meeting and the Southwest Physics Institute[8] and presented my proposal for dividing the development of fusion in China into the two stages of a hybrid reactor and a pure fusion reactor. It was unanimously supported by the leadership and science and technology personnel of the Southwest Physics Institute. In 1985, this institute completed a concept design of a rather complete magnetic mirror hybrid reactor (CHD).[9] In December 1985, China's first Hybrid Reactor Symposium was convened at Leshan in Sichuan. At the meeting the strategic idea of a two-stage development of China's nuclear fusion was unanimously approved. Through efforts in a variety of areas, the fusion-fission hybrid reactor is now ranked with the fast reactor as a pre-research topic for China's Seventh Five-Year Plan to further certify the policymaking.

This paper will briefly introduce the principle of the hybrid reactor and make certain comparisons with regard to the superiority of the hybrid reactor.

I. Principle of the Fusion-Fission Hybrid Reactor

1. Nuclear Physics Foundation of the Hybrid Reactor

The hybrid fusion-fission reactor has a fusion core as driver. Outside the reactor core is breeder cladding. The cladding is a subcritical apparatus. Figure 1 is a comparative diagram of a pure fusion reactor and a hybrid reactor. The primary difference between the two is that in the hybrid reactor cladding the feiliao [5142 2436 fertile material] nuclei ^{238}U or ^{232}Th is increased and there are sometimes also other fissionable nuclei ^{235}U and ^{239}Pu or ^{233}U.

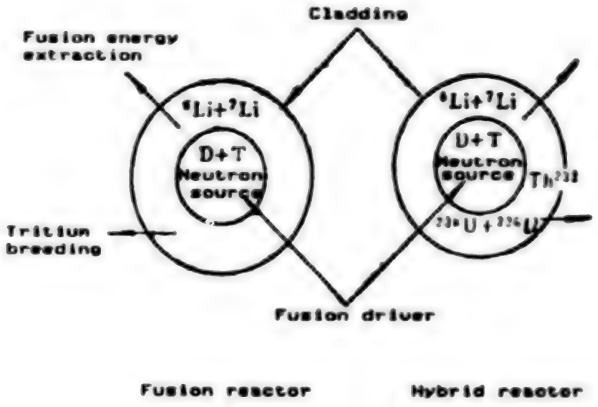

Figure 1. Comparison of Fusion Reactor and Hybrid Reactor

The first generation fusion reactor will be a deuterium-tritium reaction fusion reactor. The thermonuclear reaction which takes place in the high temperature plasma in the fusion reactor core is:

$$D + T \longrightarrow \alpha(3.52\ MeV) + n\ (14.06\ MeV) \qquad (1)$$

produces 14 MeV fast neutrons which enter the cladding through the first barrier. Like a pure fusion reactor, the fast neutrons enter the hybrid reactor cladding and the reaction with lithium creates tritium to supplement the tritium consumed in the fusion reaction:

$$^6Li + n \longrightarrow \alpha + T + 4.78\ MeV \qquad (2)$$

$$^7Li + n \longrightarrow \alpha + T + n' - 2.82\ MeV \qquad (3)$$

However, the difference between a hybrid reactor and a pure reactor is that after the fast neutrons enter the cladding, in addition to creating a tritium reaction, a (n, γ) capture reaction occurs with ^{238}U or ^{232}Th and the nuclear fuel ^{239}Pu ^{233}U which is created thus plays a role as fertile nuclear fuel.

The fusion neutrons can also have a fast fission reaction with the ^{238}U and ^{232}Th (threshold values are 0.7 MeV and 1.2 MeV, respectively), and after

slowing, hot neutron fission can occur with ^{235}U, ^{239}Pu or ^{233}U. The fission energy deposited in the cladding by each fission is approximately 190 MeV, and thus acts to multiply the energy.

The fusion neutrons, through (n, 2n), (n, 3n) reactions with the first barrier material, feiliao nuclei and neutron multiplier (such as Be, and Pb) can achieve the goal of multiplying neutrons.

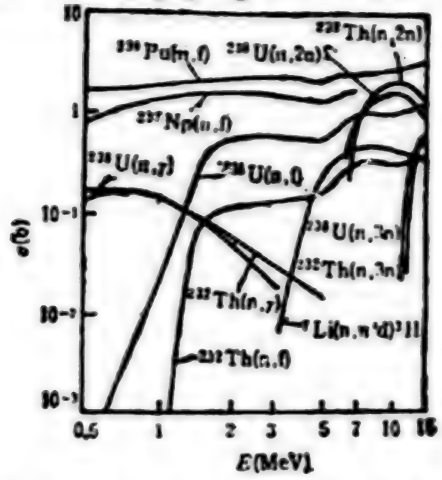

(a) Cross section of various fuel nuclear fast neutrons

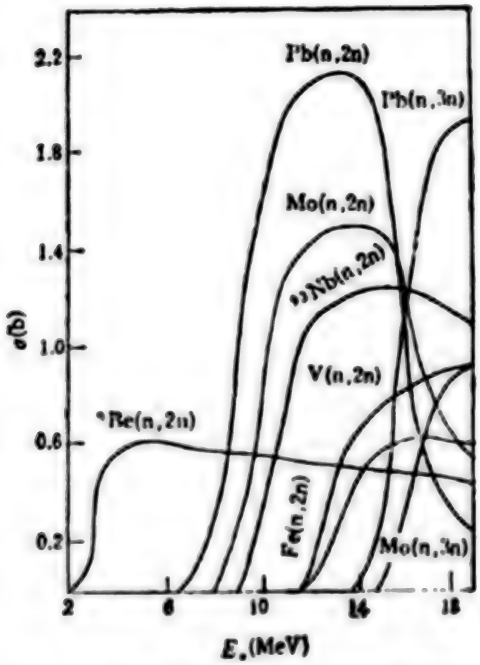

(b) Cross section of several types of neutron multiplier (n, 2n), (n, 3n)

Figure 2.

Figure 2(a) is a cross section of significant fuel nuclei fast neutrons in a hybrid reactor. Figure 2(b) is a cross section of several non-fuel

nuclei (n, 2n), (n, 3n). Through fission, (n, 2n), and (n, 3n) reactions, a fission neutron in the hybrid reactor cladding can generally be multiplied to 2-4 neutrons. Apart from one neutron which is used for breeding tritium, 1-3 neutrons can be used for breeding nuclear fuel or increasing fission. This is called the net breeder ratio (C_{BR}^{H}). The fast reactor neutron spectrum is rather soft, in a fast reactor, ^{238}U and ^{232}Th fast fission is rare, there is no (n, 2n), (n, 3n) reaction, neutron multiplication is poor, and the breeding ratio is low. When hybrid sodium oxide cools the fast reactor, the breeding ratio can only reach 1.1-1.3. In future use of carbides or metallic fuel it may reach 1.4-1.5 The fuel of each fission breeding has one used for production nuclear fuel to compensate for consumption, the net breeder ratio (C_{BR}^{FB}) can only be 0.1-0.3, and in the future at most can be 0.4-0.5.

The ratio of annual neutron fuel production capability of hybrid reactors (Y) is the ratio of product of the fusion reaction rate (R_f) and the cladding net breeder ratio of the hybrid reactor and the product of the fission rate (R_F) and the net breeder rate of the fast reactor.

$$Y = R_f C_{BR}^{H} / R_F C_{BR}^{FB} \tag{4}$$

For power, it is the same for the P(MW) hybrid reactor and fast reactors

$$R_f R_F = 190/(3.52 + 14\ M), \tag{5}$$

in which M is the hybrid reactor cladding energy multiplication factor. Therefore,

$$Y = 190\ C_{BR}^{H}/(3.52 + 14M) C_{BR}^{FB} \tag{6}$$

This is because $C_{BR}^{H} > C_{BR}^{FB}$, therefore when M is not too great, $Y \gg 1$. It is clear that the hybrid breeding ability of the reactor is much greater than that of the fast reactor.

2. Two Types of Hybrid Reactors

Any deuterium or tritium neutron source can be the driver of a hybrid reactor, even if the accelerator neutral source, such as a spallation source also can be the driver of a hybrid reactor. Hybrid reactors can be divided into two major classes of magnetically confined hybrid fusion-fission reactor and inertially confined hybrid fusion-fission reactor depending on the differences in hybrid reactor driver. Examples of the former are tokamak hybrid reactors and tandem magnetic mirror hybrid reactors; examples of the latter are laser inertially confined hybrid reactors and hybrid particle beam fusion reactors. Inertially confined hybrid reactors do not require a strong magnetic field, structure is simple, reactor core power density is high, economics are good, and maintenance is easy. The structure of magnetically confined hybrid reactors is complex; they require a strong magnetic field, reactor core power density is low, and economic performance is relatively poor. However, research on tokamak fusion devices is well advanced and first generation hybrid reactors will be tokamak hybrid reactors.

Hybrid reactors are divided on the basis of fuel systems into U/Pu system hybrid reactors and Th/U system hybrid reactors. After breeding nuclear fuel generally goes through postprocessing to extract the breeder Pu or ^{233}U. Recently with the development of neutronics, a new idea has been suggested, i.e., after breeding to a certain isotope density, such as 3 percent ^{233}U content, it can be used in a thermal reactor without going through processing. This type is called the direct enriched hybrid reactor. It can save the expenses of postprocessing which is beneficial for lowering fuel costs and advancing commercial use.

Fission hybrid reactors and retarded fission reactors can be designed on the basis of the differences between the nature and degree of the fission induced after 14 MeV neutrons enter the cladding. Hybrid fission reactors use ^{238}U and ^{232}Th fast neutron fission (fast fission hybrid reactor) or post-moderation thermal neutrons and ^{235}U in the cladding and the thermal neutron fission of the ^{239}Pu or ^{233}U produced (thermal neutron fission hybrid reactor). Since fission hybrid reactors use fission energy, the energy accumulated in the cladding can be many times greater than that of the pure fusion reactor. If in the design of the hybrid reactor, 14 M neutrons are rapidly moderated below the fission threshold of ^{238}U or ^{232}Th so that fast fission is avoided as much as possible and at the same time the ^{239}Pu, ^{233}U, and ^{235}U content of the cladding is lowered as much as possible to avoid thermal fission, then the fusion neutrons which are multiplied in the cladding can be used as much as possible as nuclear breeder fuel and such a hybrid reactor is called an inhibited fission reactor. The energy multiplication of such a reactor is not great, but the nuclear fuel production is considerable, so it is called a nuclear fuel plant.

$$N = \frac{\text{Energy released by each fission reaction} \cdot \frac{C_{BR}}{(1-c)}}{\text{Energy released by each fusion reaction in a hybrid reactor}}$$

$$= \frac{190}{14.06\,M + 3.52}\,\frac{C_{BR}}{1-c}$$

$$= \frac{13.5}{1-C}\,\frac{C_{BR}}{M}\,f(M),$$

in which C_{BR} is the net breeder ratio, M is the cladding energy multiplier factor, c is the fission reactor fuel conversion ratio.

$$f(M) = 14.06\,M/(14.06\,M + 3.52),$$

$$N = 33.7\,\frac{C_{BR}}{M}\,f(M)$$

for ^{239}Pu pressure water reactor (c = 0.6), (7)

$$N = 54.0 \frac{C_{3R}}{M} f(M)$$

for ^{233}U pressure water reactor (8)

Table 1 is a representative example of the support ratios of different hybrid pressure water reactors. On the basis of different demands, hybrid reactors which are primarily for production of nuclear fuel or primarily to power production or a combination of the two can be designed.

Table 1. Support Ratios of Different Cladding Hybrid Reactors Relative to Pressure Water Reactors

	M	C_{3R}	N ^{239}Pu	^{233}U
Fast neutron fission (power reactor)	25	1.04	-1	-2
Fast fission	10	1.6	-5	-8
Controlled fission	2	0.92	-14	-22

3. Hybrid Reactors Can Advance Use of Fusion Energy

The more fission energy produced by hybrid reactor cladding, the greater the increase in cladding energy, the lower the demands on the fusion driver, which is beneficial for advancing the implementation of fusion energy use. The average deposited energy of each fusion neutron in the cladding is

$$E_b = Mq_n, \quad (9)$$

q_n is the fusion neutron energy. The hybrid reactor cladding power is

$$P_B = R_f E_b = Mq_n R_f, \quad (10)$$

R_f is the fusion reaction rate of the fusion reactor core. For a hybrid reactor with a definite cladding power,

$$R_f = \frac{P_B}{q_a} \cdot \frac{1}{M}, \quad (11)$$

P_F = fusion power = $R_f(q_a + q_n)$

$$= \frac{P_B(q_a + q_n)}{q_a} \cdot \frac{1}{M}, \quad (12)$$

$$Q = \text{energy gain} = \frac{R_f(q_n + q_a)}{\gamma P_a}$$

$$= \frac{(q_n + q_a)}{\gamma q_a} \cdot \frac{1}{M}, \tag{13}$$

$$I = \text{first barrier neutron load} = \frac{R_f q_n}{A}$$

$$= \frac{P_h}{A} \cdot \frac{1}{M}, \tag{14}$$

in which q_a = 3.52 MeV, A is the first barrier area, γ is the portion of a cladding power used for reactor core input energy. The demands of a fusion reactor or hybrid fusion-fission reactor with a fixed cladding power on the fusion driver forms an inverse ratio with M. Therefore, the hybrid reactor (especially the hybrid fission reactor) can greatly lower the difficulty of a fusion driver technologically. Table 2 is the demands of different cladding on the Q value (assuming γ = 5 percent).

Table 2. Demands of Different Cladding on Fusion Reactor Core Q Value

	Thermal neutron hybrid reactor	Fast fission hybrid reactor	Controlled fission hybrid reactor	Pure fusion reactor
Av cladding energy multiplier factor (M)	25	10	2	1.3
Demand on effective power output gain (Q)	1	2.5	12.5	19

It is all right if the demands of hybrid fission reactors on the Q value reach 1-2. The Q value of the current four major ignition devices internationally TFTR, JET, JT-60, and T-15 are about 1-4. After these devices realize ignition, an engineering experimental hybrid fusion-fission reactor can be constructed on the basis of this generation of devices. The tokamak fission hybrid reactor can be implemented first of all. According to statistics, it can be about 20 years ahead of the pure fusion reactor. If at first it is only used for producing nuclear fuel and not connected to a network for transmission of electricity, it still can be moved ahead. A controlled hybrid fission reactor is the ideal nuclear fuel plant. Since the demands on the driver are not lowered much, the construction time will be more delayed than the hybrid fission reactor.

II. Comparison of Two Types of Breeder Reactors

To explain the advantages of hybrid reactors, we will first make some comparisons of the fusion breeder reactor (hybrid reactor) and the fission breeder reactor (fast reactor).

1. Hybrid Reactor Breeder Energy Is Much Greater Than Fast Reactors

Above we have mentioned that the pure breeder ratio of fast reactors is small, multiplication time is long (for example Super-Fenghuang-1 breeder ratio is 1.1 and multiplication time is 40 years), the nuclear fuel breeder capability is poor, and the support ratio is much smaller than that of the hybrid reactor. Table 3 is the typical range of a fast reactor and hybrid reactor with regard to pressure water reactor support ratio.

Table 3. Fast Reactor and Hybrid Reactor Support Ratios Relative to Pressure Water Reactors

	Oxide fast reactor	Carbide fast reactor	Metallic uranium fast reactor	U/Pu fast fission hybrid reactor	Th/U fast fission hybrid reactor	Th/U controlled fission hybrid reactor
C_{BR}	0.1-0.3	$\leq$0.4	$\leq$0.5	1.5-2	1.8-2.5	0.6-0.85
M				8-12	10-14	2.5-1.6
N	0.25-0.7	$\leq$1.25	$\leq$1.25	4-6	8-12	12-25

P. Fortescue has carried out theoretical comparison of the breeder energy of a fusion breeder reactor and a fission breeder reactor.[10] See Figures 3(a) and (b). Q is the energy multiplication, relative to the support ratio (here the fast reactor C_{BR}-1 is the pure breeder ratio).

2. The Hybrid Reactor Is Not Inhibited by Industrial Plutonium

Fast reactor power station construction was inhibited by initial fueling with industrial plutonium, but the hybrid reactor does not have this problem. The Super-Fenghuang-1 fast reactor initial fueling required 8 t of industrial plutonium in the reactor with an annual output of 200 kg of plutonium. After the oxide sodium cooled fast reactor was transformed, the best circumstances were estimated to be initial fueling of 5 t and annual output of 250 kg of plutonium. In the future, using carbide or metallic uranium fuel, the initial fueling can reach 3 t with annual output of 300 kg of plutonium, but it will still be inhibited by the initial fueling with industrial plutonium.

China's rated electric power generating capacity by the year 2000 is estimated to reach 230 GWe and if the average annual increase after the year 2000 is 4 percent then the gross rated capacity by the year 2050 will be about 1,635 GWe (curve IV in Figure 4). It is said that China's uranium mine explored reserves can only supply 15 GWe pressure water reactors for 30 years. With U-Pu circulation it also can only be 21 GWe. China's nuclear power station construction is too late and too slow and extremely unfavorable for accumulating industrial plutonium growth fast reactors. If 15 GWe nuclear power is built before the year 2010, and another 10 GWe

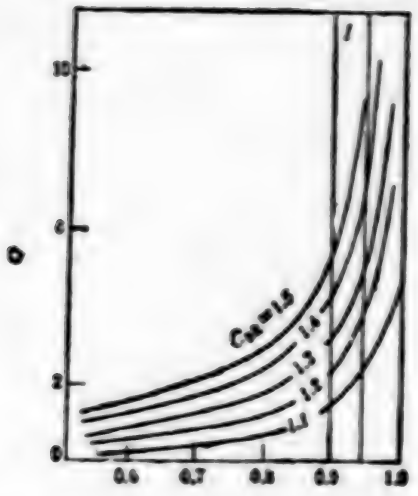

(a) Fast reactor breeder capability (Q = conversion reactor power/ fast reactor power, α is the thermal reactor conversion ratio. C_{BR} is the breeder ratio)

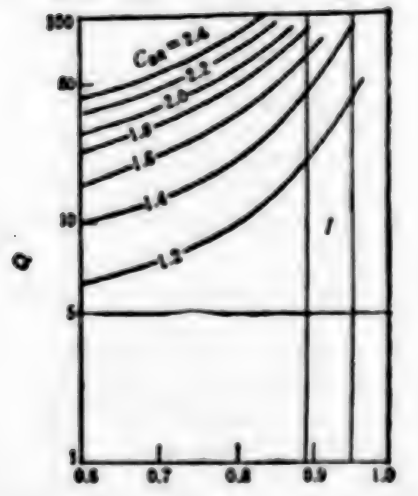

(b) Hybrid reactor breeder capability (Q = fission energy/fusion energy. α is the thermal reactor conversion ratio. C_{BR} is the net breeder ratio)

Figure 3.

added between the years 2011 and 2015, then the total will reach 25 GWe by the year 2015. If fast reactors are introduced beginning in the year 2010 and all industrial plutonium produced by pressure water reactors and fast reactors is used to develop fast reactors, then the nuclear power rated capacity provided by pressure water reactors and fast reactors with different breeding capabilities together are illustrated by curves I, II, and iII in Figure 4. From Figure 4 it is clear that fast reactors cannot resolve China's energy problem in the 21st century.

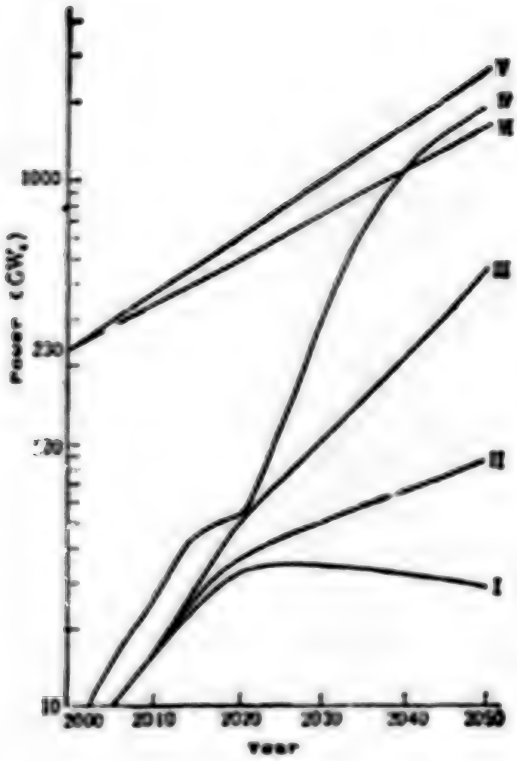

Figure 4. Nuclear Power Which Can Be Provided By Different Breeder Reactor Systems
Curve I is fast reactor + LWR, initial fueling 6 t, annual output of plutonium is 150 kg;
Curve II is fast reactor + LWR, initial fueling 5 t, annual output of plutonium is 250 kg;
Curve III is fast reactor + LWR, initial fueling 3 t, annual output of plutonium is 300 kg;
Curve IV is hybrid reactor + LWR, year 2020 introduction of fission hybrid reactor (support ratio 6),
Year 2025 introduction of controlled fission hybrid reactor (support ratio of 20);
Curves V and VI are China's needs for electric power increase (V is annual increase of 4 percent after the year 2000, VI is annual increase of 5 percent after the year 2000)

Hybrid reactor construction is not inhibited by accumulation of industrial plutonium, and as soon as the technology matures and economic forces permit, development can be accelerated. If we can concentrate our forces and work hard, then hybrid fission reactors can go into operation in China in the year 2015, and it is possible that about the year 2020-2025 controlled fission hybrid reactors can go into use. Since the hybrid breeder reactor's capacity is powerful, soon after construction it can supply fuel for pressure water reactors. The above-mentioned 25 GWe nuclear power station fuel can be used for a total of 750 reactor-years. While the pressure water reactors will use low concentration natural

uranium for the first 15-20 years, later they can use fuel supplied by hybrid reactors. Thus in the early period, more pressure water reactors can be built. If each year we begin to construct one fast fission hybrid reactor-pressure water reactor system with a support ratio of 67 and after the year 2025 add two more per year; then after the year 2025 we construct one controlled fission hybrid reactor co-generation system (support ratio of 20) and after the year 2030 add two per year, then according to this plan the nuclear power electricity rated capacity of the hybrid reactor-pressure water reactor co-generation system will be as illustrated by curve VI in Figure 4. This shows that the hybrid reactor-pressure water reactor co-generation system will provide a possible road for resolving the problem of the energy shortage in China in the 21st century.

3. The Price of Electric Energy of the Hybrid Reactor-Pressure Water Reactor Co-Generation System Is Cheaper Than the Fast Reactor-Pressure Water Reactor Co-Generation System

Figure 5 [omitted] is the U.S. EPRI evaluation of power plant prices of several types of fuel circulation.[11] In the figure, OT + F is the fast reactor (construction cost ratio for LWR is higher by 30 percent, multiplication time is 15 years) + LWR (one pass) co-generation system; D + H_1, D + H_2, D + H_3, D + H_4 are hybrid reactor + LWR (U/Pu circulation) co-generation systems. Hybrid reactor co-generation system power plant prices are cheaper than fast reactor co-generation systems. OT is one pass LWR; D is U-Pu circulation LWR, H is the hybrid reactor, whose performance is illustrated in Table 4.

Table 4. Various Hybrid Reactor Conditions

Hybrid reactor	Construction cost (LWR)	Support ratio	Net electricity output (MWe)
H_1	1.5	4	800
H_2	2.5	4	800
H_3	2.5	12	100
H_4	2.5	8	800

4. Hybrid Reactor-LWR Co-Generation System Consumption of Uranium Resources Is Lower Than Fast Reactor-LWR Co-Generation Systems

Figure 6 is the relationship of world uranium consumption according to the OECD world nuclear power prediction low scheme analysis and different systems and fuel circulation.[12] In the figure, FB is LMFBR + LWR, HP is U/Pu circulation hybrid reactor + LWR, HU is Th/U circulation hybrid reactor + LWR. Obviously, HP and HU are lower than FB. The horizontal line is the believed world uranium reserves. Clearly, only the hybrid reactor co-generation system can maintain the use of uranium consumption below 5 x 10^6t. In Figure 6, OT is one pass LWR; LU is LWR uranium circulation; LU-1P is LWR U/PU circulation.

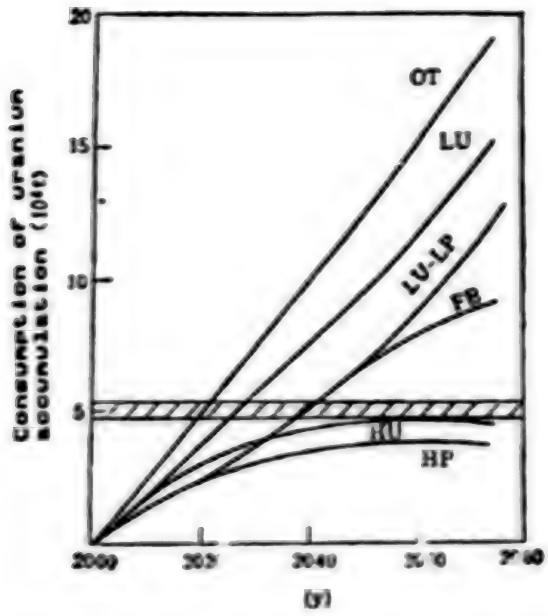

Figure 6. World Uranium Consumption According to Predicted Low Nuclear Power
(Assuming new type reactors are introduced in the year 2000 and according to market penetration model)

From Figure 6 it is clear that if it is one-pass LWR, then the world uranium deposits will be used up by the year 2020. Using the U/Pu circulation and fast reactor + LWR co-generation system, it will be used up before the year 2040. If the time that the fast reactor is introduced and promoted is retarded, then the time when the uranium consumption ends will be advanced.

5. Th/U System Hybrid Reactor-LWR Co-Generation System Is Economical Compared to Use of Thorium Resources, and Fast Reactors Cannot Economically Use Thorium Resources

Since the ^{232}Th fast neutron fission cross section is much smaller than the ^{238}U fast fusion cross section, the ^{232}Th fission threshold (1.2 MeV) is much higher than that of ^{238}U (0.7 MeV), in a hybrid reactor Th/U system has many more neutrons than the U/Pu system to be used for breeding nuclear fuel but the ^{232}Th and ^{238}U's capture surfaces are about the same. Therefore, in a hybrid reactor, the Th/U system breeder performance is better than the U/Pu system and under controlled fission circumstances it is even more the case. In addition, the η value of the ^{233}U in the thermal zone is higher than ^{239}Pu (for ^{233}U, η = 2.2966; for ^{239}Pu, η = 2.1137), therefore in thermal reactors burning ^{233}U is more economical than burning ^{239}Pu (^{233}U is 0.14 kg/MW·y, ^{239}Pu is 0.2 kg/MW·y). In the hybrid reactor-LWR co-generation system, the support ratio of Th/U system is greater than that of U/Pu system, thorium utilization is also more economical, and the controlled fusion hybrid reactor Th/U system is especially beneficial.

In the fast reactor, because the η value of ^{233}U in the high energy neutron zone (> 100 keV) is much lower than that of ^{239}Pu, ^{232}Th fast fission cross section is much smaller than that of ^{238}U, but the fission threshold happens to be higher than that of ^{238}U so the capture cross section is about the same as for ^{238}U. Therefore, in fast reactors, the breeder performance of both ^{233}U and ^{232}Th is poor, in the overall breeder performance, the Th/U system is about 20 percent lower than the U/Pu system. If a fast reactor uses the Th/U system, ^{233}U initial fueling and multiplication times are greater than the U-Pu system, economic performance is worse than that of the present uranium plutonium hybrid oxide fast reactors, breeding capability is lower, and even more lacks competitive ability.

China's thorium resources are abundant: surveyed reserves are over 200,000 tons. Developing hybrid reactors may effectively use thorium resources so that China's nuclear fuel resources will be expanded over three-fold.

6. Hybrid Reactors Are Safer Than Fast Reactors

First, hybrid reactors are a one time critical device; second, the reactor after heat problems are fewer than the fast reactor's, the controlled fission hybrid reactor is safer than the LWR, fission rate is extremely low (each fusion in the cladding induces a fission number of <0.05), unloaded fuel fission product is only 1/60 that of the LWR; third, in fluidized bed combustion circulation nuclear fuel in the reactor can leak out during an emergency shutdown and there is the problem of melting inside the reactor; fourth, direct enriched hybrid reactor does not have a post-processing problem; fifth, when the hybrid reactor-satellite reactor co-generation system requires post-processing, all the waste elements in the satellite reactors can be concentrated in the hybrid reactor plant for processing.

7. Other Advantages

Hybrid has a series of advantages which the fast reactor lacks. For example, the hybrid reactor can produce isotopes of ^{239}Pu which can be more than 95.5 percent pure; it can build a tritium reactor, there is the possibility that it can become a way for final processing of wastes with long radioactive lives; it can construct a high temperature heat source of more than 1,000°C taking the place of high temperature gas-cooled reactor and used for coal gasification, production of hydrogen and organic synthesis of methane, alcohol, gasoline.

Another important function of hybrid reactors is that they act as an intermediate stage in the transition to pure fusion reactors and can be second degree test reactors for pure fusion development to test materials and equipment, and accumulate design, construction and operational experience. Yet the fast reactor serving as a transitional reactor is completely independent and has no direct relationship to fusion development.

From the several points cited above it can be seen that the superiority of the hybrid reactor compared with the fast reactor is clear. The issue that concerns everyone now is what is the feasibility of the hybrid reactor. With regard to this point, development of the fast reactor is naturally mature, prototype reactors are already connected to networks and transmitting electricity. For a hybrid reactor to develop to today's stage of the prototype fast reactor would take about 15 years. There are many engineering and technical problems that must be resolved in hybrid reactor development. However, construction of a hybrid reactor has already been resolved in principle, and at the same time since in terms of engineering and technology it is based on the foundation of existing fission reactor and fusion reactor engineering research, there are no insuperable problems, construction is possible; there is only the problem of time. China's development of breeder reactors is to resolve the energy shortage in the 21st century. Technological maturity is a necessary condition for introducing an energy source system, but it is not a complete condition. Whether or not it can, or to what degree can resolve China's energy shortage in the 21st century is the complete condition. From this angle, proceeding from the actual circumstances in China, China's development of breeder reactors by taking the path of hybrid reactors seems to be the best policy.

III. Developing Hybrid Reactors Is an Important Challenge and Opportunity Facing China

It was mentioned above that although there are difficulties in developing hybrid reactors, a feasible path has already been realized. Internationally, since there are great difficulties in developing pure fusion reactors, construction time may be more retarded than previously thought. Thus the cry for hybrid reactors as an intermediate stage has been higher and higher. For the USSR making the hybrid reactor the first stage in utilizing fusion energy is already policy. At the 10th International Plasma and Nuclear Fusion Conference, Soviet Academician E.P. Velikhov announced that the Soviet Union would make hybrid reactors for generating electricity and producing nuclear fuel the first step in utilizing fusion energy and announced the indicators of a tokamak hybrid reactor engineering test reactor OTR based on the T-15.[13] This reactor is estimated to be completed before the year 2000. The Soviet Academician Basov pointed out in a 1984 article,[14] that in laser fusion the Soviet Union had planned a pure fusion reactor, a fission hybrid reactor for motive power, controlled fission hybrid reactor-fission reactor power station co-generation system. And he pointed out that the hybrid reactor's demand for laser efficiency could be lowered from 5 percent to 0.5 percent. At the 1986 Madrid Conference, Soviet Academician Basov and others gave reports on the concept and design of laser constraint hybrid reactor[15] and pointed out that costs of generating electricity could be lower than conventional nuclear electricity.

U.S. hybrid reactor research was the earliest and they have done the most work. Uranium and oil prices dropped due to the energy glut and at the same time because of preventing nuclear proliferation and anti-nuclear influence fast reactors and hybrid reactors did not receive congressional

support. Recently, due to the great difficulties of pure fusion, seeing that the Soviet Union is committed to developing hybrid reactors, the call for hybrid reactors in the United States has also increased. In 1985 the Department of Energy organized a committee of specialists to conduct 9 months of evaluation of hybrid reactors. Due to economic, political, and social factors, U.S. development of hybrid reactors will not go smoothly.

The person in charge of West European fusion, D. Palumb, indicates that Western Europe is engaging in pure fusion reactors and is not prepared to engage in hybrid reactors, because 1) Western Europe has invested in the development of fast reactors, that have enough industrial plutonium; 2) the anti-nuclear movement is too powerful; 3) they have no place to build hybrid reactors. He recognizes that only the Soviet Union and China have the conditions to engage in hybrid reactors.

After the Third International New Nuclear Energy System Conference in 1983, the hybrid reactor began to be taken seriously by more countries. Japan[16] and India have begun actively developing hybrid reactors.

Western Europe, the Soviet Union, and the United States have a history of development of hybrid reactors of more than 30 years. They have sufficient accumulation of industrial plutonium. It is natural for them to take the fast reactor route. Developing hybrid reactors would not be difficult for them technologically speaking. However, due to political, economic, and social influences, except for the Soviet Union, it will be difficult for them to take the hybrid reactor route.

China has a foundation of 30 years of fast reactor work, does not have accumulation of industrial plutonium, and development of fast reactors would not resolve the long-range energy problem. Compared with fast reactors, China's fusion research has two bases and a good foundation. China's path of developing nuclear energy need not take the crooked road of thermal reactor-fast reactor-fusion reactor. In the new technological revolution, we must be far-sighted, strengthen leadership, concentrate forces, and take the path of developing hybrid reactors. In this way we may later dominate. "The opportunity should not be lost, the time will not come again," we cannot let this opportunity pass us by.

References

1. P.F. Powell, LWS-24920, California Research and Development Company (1953); J.D. Lawson, AERE-GP/M (1955), 185.

2. J.W. Weale, et al., J. NUCLEAR ENERGY A/B, 14 (1961), 91.

3. L.N. Lontai, MS Thesis, Technical Report, No 436, MIT (1965).

4. L.M. Lidsky, CLM-NFR (1969), 41-53.

5. J.D. Lee, Proceedings 7th Intersociety Energy Conversion Engineering Conference, American Chemical Society (1972), 1294.

6. L.M. Lidsky, Proceedings 2d Fusion-Fission Energy Systems Review Meeting (1977), 83.

7. Qiu Lijian [6726 0536 0313], Yang Yaochen [2799 5069 5256], et al., HEFEI TOKAMAKE JUBIAN-LI-BIAN HYNHEDUI (HTHR) WULI GAINIAN SHEJI [PHYSICAL CONCEPT AND DESIGN OF THE HEFEI TOKAMAK FUSION-FISSION HYBRID REACTOR (HTHR)], Zhongguo Kexueyuan Dengliziti Wuliso Chuban (1985).

8. Li Shounan [2621 1108 2809], GUOWAI HEJIBIAN [NUCLEAR FUSION ABROAD], No 1 (1985), 1.

9. Huang Jinhua [7806 6930 5478], CIJING HUNHEDUI (CHD) GAINIAN SHEJI CHUBU BAOGAO [PRELIMINARY REPORT ON THE CONCEPT AND DESIGN OF THE MAGNETIC MIRROR HYBRID REACTOR (CHD)], Hegongyebu Xinan Wuli Yanjiuso Chuban (1985).

10. P. Fortescue, SCIENCE, 196-4296 (1977), 1326.

11. N.A. Amhred, Atomkernenergie/Kerntechnik, 44-1 (1984), 27.

12. J.D. Mantyb, S.I. Abdel-Halik, Atomkernenergie/Kerntechnik, 43-3 (1983), 156-158.

13. E.P. Velihov, IAEA-CN, 44/A.O.

14. N.G. Basov, FUSION, 6-2 (1984), 35.

15. N.G. Basor, et al., Proceedings 4th International Conference on Emerging Nuclear Energy Systems, Madrid (1986), 26.

16. M. Inoue, et al., Proceedings 4th International Conference on Emerging Nuclear Energy Systems, Madrid (1986), 70.

08226/9365

Design of Nuclear Heat, Power Co-Generation Plant Detailed

40080042a Chengdu HE DONGLI GONGCHENG [NUCLEAR POWER ENGINEERING] in Chinese Vol 8 No 6, Dec 87 pp 1-13

[Article by Liu Jukui [0491 5112 1145], manuscript received 10 November 1986: "Selection of Reactor for Small Nuclear Power and Heat Co-Generation Plant and Its Design Characteristics"]

[Text] I. Introduction

As society grows, the demand for heat also increases. More than 70 percent of primary energy resources is consumed to generate heat. Power generation, however, only consumes approximately 20 percent. Over 400 billion tons of coal are used for heating each year. In addition, a great deal of oil is also consumed. This stresses the transportation system, pollutes the environment, and wastes resources. In the future, a nuclear power and heat co-generation plant will be built near a town or city where the demand for steam and heat is centralized. This is a novel way to conserve energy, relieve transportation load, and reduce environmental pollution.

Although constructing a nuclear power and heat co-generation plant is a promising way to conserve energy, designers must first consider factors which make such a plant truly clean, safe, and cost effective. A summary of past experience tells us that the design objectives of a small nuclear power and heat co-generation plant are as follows:

(1) low capital requirement, in the range of 2,500-2,800 yuan/kW;

(2) construction time--4 years with one reactor and 5 years with two reactors;

(3) reliability--usable rate 85-90 percent, load factor over 80 percent;

(4) no major incident involving the fracture of a large-diameter pipe (more than 100) and loss of water. Core meltdown probability is less than 10^{-6} reactor/yr. In the absence of normal internal and external power, the device itself and battery power can cool the reactor. Due to its high safety and reliability, it may be used in populated areas;

(5) simplicity, compactness, and small scale construction;

(6) eliminating the need for a huge reactor building to reduce the load on the foundation. Hence, the nuclear power and heat co-generation plant may be built on a beach, on soft soil, and in earthquake areas. The degree of freedom in site selection is similar to that for a train station;

(7) no radioactivity in heat and hot water supplied, based on natural background level;

(8) double layer structured reactor building that can withstand pressure and can be sealed. In the event of leakage, the surrounding environment will not be contaminated by radiation.

II. Selection of Reactor Type

The bases for the selection of the reactor are that the eight designed objectives discussed above are met, it is technically feasible and it satisfies the demand for steam.

A pressurized-water reactor, boiling water reactor, or high-temperature gas-cooled reactor may be chosen for the small nuclear power and heat co-generation plant. We are more experienced in the experimental research, design, manufacture, installation, and operation of pressurized-water reactors. Based on practicality, we should choose a pressurized-water reactor.

The demand for steam is the basis for the selection of the type of reactor to use. Table 1 shows the demand parameters of several major steam users.

Based on the steam consumption parameters shown in Table 1, the majority is low and medium pressure steam. Therefore, either a pressurized-water reactor or a boiling water reactor can meet the steam requirements. However, the pressure of a boiling water reactor is generally 6.86 MPa and the core outlet temperature is 285°C. Hence, the steam temperature in the tertiary loop is less than 225°C. The core outlet temperature of a pressurized-water reactor is 310-325°C. As it is capable of generating medium pressure steam in the tertiary loop, it has a wider range of applications.

In summary, our first choice should be to use pressurized-water reactors for the heat and power co-generation nuclear plants. In addition, because the steam requirement is usually less than 100 t/h, reactor power should be under 600 MW. It is more appropriate to build two reactors in the same plant to supply both heat and power.

Table 1. Steam Consumption by Chemical Plants

Plant	Pressure 10^5Pa	Temperature °C	Amount t/h	Percentage
Shanghai Jinshan	10-16	270-285	700-1,000	77.8
Petrochemical Plant	35-40	320	285	22.2
Liaoyang Chemical	8-13	260	665-865	67.2
Fiber Company	39	450	417	31.6
	100	540	5	0.40
Jilin Chemical	8-13	280	1,121	86.1
Company	20	320	61	4.7
	30	260	104	8.0
	70	360	16	1.23
Dalian Ganjingzi	1.2-1.5		65	6.50
Area	8-13		839.7	84
	16		12	1.20
	32		86	8.60

The following discussion is based on a 450 MW reactor.

There are many types of pressurized-water reactors, including the classical circulation design, compact design (NP-300, CAS-3G), integrated layout, and pool layout (PIUS, ISER). The circulation design is a large, complicated system which takes a long time to build and costs more. It is not suited for a small plant.

III. Design of Small Nuclear Plant for Heat and Power

1. Principal Parameters and Primary Process Flowchart

The key issue in the design of a heat and power co-generation nuclear plant is the selection of the principal parameters and primary process flow. Based on the classical way of thinking, a water-steam-steam process is chosen for the plant to be constructed at Shanghai Jinshan Chemical Plant (Figure 2). The operating pressure of the reactor and the primary loop is 15 MPa. The steam pressure in the secondary loop is 5 MPa. The tertiary loop generates 75 t/h of saturated steam at 4 MPa, 320 t/h of saturated steam at 1.6 MPa and 52,000 kW of electricity (per reactor). The disadvantages of this flow process are: 1) leakage of the heat exchanger may bring radioactivity into the steam in the tertiary loop. Therefore, it is necessary to install detectors and the associated emergency equipment. 2) The thermal efficiency of the steam-steam heat exchanger is poor. It requires several heat exchangers (nine units per reactor) and takes a lot of space. 3) It requires too many water pre-heaters in the tertiary loop. The system is complex and the construction cost is high.

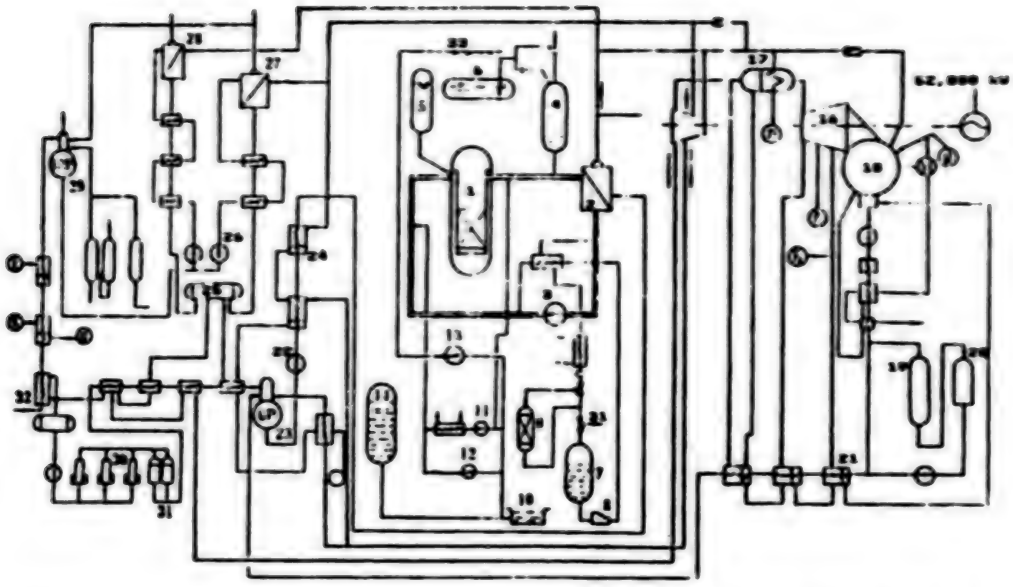

Figure 2. Flowchart of Nuclear Power Plant for Heat and Power*
* P = 98066.5 Pa

Key:

1. Reactor
2. Steam generator
3. Main Pump
4. Pressure stabilizer
5. Safety tank
6. Pressure release box
7. Volume control box
8. Filling pump
9. Resin bed
10. Safety shield pit
11. Reactor shutdown cooling pump
12. Safety pump
13. Sprinkle pump
14. Water exchange tank
15. High pressure turbine
16. Low pressure turbine
17. Steam-water separation re-heater
18. Condenser
19. Hydrogen ion exchanger
20. Mixer
21. Low pressure heater
22. Main water pump
23. High-pressure gas removing pump
24. High-pressure heater
25. Water tank
26. Relay pump
27. Low-pressure evaporator
28. Medium-pressure evaporator
29. Low-pressure de-oxygenator
30. Electromagnetic filter
31. Mixer
32. Tertiary loop water supply
33. Safety shield sprinkle
34. To boron recovery system

Based on the experience in the water-steam-steam process, in order to ensure that there is no radiation in the steam, the plant still uses three loops. To simplify the system, downsize the equipment, and improve reliability and safety, we choose to use the water-water-steam process. Figure 3 shows the major parameters and the flowchart.

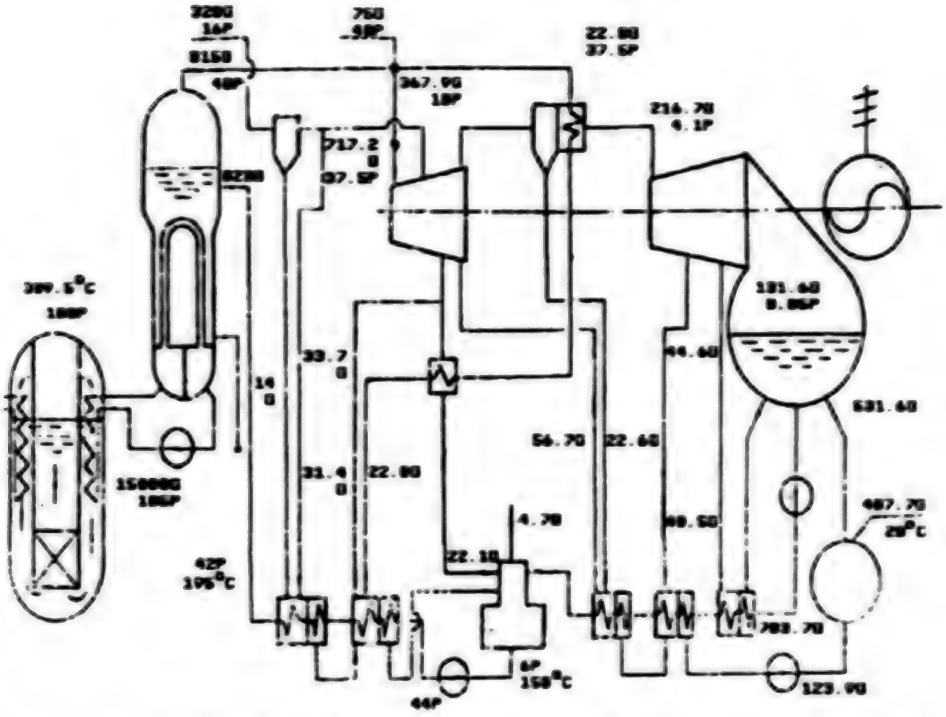

Figure 3. Flowchart for Thermal System of a Small Nuclear Power and Heat Co-Generation Plant*
* G - 1 t/h

The operating pressure and temperature in loops 1, 2, and 3 are selected based on the premise that the tertiary loop must supply saturated steam at 3.92 MPa and by judging the relative size of the heat exchangers in loops 1 and 2 to ascertain that the pressure in loop 1 is 10 MPa. Because the reactor operates at a stable pressure, the average core outlet pressure is 309.5°C, the coolant flow rate is 14,000 t/h, and the core inlet temperature is 289.5°C.

The intermediate loop is a high pressure water loop which operates at 10.5 MPa. This makes it difficult for radiation to leak into the tertiary loop. The intermediate circuit may be a two, three, or four turn loop. In this case, it is temporarily designed as a two turn loop.

The flow is 15,000 t/h. The main pump is a wet spindle pump. The hot end temperature is 280°C and the cold end 258.5°C.

The tertiary loop steam pressure is 4 MPa. There are two U-shaped steam generators. The heat exchange area is 2,666.5 m^2 per unit. The design area is 3,066.5 m^2 with 15 percent excess.

The pipes, valves, and equipment in loops 2 and 3 are made of low alloy steel or carbon steel.

Table 2 shows the effect of the water-water-steam process and the water-steam-steam process on heat exchange. It is not difficult to see that the advantage of the design is that the pressure in the primary loop is significantly reduced while the steam temperature in the tertiary loop remains the same. Furthermore, the temperature difference between loops 2 and 3 is larger, which reduces the size and volume of the major equipment. Consequently, the scale of the plant can be reduced and the construction cost can be lowered.

Table 2. Comparison of the Two Processes

Item		Water-water-steam process	Water-steam-steam process
Reactor power	MW	450	450
Primary loop pressure	MPa	10	15
Primary loop flow	t/h	14,000	12,000
Core outlet temperature	°C	309.5	307.5
Core inlet temperature	°C	289.5	282.5
Loop 3 steam pressure	MPa	4	4
Loop 3 steam temperature	°C	250	250
Temperature difference between loops 1 and 2	°C	30.3	30.6
Temperature difference between loops 2 and 3	°C	22.4	16.2 (Low pressure evaporator) 17.5 (Medium pressure evaporator)
Heat exchanger area in loops 1 and 2	m^2	2,832	3,000
Heat exchanger area in loops 2 and 3	m^2	6,133	12,674

Under the same demand for steam, the water-water-steam process can generate 5,000 kW of power per reactor.

In summary, the water-water-steam process can better insure that the steam in the tertiary loop is radiation free. The heat exchanger is smaller and it operates reliably. The construction cost is low and the thermal

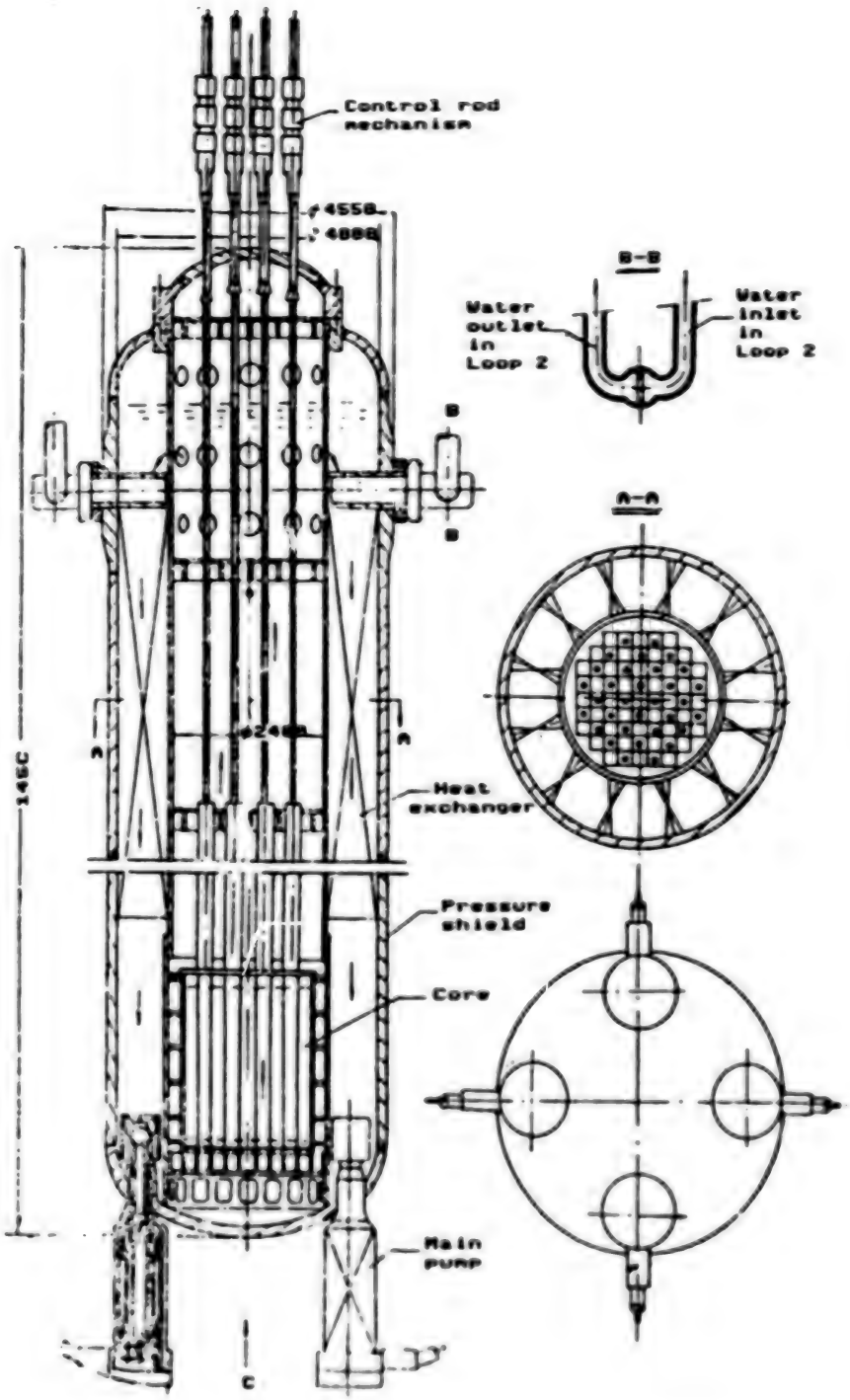

Figure 4. Integrated Pressurized-Water Reactor

efficiency is improved. Therefore, it is appropriate to choose the water-water-steam process for a small heat and power co-generation nuclear plant.

2. Reactor Design

Figure 4 shows an integrated reactor. It consists of a core, 12 U-shaped heat exchanger tubes, 4 main pumps, 32 sets of control rod driving mechanisms, a pressure shield, and other reactor components. The reactor pressure is self-stabilizing. On the average, the core contains 0.1 percent of steam. The steam space at the top of the pressure shield is 12.5 m^3, which is 60 percent larger than that in the pressure stabilizer of an ordinary reactor (of the same power) with a scattered layout.

Figure 5 shows the core layout and the fuel component cross-section. The core consists of 69 fuel components. The diameter of the fuel rod is 8 mm. The average heat flux is 0.27×10^6 kcal/m^2 h and the mean thermal output is 7.9 kW/m. The volumetric power density is 64 kW/ℓ and the mean coolant flow rate is 3.53 m/s. The temperature at the center of UO_2 is 485°C and the maximum temperature is 1,500°C. UO_2 is doped with Gd_2O_3 which is toxic and combustible. Boric acid is not used to control reactivity.

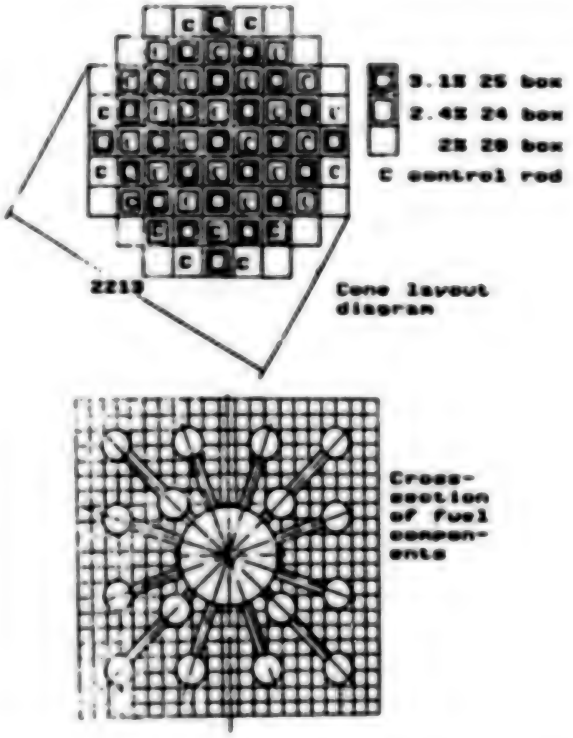

Figure 5. Reactor Core Layout and Fuel Component Cross-Section

Figure 6 shows the structure of the heat exchanger inside the core. Twelve water-water heat exchangers are placed at the upper part of the core. The area of each exchanger is 236 m^2 and the tube is made of OCr18N19Ti. The U-shaped tube is connected to the tank through an in-welded hole inside.

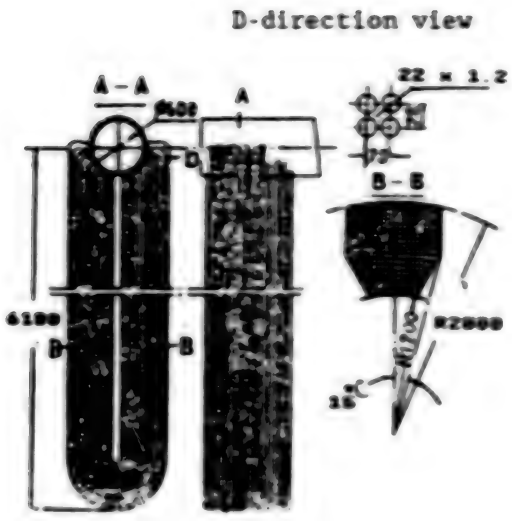

Figure 6. Heat Exchangers Inside Reactor

The vertical distance between the bottom of the heat exchanger tube and the top of the core is 1 m to prevent the secondary loop from becoming seriously radioactive.

The four main pumps are located at the bottom of the pressure shield. It is similar in structure as the main pumps in a boiling water reactor. They are reverse wet spindle pumps. The head pressure of the main pump is 0.13 MPa and the flow rate is 3,500 t/h. The hot pump power is 210 kW. The electrical power for the main pump is rated at 300 kW. Since natural circulation of the coolant in the primary loop is good, the main pump will not be equipped with an idle flywheel.

The largest pipe connecting the reactor to the outside is the drain pipe of the purifying system with an inner diameter of 50 mm. Thus, only small water leak incidents must be considered. The outgoing pipe of the purifying system extends from the upper part of the pressure shield through the heat exchangers in the reactor to the lower part of the shield. Other outlets in the primary loop are higher than the common tank for the heat exchangers. In case there is a small water leak, steam escapes first. In addition, the core is buried under 8 m of water, corresponding to 100 m^3 of water. Therefore, it is highly impossible to expose the core.

3. Primary Loop Auxiliary System

Figure 7 shows the reactor and the primary loop auxiliary system. It mainly consists of a safety injection and sprinkle system, purification system, gas removal system, equipment cooling water system, water and chemical additive makeup system, pressure suppressing system for the

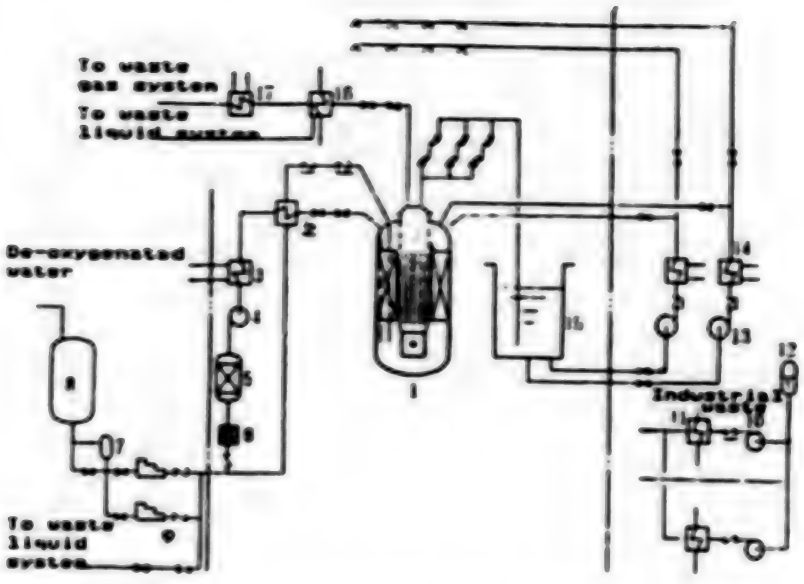

Figure 7. Flowchart of Primary Loop Auxiliary System

Key:

1. Reactor
2. Regenerative heat exchanger
3. Nonregenerative heat exchanger
4. Purifying pump
5. Purification bed
6. Filter
7. Chemical container
8. Makeup water tank
9. Makeup water pump
10. Equipment cooling water pump
11. Equipment cooling heat exchanger
12. Wave box
13. Low-pressure injection and sprinkling pump
14. Recirculating condenser
15. Pressure suppressing pool
16. Condenser
17. Gas condenser

reactor, and its pressure shield, pressure safety system, and sampling and decontamination system.

4. Intermediate Loop and Its Auxiliary System

The system in the secondary loop (Figure 8) is as follows:

(1) The Primary System

The operating pressure in the intermediate loop is 10.5 MPa. It consists of two circuits. Each circuit has a main pump and a steam generator. The main pipe is made of No 20 carbon steel. The outer diameter is 600 mm and the wall thickness is 25 mm. The circulation flow rate is 7,500 t/h and the flow speed is 11.20 m/s. The main pump is a wet spindle pump with a lift of 80 m. Its hot power is 2,040 kW and its cold power is 2,800 kW. Each circuit is equipped with a steam generator. Its heat exchange area

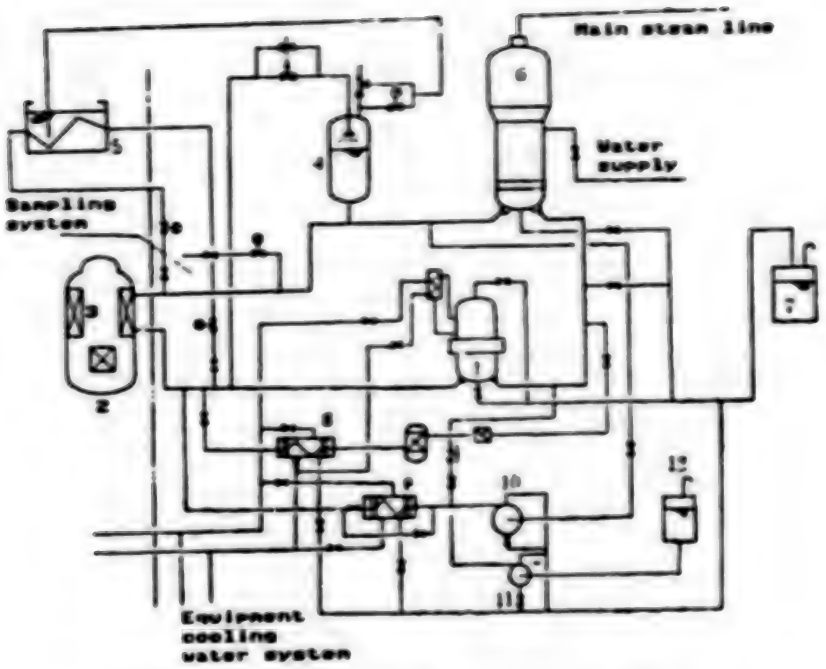

Figure 8. Flowchart of Secondary Loop

Key:

1. Circulating pump
2. Reactor
3. Main heat exchanger
4. Pressure stabilizer
5. Pressure relieving pool
6. Steam generator
7. Water tank
8. Purifying condenser
9. Shutdown condenser
10. Shutdown cooling pump
11. Water makeup pump
12. De-oxygenated water tank

is 3,066.5 m^2, maximum outer diameter is 3.8 m, total height is 17 m and total weight is 180 t. The steam generator is made of 16 MnR steel and the pipes are made of No 20 steel. The construction cost is low (approximately 3 million yuan each). Its structure and parameters are shown in Figure 9.

The heat exchanger in the reactor and the intermediate loop are connected by a tank. Each tank is connected to six heat exchangers. Furthermore, an isolating valve is installed to isolate the heat exchanger from the outside environment in the event of a leak to prevent the escape of radiation.

(2) Pressure Safety System

The pressure safety system consists of a pressure stabilizer and its associated valves and pipes. Because the water in the intermediate loop is radiation free, it may be discharged into the pool.

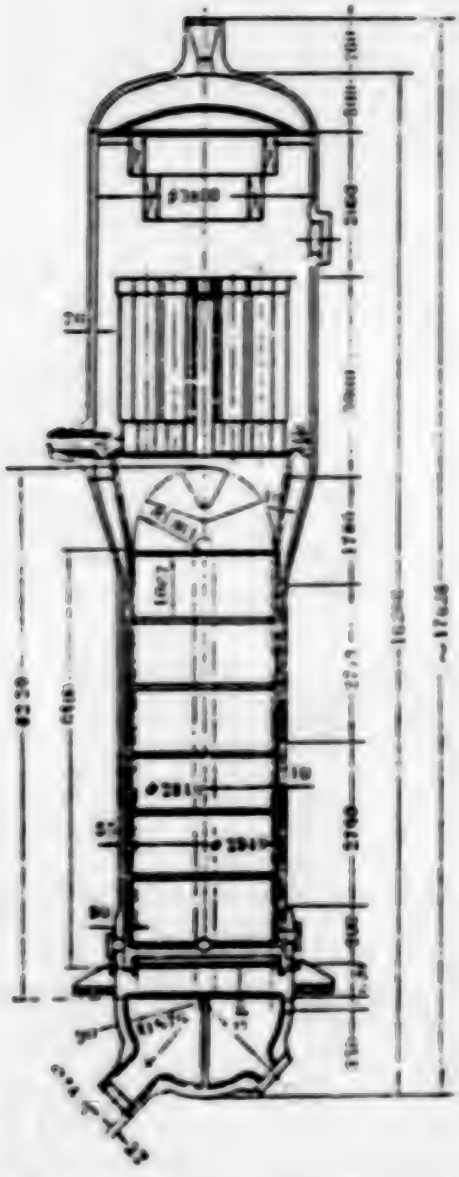

Figure 9. Steam Generator in Loops 2 and 3

(3) Purification System

Each loop is equipped with a purification system. The system is very simple. A continuous flow is established by the head pressure of the pump. The downward flow decreases the temperature, but not the pressure. The flow in the loop is 2-3 percent of the total flow. It is primarily composed of regenerative and nonregenerative heat exchangers, electromagnetic filters, and ion exchangers.

(4) Shutdown Cooling System

Heat is transferred from the primary loop to the water in the heat exchanger in the reactor by natural circulation. The water in the intermediate loop is circulated by the shutdown cooling pump and the heat is transferred through the shutdown condenser.

The equipment cooling water system is shred by the primary loop equipment cooling water system. In addition, it includes a sampling system, a water make-up system, and a drain system.

IV. Reactor Building and Nuclear Annex

Because of the integrated layout of the reactor building, no major pipe fracture incident is possible. Also because the pressure in the primary loop is only 10 MPa, it only requires a pressure suppressing system and a concrete safety shell. The shell is 16 m in inner diameter and 2 m in wall thickness. It is lined with stainless plate. The pressure suppressing pool has 5.2 m of water and each reactor pool has a capacity of 750 m^2. The space on top of the fluid surface is approximately 420 m^2. In addition, the dry part of the safety shell has approximately 1,750 m^3 in volume. Other than tanks and valves connected to the heat exchangers in the reactor, there is major equipment there. The height of the safety shell is approximately 23.2 m. A small room is built at the bottom of the reactor with a passageway to enter the plant for the installation, replacement, and maintenance of the main pump. The passageway has a sealed gate to prevent the escape of radiation. This small room is ventilated.

Both reactors share a piece of fuel replacement equipment. The fuel storage pool and fuel replacement pool are located in between the two safety shells. A 50-ton bridge-type crane is installed at the upper part of the fuel replacement pool to lift up the pressure cap or the core basket.

The reactor building and the fuel plant in combination are 22 m in width and 40 m in length, and they occupy 880 m^2 in area.

The reactor building is equipped with an entrance to lift equipment in and out of the place.

The nuclear annex is equipped with systems for low pressure injection, sprinkling, equipment cooling, water drainage, purification, water make-up, waste resin processing, decontamination, waste gas processing, sampling, and isolation. It also has a physicochemical laboratory, an electrical shop, a mechanical shop, and a room for personnel on duty. The upper part is the ventilation system which occupies approximately 1,638 m^2 of space. The nuclear island covers 2,518 m^2 of area and has 20,000 m^2 of building space. In summary, the scale of the construction of the plant is approximately 33 percent of that of a scattered layout.

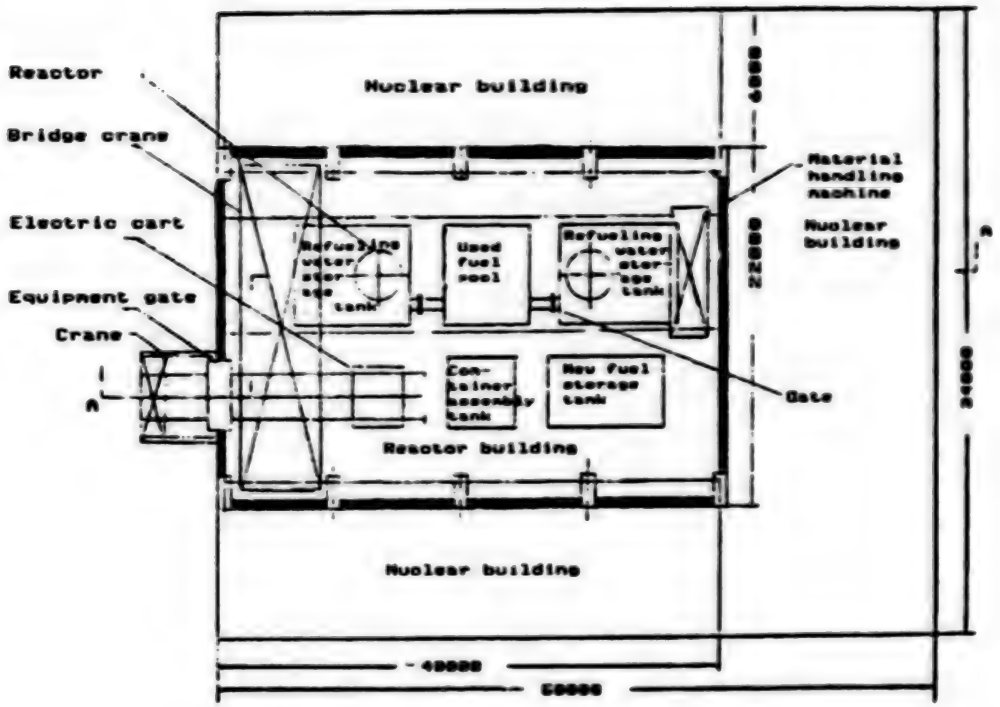

Figure 11. Layout of Nuclear Building

V. Preliminary Analysis of Total Investment, Replacement of Oil Consumption and Economic Benefit

The initial investment is approximately 680 million yuan, 30 percent lower than the original plan. Compared to the original plan, this is a conservative estimate.

The load factor of the heat and power co-generation nuclear plant is estimated to be 80 percent (as compared to 70 percent in the original plan). The major reason is the simplicity of the system. In valves alone we can reduce the number by one-third (nuclear island portion). The pressure in the primary loop is reduced from 15 MPa to 10 MPa. The reliability of the equipment can be significantly improved. Water-water heat exchangers are used between the primary and secondary loops which are far more reliable than water-steam heat exchange type of steam generators. Thus, the calculation of replacement of oil consumption is made based on 7,008 hours of continuous operation per year.

The water pumps in the primary loop consume relatively little power. In hot working conditions, the eight pumps for both reactors use 1,600 kW of electricity. The power consumed by the water pumps in the tertiary loop can be saved by 20 percent. However, the main pumps in the secondary loop consume more power. They more or less cancel each other. Nevertheless,

consume more power. They more or less cancel each other. Nevertheless, some power can be saved in the pressure stabilizer, waste treatment and boron recovery systems, as well as by the high-pressure safety injection pump. Therefore, the power requirement for a two-reactor plant is estimated to be 16.5 MW. Other factors to be taken into account are based on the parameters in the feasibility study report on the heat and power co-generation nuclear plant at Shanghai Petrochemical General Plant (September 1985). The calculation is as follows:

The amount of oil replaced by the power generated is Q_1.

$$Q_1 = (E_1 - E_2)\ Te \times q_1 = 1.45 \times 10^5\ t/a$$

The amount of oil replaced by the low-pressure steam generated is Q_2.

$$Q_2 = [(W_1 \times Te) - W_3] \times (1{,}000\Delta h_1/1000000) \times q_2 = 2.99 \times 10^5\ t/a$$

The amount of oil saved by the medium-pressure steam generated is Q_3.

$$Q_3 = W_2 T_2\ (\Delta h_2/1000) q_2 = 7.10 \times 10^4\ t/a$$

The total amount of oil replaced per year is $Q = Q_1 + Q_2 + Q_3 = 5.15 \times 10^5$ t/a. E_1 is the power generating capacity of the nuclear plant in kW. E_2 is the power consumed by the plant in kW. W_1 = 640 t/h is the amount of low pressure steam supplied to the outside. W_2 = 150 t/h is the amount of medium pressure steam supplied externally. W_3 = 44,000 t/a is the amount of steam used by the plant itself. q_1 = 0.212 kg/kW·h is the oil consumed to generated power. q_2 = 104.8 kg/Mcal is the oil consumed for heating. Δh_1 = 642.1 kcal/kg is the enthalpy rise in the low pressure steam and Δh_2 = 645.1 kcal/kg is the enthalpy rise in the medium pressure steam.

Since q_1 and q_2 are fairly advanced in China, the oil replacement figure is very conservative.

The economics of the small heat and power co-/generation nuclear plant is briefly described in the following:

(1) Heat and Power Costs

Based on the facts that the cost is 70 to 50 yuan per ton, the thermal value is 4,800 kcal/kg, the price of oil is 150 yuan per ton, and the fuel cost is estimated by assuming one-third of the total nuclear fuel loaded can operate at full capacity for 7,008 hours (load factor at 80 percent), the total costs and power generating costs of heat and power co-generation nuclear plants at various capacities are shown in Table 3. We can see that only when the price of high grade is reduced to 50 yuan per ton that it is equivalent to nuclear power. Considering the fact that the price of uranium is falling and the cost of coal is rising, it is more economical to run a nuclear plant.

Table 3. Comparison of Costs of Three Types of Heat and Power Co-Generation Plants (at 450 x 2 MW Thermal Power)

Item	Nuclear plant	Coal plant 70 yuan/t	Coal plant 50 yuan/t	Oil plant
Total cost, 10^4 yuan/a	7,978	10,309	7,976.4	9,583
Fuel, 10^4 yuan/a	3,610	6,064	4,331.4	7,674
Basic depreciation, 10^4 yuan/a	2,563	1,955	1,955	794
Maintenance, 10^4 yuan/a	905	690	690	395
Other expenses, 10^4 yuan/a	900	1,000	1,000	720
Heat cost, yuan/10^6 kcal	17	17	17	17
Power cost, cents/kWh	2.42 (gross) 2.83 (net)	5.34 6.24	2.416 2.83	4.43 5.20

(2) Return of Capital

Production cost per year is 7.98x 10^7 yuan. It replaces 5.15 x 10^4 tons of oil. Based on the price of high grade oil, it corresponds to 2.37 x 10^8 yuan. The difference is 1.57 x 10^8 yuan.

(3) Thermal Efficiency

The thermal efficiency of a large nuclear plant is approximately 33 percent. The thermal efficiency of this plant is 80 percent.

In conclusion, the small heat and power co-generation nuclear plant is economically viable.

VI. Characteristic and Prospect of the Plan

(1) The reactor is a self-stabilizing integrated pressurized-water reactor.

(2) The reactor operates at low pressure, low core power density and low fuel temperature. The primary loop operates at a high mean temperature. Thus, it is possible to ensure safety and economical steam parameters. Under the condition that the pressure in the primary loop is 10 MPa, the steam in the tertiary loop can reach 4 MPa. The thermal efficiency is approximately 80 percent.

(3) A water-water-steam process is employed to improve the reliability of the heat exchangers in the reactor. In addition, the pressure in the secondary loop is higher than that in the primary loop to prevent radioactivity in the primary loop from leaking into the tertiary loop. The heat exchange for a water-water-steam system is better than that for a water-steam-steam system. It also reduces the size of the evaporators and the associated plant building.

(4) The reactor and the primary loop are integrated. The inner diameter of the safety containment s only 16 m. Thus, the reactor building is reduced to a minimum. The nuclear island is only 2,518 m^2 in area, which is 33 percent of that in a scattered design.

(5) Because of the small building size, the amount of cement and steel required is greatly reduced. Consequently, the construction cost is reduced by 200 million yuan. It replaces over 500,000 tons of oil per year. It is expected that the capital can be returned in approximately 6 years.

(6) The system is inherently safe and reliable. Because approximately 15 percent of the heat can be carried out by the natural circulation of the coolant after the main pumps are shut off, core melt-down will not occur due to loss of power. The intermediate loop is a high pressure water loop which makes it difficult for radiation to leak into the tertiary loop. The system is simple and the number of valves and pumps is significantly reduced. Therefore, it is less probable to have an incident. It uses water-water heat exchangers in the reactor which are more reliable than steam generators. All these factors can decrease the number of unplanned shutdowns.

(7) Due to its inherent high safety, it is possible to build it near a city or a large industrial site with a double layer safety shell.

(8) The reactor and the primary loop can be manufactured and assembled at the factory. The amount of work involved in on-site installation, welding, and testing is less. The scale of the construction of the safety shell and the nuclear and non-nuclear islands is relatively small. It only takes 5 years to complete a twin reactor plant.

(9) The shape of the plant buildings is simple and easy to build. The construction cycle is reduced.

Table 4 compares the major specification of an integrated reactor to those of a circulation type pressurized water reactor. The data in the table demonstrate that the design can meet the basic requirements of the nuclear plant.

In conclusion, a small heat and power co-generation nuclear plant is economically competitive. Based on the requirements of more than 20 potential steam users, it is more appropriate to build 400-600 MW reactors.

Table 4. Comparison of Major Performance Characteristics

No	Item		Integrated design	Scattered layout
1	Reactor power	MW	450 x 2	450 x 2
2	Steam generated	t/h	75 x 2 (medium pressure) 320 x 2 (low pressure)	75 x 2 (medium pressure) 320 x 2 (low pressure)
3	Power generated	kW	56947 x 2	52000 x 2
4	Thermal efficiency	%	- 80	79.15
5	Load factor	%	80	70
6	Oil replacement	10^4 yuan/a	51.455	43.6
7	Primary loop operating pressure	MPa	10	15
8	Safety shell id/od	m/m	16/20	29/33.30
9	Nuclear island area	m^2	2,518	7,884
10	Nuclear island construction area/volume	m^2/m^3	20,000/140,000	23,320/353,185
11	Regular island area	m^2	6,000	8,522.7
12	Regular island construction area/volume	m^2/m^3	22,800/190,000	31,728/229,808
13	Total investment	10^8 yuan	6.80	8.80
14	Construction cycle	a	5	6-7
15	Worst incident		drain pipe (ϕ50) fracture	main pipe (ϕ510) fracture

A heat and power co-generation nuclear plant should focus on heat. The amount of power generated is determined by the heat requirement. Power generation should not be very high in proportion to avoid the high cost of steam turbines. If heat is primary and power is secondary, it is more appropriate to adopt a water-water steam flow process. In the choice of reactor, either pressurized and boiling water reactors may be used. However, a pressurized water reactor should be preferred in order to raise

the temperature to produce steam in the tertiary loop for heating. An integrated layout and forced circulation should be adopted for the reactor and the primary loop. This is more compact than a natural circulation boiling water reactor. Figure 12 shows a 640 MW self-stabilizing pressurized reactor. The inner diameter of the pressure shell is 4.5 m, the total height is 16 m and the total weight is approximately 320 tons. A natural circulation boiling water reactor (with heat exchangers inside the reactor) with a comparable pressure shell is only around 450 MW. Based on the steam requirements of the chemical industries in China, the operating pressure of the reactor should be 10 MPa. Therefore, the following conclusions are derived.

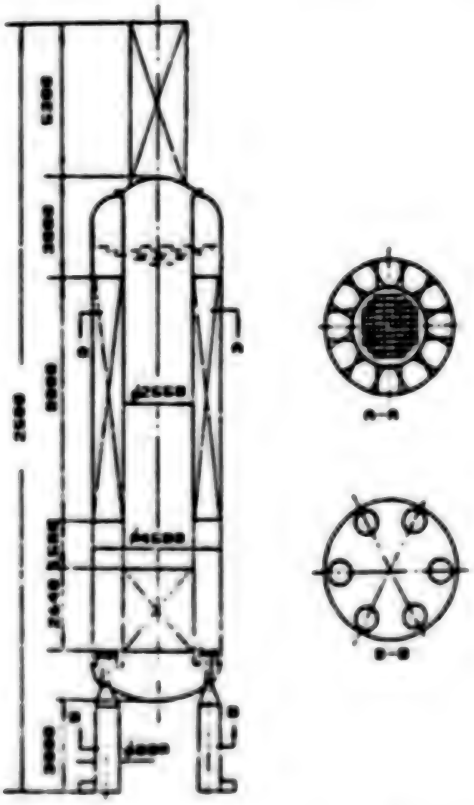

Figure 12. 640 MW Integrated Self-Stabilizing Pressurized-Water Reactor

An integrated, self-stabilizing, forced circulation pressurized-water reactor should be chosen for a small heat and power co-generation nuclear plant. The reactor operating pressure is 10 MPa. The power per reactor is 400-600 MW and the maximum power is 1,000 MW. The primary process is water-water-steam and the amount of power is determined by the steam demand. Boric acid is eliminated to simplify the system. This plan is also applicable to a small nuclear power plant. However, the heat exchangers in the reactor would be replaced by steam generators. If the steam-water separator is placed outside the reactor, then the schematic

diagram of the system becomes Figure 13. Under the condition that the structural dimensions and parameters remain unchanged, the secondary loop produces saturated steam at 44-60 atmospheric pressure.

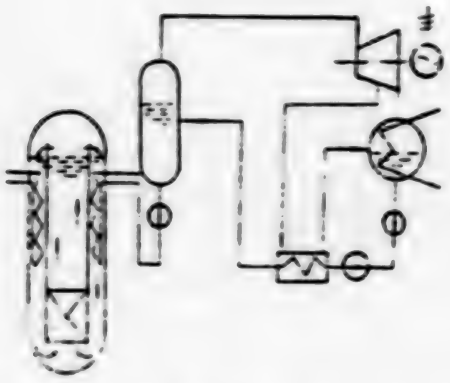

Figure 13. Schematic Diagram for a Nuclear Power Plant

This plan may also be applied to supply heat to cities and towns. With the same reactor and auxiliary system, it becomes a nuclear heat generating plant by reducing the operating pressure and the temperature and by replacing the steam generator with a heat exchanger in the tertiary loop. It does not require any additional study and experimentation.

Of course, this plan can also be used for seawater desalination and power generation. It only requires a modification of the flow process.

The advantages and disadvantages of natural and forced circulation will be investigated further. The driving mechanism of the control rods will be modified. The use of a high conversion ratio reactor in a small plant will also be investigated.

The basic investment for a small 200 MW nuclear plant can be controlled within 400 million yuan. It can be completed in 4 years. The majority of the equipment can be manufactured in China. Moreover, it can meet the basic requirements of heat and power co-generation and urban heating.

In summary, this type of a small heat and power co-generation nuclear plant can become an economical, safe, and clean energy source for cities and large industries in the future. Its initial investment is low, the constructing period is short, the range of applications is wide, and the prospect is bright. It should have a role in the development of energy resources in China.

12553/9365

CORE POWER DISTRIBUTION ANALYSIS FOR QINSHAN 300 MWe PWR PLANT

40090062a Beijing HE KEXUE YU GONGCHENG [CHINESE JOURNAL OF NUCLEAR SCIENCE AND ENGINEERING] in Chinese Vol 7 No 2, Jun 87 pp 97-107

[English abstract of article by Tang Bowan [0781 0130 3834], et al., of Shanghai Nuclear Engineering Research and Design Institute]

[Text] The objectives and significance of core power distribution analysis are discussed in this article. The factors affecting PWR core power distribution are detailed, and many kinds of core power distribution methods are investigated. The designed core power distribution for the Qinshan 300 MWe PWR plant has been obtained as follows: nuclear hot channel factor $F_q^N \leq 2.50$; nuclear enthalpy rise hot channel factor $F_{\Delta H}^N \leq 1.58$. In addition, a comparison between the designed power distribution of the Qinshan 300 MWe PWR and similar PWRs abroad is presented.

9717

MIRROR FUSION BREEDER CONCEPTUAL DESIGN

40090062b Beijing HE KEXUE YU GONGCHENG [CHINESE JOURNAL OF NUCLEAR SCIENCE AND ENGINEERING] in Chinese Vol 7 No 2, Jun 87 pp 164-173

[English abstract of article by Huang Jinhua [7806 6930 5478], et al., of Southwestern Institute of Physics]

[Text] A mirror fusion breeder, CHD, has been designed to provide plenty of nuclear fuel for light water reactors as a means of meeting the need for rapid development of nuclear power in the first half of the next century. This reactor can support more than 10 LWRs of equal scale in power, with the fuel enriched directly in the CHD without reprocessing. The CHD consists of end plugs and a central cell. The leakage of plasma from the central cell is plugged by an ambipolar electrostatic potential combined with a high magnetic field, and an octopole field is applied to stabilize the plasma. The central cell, which is 128 meters long, consists of 40 identical modules. Measures have been taken to flatten the power density distribution in the blanket so that fission is suppressed in the region close to the plasma, thereby effectively improving the fuel production. Although the tritium inventory in the reactor is very low, special materials and designs must be developed to reduce the permeation of tritium through the coolant pipes. The cost of electricity from the system, consisting of 11 LWR plants and one fusion breeder, is predicted to be 1.05 times that from a traditional LWR plant. This figure does not take into consideration the cost of the CHD or its support ratio.

9717

AIR FORCE ADOPTS NETWORKED MANAGEMENT SYSTEM

40080071a Beijing JISUANJI SHIJIE [CHINA COMPUTERWORLD] in Chinese 20 Jan 88 p 2

[Article: "The Air Force Enhances Its Efforts in Ordnance Automation and Management as It Builds a Comprehensive Networked Management System"]

[Text] Recently the PLA "Ordnance Tasking Management Automation System" successfully passed its evaluation. This system was jointly developed by the Jiangsu Computer Institute and the Air Force Ordnance Unit.

This system is a multi-level, hierarchical, multi-function microcomputer system for managing information and is based upon local-area networks [LAN's] and telecommunications networks. This system rather systematically covers all Air Force ordnance tasking, and its four major components are: an Ordnance Unit LAN, a central database, a telecommunications network, and management software.

The LAN is based on Ethernet and can handle hierarchical tasking management at the three levels, which are: the unit commander's office, the office of project financing, and the office of each particular task, as well as the sharing of the central database. The management software contains 11 subsystems and 2 independent modules. It can do management coordination of the various areas of equipment, materials, aircraft ammunition, warehouses, factories, repair facilities, troop units, scientific and technical training, finances, organizational budget proposals, archive materials, and information for the commander, and it can also effectively handle the processing of office tasking and of communications with the two modules for office tasking and communications, respectively. The successful development of this system has provided powerful support for the modernization of Air Force ordnance management.

12586/6091

ANNOUNCEMENT OF CAD SOFTWARE FOR PLANNING NETWORK CHARTS

40080071b Beijing JISUANJI SHIJIE [CHINA COMPUTERWORLD] in Chinese 20 Jan 88 p 2

[Article by Peng Jianhua [1756 1696 5478]: "Planning Network Chart Software for CAD and Drafting Methods Has Been Announced"]

[Text] Ning Xuanxi [1337 1357 3556] and Lei Weizhong [7191 5898 0022] of the Nanjing Aeronautics Academy have successfully developed a package of CAD and plotting methods software for planning network charts, and this software has recently passed the provincial technical evaluation.

"Tabular design methods for planning network charts" is a new method that does not use plotting for designing network charts. Based upon job analysis tables or single-code-name network charts, it arranges each job into a list according to definite rules. Then it uses a logical algorithm to calculate the initial and terminal node serial numbers for each job. The "Program for CAD and Plotting for Planning Network Charts" is applied network chart design and plotting software based upon a listing algorithm and developed on an IBM PC/XT. The entire program was written in high level BASIC, and can automatically convert job analysis tables or single-code-name network charts into optimal dual-code-name network charts, completely replacing efforts at the manual design and plotting of network charts.

The main functions of this program are: it designs network charts in accordance with the sequential ordering of jobs as determined by job analysis tables or a single code name, calculating the correct serial number for each node in the network chart; indicates logical errors in the input of data, and increases or revises the originally entered data; calculates the time parameters for networks, indicating key routes; uses three different plotting modes for the automatic topology for nodes, as well as displaying the network chart on the screen; permits audio-visual-style interactive editing of the network charts; provides the working network charts with print-time parameters, printer-output graphics, and a choice between using or not using plotter drafting time coordinates; and it provides Chinese-language prompts for everything for the convenience of planning personnel. It only takes about 12 minutes for it to design a project network chart for 74 jobs (of which 10 minutes, 30 seconds is printing time). With an IBM PC/XT (512K RAM), where maximum look-ahead for the number of jobs is 8, a project network chart can

be designed that has 150 jobs. Experts who took part in the evaluation felt that the design philosophy of this software is innovative, and that it has reached the domestic state-of-the-art in the categories of logical design and screen display. The software has been rationally designed, has many features, performs quite well, is convenient to use, is suitable for microcomputers, and is worth disseminating for wider use.

12586/6091

LATEST DEVELOPMENTS IN COMPUTER NETWORKS OUTLINED

40080071c Beijing JISUANJI SHIJIE [CHINA COMPUTERWORLD] in Chinese 20 Jan 88 pp 5-6

[Article by Ju Jiubin [7263 0046 3453], Department of Computer Sciences, Jilin University: "The Current Situation Regarding Developments in Computer Networks"]

[Excerpt] At present, the primary LAN [local area network] products being imported to China are various implementations of CSMA/CD [carrier sense, multiple access with collision detection] (or CA) bus networks (Ethernet), as well as products such as the token-passing LAN (PLAN), and all are compatible with Chinese characters. The data transmission rates employed in these LAN's are around 1 million bits per second (bps), with the actual number of nodes at from 5 to 40. In addition to this kind of system, we have also imported OpenNet and Decnet.

China has independently developed some LAN's. These are currently domestic products for Ethernet and Omninet. The Cambridge Ring has also been successfully developed, and can be produced in small quantities. The new international standard IEEE 8802/7 (time-sliced ring) was issued in 1987, and the Cambridge Ring complies with this standard.

We have built several systems using the LAN's just described, the majority of which are used for office automation and the management of various businesses and enterprises. A small number are issued for scholastic scientific research and teaching. We have built preliminary remote network systems for some qualified systems (such as for planning commissions, banks, units, and railways).

We have also done some research on interconnecting LAN's with LAN's and LAN's with WAN's [wide-area networks] domestically. On certain networks we have also had success with optical cables. The IBM PC series has been the primary computer connected to LAN's, but higher-grade microcomputers and even mainframes can participate in networks through the RS-232C serial interface. High-speed exchange of data through direct parallel connections to LAN's is still rare. Aspects of software development include the implementation of point-to-point communication, file access, electronic mail, printers, and the sharing of disks. Remote process calls, and the facilities for other

network operating systems are still at the development stage. We have also begun research on network security.

Chinese computer networks, and especially LAN's, have begun to be widely disseminated throughout China. But whether we are speaking of quantities or of scale, there is still quite a gap between us and other countries in the development of high-level software and extensive applications, and much more must be done.

12586/6091

TIANJIN'S HETEROGENOUS COMPUTER NETWORK SYSTEM

40080071d Beijing JISUANJI SHIJIE [CHINA COMPUTERWORLD] in Chinese 27 Jan 88 p 10

[Article by Li Jun [7787 4596] and Chang Jiang [7022 3068]: "Tianjin's PLAN 5000 Networking System Development Project Enables Different Chinese-Character Systems and Different Types of Computers To Join a Network"]

[Text] The PLAN 5000 high-level microcomputer local-area network system development project has passed its municipal technical evaluation. This network was specifically developed for domestic use by the Tianjin Institute of Computer Applied Technology, and was developed in accordance with user needs. Through systematic development, different Chinese-character systems were built into this network, the printing environment is shared, and the database and communications environments are also shared. Now at a practical level, this system provides an excellent support environment for the development of user applications.

The features of this system development are as follows:

1. The three domestically most popular Chinese-character systems were built into the network. These included CCDOS software Chinese characters, the Associative Chinese Character Card, and the Great Wall 0520CH firmware Chinese characters. Problems were also resolved regarding the networking of various microcomputers of different types, so that in addition to the IBM series of micros and their compatibles, the IBM PS-2/30 and the Compaq 386 and Leo 386 can also be networked.

2. A dBASE III Plus multi-user shared database system has been developed. This system can be used simultaneously by different micros on the system and through different Chinese character environments.

3. The PLAN 5000 network-level protocol software was thoroughly analyzed.

The Tianjin Municipal Institute of Computer Applied Technology has received unanimous praise from experts and representatives for the systems development of PLAN 5000. After expert testing and evaluation, they felt the systems development effort had strengthened the power of the network, had expanded the scope of applications for the network, and had reached the domestic state-of-the-art in technology and performance.

12586/6091

IMPROVED DECnet-DOS COMMUNICATION SYSTEM

40080071e Beijing JISUANJI SHIJIE [CHINA COMPUTERWORLD] in Chinese 27 Jan 88 p 11

[Article by Fei Zhang [6316 1728]: "Results Achieved From the Analysis and Transformation of DECnet-DOS"]

[Text] After arduous and meticulous work, a certain Air Force institute in China has recently completed a full-scale analysis and series of modifications for DECnet-DOS 1.0. This has laid an excellent foundation for the final development of software using DECnet-DOS and the DECnet network. They first fully analyzed all the driver routines and applications programs for DECnet-DOS 1.0, from which they clarified the implementation principles of DECnet-DOS, the control structures and data structures of each routine, and the principle working units, at the same time discovering some errors of implementation in the original version.

On this basis, they connected the 3Com Ethernet with the DEC network. The method of implementation was to allow a PC with RS-232C interface on any line to be a route node, and any workstation on Ethernet just needs to install and operate the modified software in order to become a terminal on the DEC network through the route node. This accomplishes the features of the original DECnet-DOS, and can as well achieve communication between tasks with any user on the network, as well as the sharing of resources.

They have also successfully developed real-time terminal interaction routines. Because the DECnet-DOS implementation environment does not allow concurrent dispatching, this prevents other nodes from initiating the copying of files to their node. To this end, the application program TLK was added, the function of which is the same as the TLK function on DECnet networks.

Chinese-character processing was added to DECnet-DOS. This primarily accomplishes the effect of bringing Chinese characters to the SETHOST application program, and allows the terminal node to directly use the Chinese-character resources on the host node.

Finally, they resolved the connection of the DECnet-DOS with DECnet networks. DECnet-DOS is itself one implementation of the DNA [digital network architecture] of the DECnet network, but the majority of users in China are

running the Type III network, and it was for them that DECnet-DOS was modified, allowing Type III networks to connect through nodes and the PC's to be networked.

In this analysis and modification effort, more than 410K of code files and 81K of data files were disassembled, and a report on the analysis was written.

This series of achievements recently passed a technical evaluation by experts in Beijing. It received a high degree of praise and affirmation from these experts.

12586/6091

KSJ-HN2220 MICROCOMPUTERIZED 32-BIT SUPERMINICOMPUTER

[Editorial Report] Beijing JISUANJI SHIJIE [CHINA COMPUTERWORLD] of 3 February 1988 carries on page 1 an announcement of the KSJ-HN2220 microcomputerized 32-bit superminicomputer jointly developed by the Chinese Academy of Sciences' (CAS) Shenyang Computer Technology Institute and the Huanan (South China) Computer Company and jointly evaluated by the CAS and the Ministry of Electronics Industry (see JPRS-CST-88-006, 5 Apr 88, pp 98-99). The article includes the following passage:

"The QU bus converter board and various disk- and tape-control boards developed for the new system by the manufacturing unit completely conform to the appropriate international technical conventions and protocols, so the KSJ-HN2220 computer can be connected to imported CAD workstation hardware, and can handle transplanted system software and CAD software packages, creating broad applications for this computer. The applications system, also developed for this computer by the manufacturer, has permitted the first domestic realization--using the KSJ-HN2220 as the main computer--of a perfected practical network: the workstation system."

CSO 40080098

STRUCTURED ADDITION ANTIALIASING ZOOM ALGORITHM FOR BINARY IMAGES

40[illegible]a Aeiji-; YICHANJI XUEBAO [CHINESE JOURNAL OF COMPUTERS] in Chinese Vol 11 No 1, Jan 88 pp 1-12

Article by Zhang Zhiji [6774 5347 3444] [Institute of Computer Technology, Chinese Academy of Sciences]

[Abstract] A structured pixel addition method is presented and a new high-speed antialiasing zoom algorithm for binary images is constructed. Described in vector Boolean algebra and Boolean matrix, the algorithm can process any (0, 1) matrix images and have arbitrary antialiasing and zoom performed in one pass. To complete a MxM (0, 1) matrix, the complexity of the logic operations is O MxM in serial or xMxM in parallel. [Received 13 Jan 87].

[illegible]

NEW SCAN-LINE ALGORITHM FOR COMPUTER 3-D REALISTIC GRAPHICS DISPLAY

40090063b Beijing JISUANJI XUEBAO [CHINESE JOURNAL OF COMPUTERS] in Chinese Vol 11 No 1, Jan 88 pp 22-30

Article by Zheng Zhuojia [6774 0587 0857], Wu Youshou and Li Shuliang (Tsinghua University)

[Abstract] Based on the combination of scan-line and priority algorithms, an improved scan-line algorithm for computer three-dimensional (3-D) realistic graphics displaying is presented. In this approach, sorting is performed according to YF order, and the priority criteria are simple and normalized; therefore, the spatial-correlation can be used more effectively. Some pictures of 3-D graphics produced with the algorithm are also given. (Received 11 July 86).

/12223

TERNARY MIXED-MODE PLANAR CELLULAR ARRAY, ITS PROPERTIES

40090063c Beijing JISUANJI XUEBAO [CHINESE JOURNAL OF COMPUTERS] in Chinese Vol 11, No 1 Jan 88 pp 31-42

Article by Han Shu [7281 2562] (Zhengzhou University) and Gu Weixin [7357 4429 1800] (Harbin Institute of Technology)

[Abstract] In this paper a ternary mixed-mode planar cellular array is proposed. Its properties are studied. The advantages of this type of cellular array compared with others are: more regular in design, simpler in layout, and easier to realize in designing universal logic cellular arrays. Moreover, it can be easily generalized to n-valued (n≥2) arrays. Its applications and the realization of basic cells are also discussed.
(Received 4 July 86).

/12223

NEW APPROACH TO STEREO IMAGE MATCHING

40090065 Beijing DIANZI XUEBAO [ACTA ELECTRONICA SINICA] in Chinese, Vol 16 No 1, Jan 88 p 6

[Article by Li Jincheng [2621 6930 2052] and Yuan Baozong [5913 0202 1350] (Northern Jiaotong University, Beijing)]

[Abstract] Depth perspective is important to image analysis. Stereo vision provides a convenient and direct way to obtain 3-D scene depth. The key problem in stereo vision is stereo image matching. A feature-based sequential stereo image-matching method is discussed. Unlike previous methods, this method uses five stereo image sequences. A relaxation algorithm is used to get unique match. (Received Jul 86, revised Oct 86).

COMPUTER SIMULATION OF LINEAR FREQUENCY-MODULATION-SIGNAL DIGITAL MATCHED FILTER FOR NON-SINGLE-POINT TARGETS

40090065 Beijing DIANZI XUEBAO [ACTA ELECTRONICA SINICA] in Chinese, Vol 16 No 1, Jan 88 pp 17-18

[Article by Su Yanguang [4725 0917 0342] and Shi Xingrong [0670 2622 2837] (China University of Science & Technology, Hefei, Anhui)]

[Abstract] A single-point target has been dealt with for earlier radars. As high target resolution is required for today's radars, the target can be regarded as a set of sequential points rather than a single point in some applications. In this paper the linear FM-signal digital matched filter for non-single-point targets is investigated and its results of rectangular window weighting are compared with those of Hamming window weighting. It shows, due to the effect of point-spread function, that the output of the matched filter could not express the target's reflected coefficients correctly. A post-processing algorithm to correct this effect and its simulation results are given. (Received Mar 86, revised Nov 86).

CHANNEL ORDERING, ROUTING FOR VLSI BUILDING-BLOCK LAYOUT

40090065 Beijing DIANZI XUEBAO [ACTA ELECTRONICA SINICA] in Chinese, Vol 16 No 1, Jan 88 p 53

[Article by Chen Lidong [7115 4539 2639] and Zhang Liangzhen [1728 5328 7201] (Anhui University) and Zhuang Wenjun [8369 2429 0689] (Institute of Semiconductors, Chinese Academy of Sciences)]

[Abstract] An efficient method of channel ordering and routing for building-block layout is presented in this paper. The concept of T-shaped constraint graph and the idea of channel classification are introduced. The cycles in the channel precedence constraints are broken by introducing a kind of channel called a predetermined channel based on the routing of 3-sided channels. On the basis of these concepts, an algorithm for channel ordering and routing is described. The algorithm is implemented in FORTRAN-77 on a UNIVAC 1100/10 with satisfactory results. (Received Dec 86, revised Apr 87).

FIXED-THRESHOLD MULTI-ACQUISITION PROBABILITY FOR FRAME SYNCHRONIZATION

40090065 Beijing DIANZI XUEBAO [ACTA ELECTRONICA SINICA] in Chinese, Vol 16 No 1, Jan 88 p 87

[Article by Sui Houtang [7131 0624 2768] (Space Science & Technology Center, CAS)]

[Abstract] In this paper, a frame synchronization multi-acquisition method is presented. The multi-acquisition probability expression for a fixed threshold is obtained. By means of theoretical analysis and computer simulation, it can be shown that on the basis of correct selection of the number of fault tolerance, the multi-acquisition probability can approach a maximum value and with an increasing number of times of acquisition, the maximum probability will also be increased, and the corresponding synchronization pattern length will be decreased. Using the multi-acquisition method presented with the synchronization length given, the frame synchronization can be achieved with probability of one under serious noise level. (Received Feb 86, revised May 87).

ELECTROSTATIC GYRO-PENIOTRON

40090065 Beijing DIANZI XUEBAO [ACTA ELECTRONICA SINICA] in Chinese, Vol 16 No 1, Jan 88 p 93

[Article by Zhang Shichang [1728 0013 2490] (Chengdu Institute of Radio Engineering)]

[Abstract] A gyro-peniotron [a millimeter-wave device] effected in a centrifugal electrostatic focusing system is proposed. The perturbation solution of 3-D model for large-orbit relativistic E-beam under the action

of HF field of TEmn or TMmn modes is derived. The dispersion equation and the analytic expression of normalized growth rate are obtained. Numerical analysis is carried out and it is found that the influence of the axial displacement of an electron should not be ignored. (Received Jan 86, revised Mar 87.)

EXTRA NOISE, METHODS TO REPRESS IT IN AGILE RADAR

40090065 Beijing DIANZI XUEBAO [ACTA ELECTRONICA SINICA] in Chinese Vol 16 No 1, Jan 88 p 98

[Article by Luan Defu [2940 1795 1381] and Zhou Guangyuan [0719 1639 0337] (Qinghua University, Beijing) and Song Hongji [1345 7703 7535] (Changhong Machine Factory, Mianyang, Sichuan)]

[Abstract] The principle of converting FM noise of the local oscillator into AM noise of the receiver due to the discrimination effect in agile radar is discussed. The phase-shifting discrimination and its effect on the receiver noise in the radar with a fast AFC subsystem are analyzed and formulated. The methods to minimize the extra FM noise of LO and the discrimination effect are proposed so that the additional receiver noise can be effectively repressed. The practical results applied to several radars have proved these methods to be successful. (Received Feb 86, revised Mar 87.)

STUDY ON SOME PROBLEMS IN MEASUREMENT OF DISPERSION OF MONOMODE OPTICAL FIBER BY PHASE-SHIFT METHOD

40090065 Beijing DIANZI XUEBAO [ACTA ELECTRONICA SINICA] in Chinese Vol 16 No 1, Jan 88 p 124

[Article by Zhou Wenjun [0719 2429 0193] (Wuhan Research Institute of Posts & Telecommunications, Hubei)

[Abstract] The effects of the factors in measuring thedispersion of a monomode optical fiber by phase-shift method are analyzed theoretically, and a new ideal to improve the minimum measurable signal-to-noise ratio is presented. Experimentally, the minimum measurable S/N ratio is achieved to lower than 20dB(E) and the measurable dynamic range is enlarged to over 20dB(O). (Received May 86, revised Nov 86.)

/9604

STUDIES OF INTERBAND MAGNETOREFLECTION SPECTRA, BAND PARAMETERS IN NARROW-GAP SEMICONDUCTOR $Pb_{1-x}Sn_xTe$

40090064 Beijing BANDAOTI XUEBAO [CHINESE JOURNAL OF SEMICONDUCTORS] in Chinese Vol 9 No 1, Jan 88 p 14

[Article by Gan Shu [3927 5289] and Chen Chenjia [7115 6591 0857], Department of Physics, Beijing University, and Wang Weiqing [3769 4850 0615], North China Research Institute of Electro-Optics]

[Abstract] The interband magnetoreflection spectra of n-type $Pb_{1-x}Sn_xTe$ single crystals have been studied for the first time for alloy composition x=0.2 in temperature range 10-50 K with Faraday configuration which is induced by CW CO_2 laser. The peak positions correspond to transitions from Landau levels in the L_1^6 valence band to the L_3^6 conduction band.

The peak positions are fit for the transition energies calculated using the model of k · p perturbation theory. The band parameters such as band-edge effective mass, g factor, anisotropy factor and energy gap have been obtained. It is found that the contribution of far-bands to effective mass is considerable, and larger than that to g factor especially for longitudinal effective mass, which would be as large as 30 percent. The conduction-valence bands symmetry is destroyed and anisotropy factor is decreased, which is about 10 for x=0.2 due to far bands interaction.
(Received 13 Feb 87)

COMPUTER SIMULATION FOR CHARACTERISTICS OF CCTS BISTABLE DH LASER AT ELECTRIC INJECTION

40090064 Beijing BANDAOTI XUEBAO [CHINESE JOURNAL OF SEMICONDUCTORS] in Chinese Vol 9 No 1, Jan 88 p 40

[Article by Wang Qiming [3769 0796 2494] and Li Jianmeng [2621 1696 5536], Institute of Semiconductors, Chinese Academy of Sciences, Beijing]

[Abstract] The results of computer simulation for stable characteristics and transient response of a CCTS bistable DH laser which is applied by crosswise light injection or axial injection arereported. The characteristics of light-switching and light-amplification at stable-state, and an output

pulsation of chaos at weak incident light intensity, an approximately single peak with fast damped oscillation at strong light intensity and an ordinary delay process at stronger incident light intensity at transient response are obtained. (Received 25 Sep 86)

COMPUTER SIMULATION FOR CHARACTERISTICS OF CCTS BISTABLE DH LASER AT OPTICAL INJECTION

40090064 Beijing BANDAOTI XUEBAO [CHINESE JOURNAL OF SEMICONDUCTORS] in Chinese Vol 9 No 1, Jan 88 p 47

[Article by Wang Qiming [3769 0796 2494] and Li Jianmeng [2621 1696 5536], Institute of Semiconductors, Chinese Academy of Sciences, Beijing]

[Abstract] The computer simulation for stable characteristics and transient response of a CCTS bistable DH laser at electric injection is reported. The source of producing bistable behaviors and self-pulsation is intrinsic saturable absorber due to non-homogeneous injection currents for this model. Some parameters which affect self-pulsation and bistability are investigated; these parameters with relation to saturable absorber are spontaneous emission factor, input normalized currents J_1, J_2 for gain and absorbed sections, respectively. (Received 10 Sep 86)

PHOTOEMISSION SPECTROSCOPY STUDIES OF Cu-GaAs (110) INTERFACE USING SYNCHROTRON RADIATION

40090064 Beijing BANDAOTI XUEBAO [CHINESE JOURNAL OF SEMICONDUCTORS] in Chinese Vol 9 No 1, Jan 88 p 73

[Article by Pan Shihong [3382 1102 1347], Department of Physics, Nankai University, Tianjin]

[Abstract] The Cu-GaAs (110) interface and Schottky-barrier formation have been studied with synchrotron radiation photoemission spectroscopy for Cu overlayers deposited at room temperature. The evolution of the Ga3d and As3d spectra shows that strong interactions occur between Cu and GaAs substrate during the interface formation. For less than 0.5 monolayer (ML) Cu only rigid band bending was observed, but no interfacial reaction could be appreciated; for Cu more than 1 ML apparent interfacial reaction appeared, by which metallic Ga formed at the interface, and some As segregated on the metal; there were evidences of clustering or island growth of the Cu overlayers observed. Using deconvolution technique it has been found that the interfacial Fermi level lies at about 0.9 eV below the conduction band maximum. The mechanism of the Cu-GaAs (110) interface and Schottky barrier formation is discussed. (Received 19 June 86)

Mn-DOPED-BASE DOUBLE COLLECTION REGIONS InGaAsP/InP HPT

40090064 Beijing BANDAOTI XUEBAO [CHINESE JOURNAL OF SEMICONDUCTORS] in Chinese Vol 9 No 1, Jan 88 p 91

[Article by Li Weidan [2621 4850 2481], Fu Xiaomei and Pan Huizhen, Shanghai Institute of Metallurgy, Chinese Academy of Sciences, Shanghai]

[Abstract] A new structure of double heterojunction phototransistor with two collection regions for high-speed data processing has been proposed. For fabricating such a structure by LPE, manganese has been employed as the p-type dopant of InGaAsP. Using these epi-wafers, mesa HPTs have been fabricated; the typical optical gain is about 144 at 1160 nm incident light and the wavelength response region is between 875 nm and 1277 nm. Transient characteristics of the HPT have been measured with 80 ps Gaussian pulse, and FWHM of the output pulse is 1.20 ns with a rise time of 400 ps.
(Received 31 Oct 86)

EXPERIMENTAL RESULTS FOR CCTS BISTABLE DH LASER UNDER OPTICAL INJECTION

40090064 Beijing BANDAOTI XUEBAO [CHINESE JOURNAL OF SEMICONDUCTORS] in Chinese Vol 9 No 1, Jan 88 p 112

[Article by Wang Qiming [3769 0796 2494], Wu Ronghan [0702 2837 3352], Li Jianmeng [2621 1696 5536] and Wu Hong [0702 3163], Institute of Semiconductors, Chinese Academy of Sciences, Beijing]

[Abstract] Experimental results are reported for a CCTS bistable InGaAsP/InP DH laser under optical injection which produces optical bistability and optical amplification. The bistability of P_{in}-P_{out} for lasers with CW or pulsated operation is shown and some analyses for the results are given.
(Received 25 June 87)

/9604

EXPERIMENTAL INVESTIGATION ON STIMULATED RAMAN SCATTERING IN HIGH-PRESSURE HYDROGEN BY RUBY LASER

40080033 Shanghai YINGYONG JIGUANG [APPLIED LASER] in Chinese Vol 7 No 5, Oct 87 pp 217-220

[Article by Zhang Guangqiu [1728 1639 4428], Xiao Junyong [5135 0193 0516], and Ma Jichun [7456 0679 2504] of the Plasma Physics Institute, Chinese Academy of Sciences, Hefei: "Experimental Research on Stimulated Raman Scattering in Ruby Laser-Pumped High-Pressure Hydrogen"]

[Text] Abstract: This article describes a system for observing stimulated Raman phenomena and discusses experimental results. The laser energy threshold for producing stimulated Raman scattering and the transfer efficiency of each level of scattered light were measured. The results showed that stimulated Raman scattering is a parameter process involving the interaction of multiple waves.

Stimulated Raman scattering is one possible method for obtaining laser light at a specific wavelength. When this technology is combined with a dye laser, for example, it might be possible to obtain laser light at the specific wavelengths required in fusion plasma diagnosis[1-3]. It also is important for studying nonlinear effects in certain media and light parameter processes.

An excitation and measurement system to observe stimulated Raman scattering was designed to meet the need for fusion plasma diagnosis. This article introduces the experimental methods and measurement results, and it analyzes and discusses them.

I. Principles

The mechanism of stimulated Raman scattering is illustrated in Figure 1.

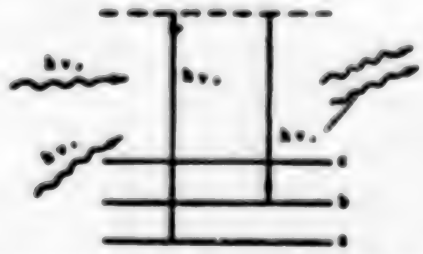

Figure 1. Stimulated Raman Scattering Energy Levels

Two photons fall simultaneously on a single molecule. One photon corresponds to the incident laser frequency v_p and the other corresponds to the frequency after scattering v_s. The scattered light is reflected back-and-forth in the medium. This sort of reflection also can occur in the absence of a resonant cavity. During this process, the laser light loses a photon hv_p, while the scattered light beam gains a photon hv_s and is thereby amplified. The excess energy $hv_p - hv_s = hv_{ba}$ is transferred to the medium. This amplification and transfer process can occur only when the laser energy density P exceeds a certain threshold energy density P_o.

It was assumed that the intensity of polarization in the medium is X and that during high energy density laser incidence, X is no longer a constant quantity but is instead an atomic position y function, thus X = X(y). X(y) was used for a Taylor series expansion near the equilibrium position (y = 0). At a first approximation, the molecular vibration formula can be considered

$$y = y_o \cos(2\pi v_e t)$$

v_e is the vibration frequency. Laser irradiation of the molecules is assumed to be

$$E = \cos(2\pi v_p t)$$

The v_p in the formula is the frequency of the incident laser light.

The electric dipole movement P_e it creates on the molecules is:

$$\begin{aligned} P_e = \chi E = &\left[\chi_0 + \frac{1}{4}\left(\frac{d^2\chi}{dy^2}\right)_0 y_0^2\right] E_0 \cos 2\pi v_p t \\ &+ \frac{1}{2}\left(\frac{d\chi}{dy}\right)_0 y_0 E_0 \cos[2\pi(v_p - v_e)t] \\ &+ \frac{1}{2}\left(\frac{d\chi}{dy}\right)_0 y_0 E_0 \cos]2\pi(v_p + v_e)t] \\ &+ \cdots \end{aligned}$$

The amount of polarization P_e includes components at frequencies $v_p \pm v_e$, $v_p \pm 2v_e$, and so on. The "-" is light at the frequency corresponding to Stokes scattering light, while the "+" is light at the frequency corresponding to anti-Stokes scattering light.

The relationship between the wavelength of the incident light and the scattered light is

$$\lambda_n = [(1/\lambda_1) \pm nv_e]^{-1} \times 10^8 \text{ Å}$$

λ_n is the wavelength of n level light, λ_1 is the wavelength of the incident scattered light, and v_e is the molecular vibration frequency of the medium.

In this experiment, we chose high-pressure hydrogen as the working medium and ruby laser light (λ_i = 6943 Å) as the incident light. The v_e = 4155 cm^{-1} of hydrogen is already known. Thus, we can derive the Stokes and anti-Stokes scattering wavelengths λ_s and λ_{as}.

II. Experiment Systems and Results

The configuration is shown in Figure 2. Monopulse laser light output is produced by using (yinhuajing) [7148 0553 5464] dye to adjust the Q of the ruby laser. The laser beam passes through incident lens 2 and enters the high-pressure hydrogen Raman. The light exiting the Raman chamber includes light at the fundamental frequency and scattered light. Pellin-Broce prismatic decomposition of this light easily provides monochromatic light at different levels. Spots of scattered light at different levels can be obtained at the focal plane of an access lens placed behind the prism (7). The energy of scattered light at different levels can be measured by placing an energy meter fitted with a suitable diaphragm at the focal plane. The reflecting lens (8) in Figure 2 can be shifted. It was put in place when photographing the light spot on the white paper screen at (11) with a camera and removed when measuring the energy.

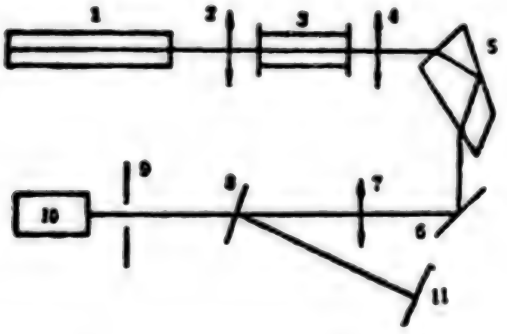

Figure 2. Experimental Configuration

Key:

1. Ruby laser with dye-adjusted Q
2. Incident lens
3. Raman chamber
4. Access lens
5. Pellin-Broce prism
6. Reflecting lens
7. Lens
8. Reflecting lens
9. Diaphragm
10. Energy meter
11. White paper screen

The resonant cavity of the laser is 84 cm long. The capacitance is 4,000 μf and the charging voltage is 1,750 to 1,850 V. The (yinhuajing) dye box is 2 cm thick. The solvent is anhydrous ethanol. Efficiency is highest at a concentration which provides He-Ne laser light transmittance of ~69 percent, and this enables stable output of single-peak laser light. The pulse width is ~120 ns and the energy is ~500 mJ.

The Raman chamber is 40 mm in diameter and 1 m long, and is made of stainless steel. The pressure can be regulated. The pressure of the gas used in this experiment was 25 atmospheres.

1. The Energy Threshold of Stimulated Raman Scattering

Color film was used for all photographs of the light spot during the experiment to enable direct observation of the scattered light. In the experiment, the light output was not prismatically decomposed at first. A reflecting lens was substituted for the Pellin-Broce prism. To enable direct observation, we used a capacitor charged to voltage V to boost the laser energy. The laser energy at various V was measured closely before the experiment.

The photograph of the light spot at a charge voltage V = 1780 V showed a red spot. Obviously, this was a spot of incident light (λ = 6943 Å), indicating the absence of stimulated Raman scattering under these conditions. A photograph of the light spot when the charge voltage V was increased to 1800 V is shown in Figure 3. This time, the light output included incident light and Raman scattering light. The white at the center of the light spot is the incident light and scattered light of all levels, and is mainly the result of Stokes scattering. The yellow circle of light, however, is produced by the combination of incident light and first-level anti-Stokes scattering light. The outer layer of green light is first-level anti-Stokes scattering light. Light spots of different colors then were obtained on the white paper screen by replacing the reflecting lens with a Pellin-Broce prism for prismatic decomposition. These light spots are shown in Figure 4. It is apparent that the light spots in the picture represent incident light (λ = 6943 Å), first-level anti-Stokes scattering light (λ = 5388.5 Å), and second-level anti-Stokes scattering light (λ = 4402.8 Å). Higher levels of anti-Stokes scattering light are at ultraviolet wavelengths and higher levels of Stokes scattering light are at infrared wavelengths, so this light could not be recorded in the photograph shown in Figure 4.

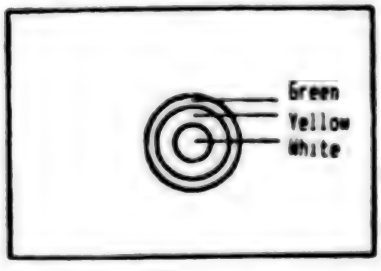

Figure 3. V = 1800 V, Light Spot not Spectrally Decomposed

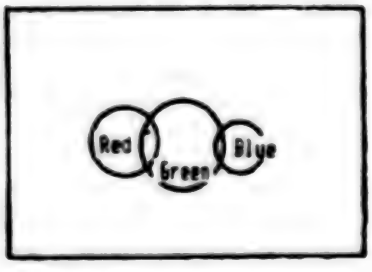

Figure 4. V = 1800 V, Scattered Light Spot After Spectral Decomposition

To observe Stokes scattering light, lens (7) in Figure 2 was replaced with a short focal length lens to increase the energy density of the light spot at the focal plane. Figure 5 shows the light spots obtained when a developed and fixed piece of black photographic paper was placed at the focal plane.

Moving from right to left in the figure are the fundamental frequency light (λ = 6943 Å) then first-level and second-level Stokes scattering light. At the time of measurement, the green and blue light spots shown in Figure 4 also were visible to the naked eye to the right of the fundamental frequency. However, they did not make a corresponding point on the black photographic paper because their energy was less than the Stokes scattering energy and therefore insufficient to make a light point on the black paper.

Figure 5. V = 1800 V, Stokes Scattering Light Spot

Key:

S_g--Fundamental frequency light (λ = 6943 Å)
S_1--First-level Stokes scattering light (λ = 9758 Å)
S_2--Second-level Stokes scattering light (λ = 16142.5 Å)

Thus, we can deduce: 1) Stimulated Raman scattering can be produced in ruby laser-pumped high-pressure hydrogen when the power of the incident light exceeds a certain threshold value. In this experiment, the power threshold was $P_0 \simeq 1.5$ MW. 2) If Stokes and anti-Stokes scattering light do not appear, then ($P < P_0$); if they do, then ($P > P_0$). This indicates that the levels of scattered light are interrelated and mutually constraining, and that they are a parameter process of interaction among multiple waves.

2. Energy Transfer Efficiency Among the Levels of Scattered Light

An energy meter was used to measure the energy of the various levels of stimulated Raman scattering light at a ruby laser energy of 500 mJ and pulse width of 120 ns (P = 4 MW), and we calculated the various transfer efficiencies η and powers P_0. It was assumed when making the calculations that the pulse width of each level of scattered light equalled the incident light pulse width. The results are shown in Table 1. The methods employed for measurement were first, to place a screen or sheet of black photographic paper in front of the energy meter to determine the location of the scattered light spots at each level. Next, the diaphragm and energy meter (Figure 2) were moved together so that the energy meter received energy from a specific level of scattered light while rejecting all other levels. The laser pulse width was measured prior to the experiment.

The results in Table 1 show that the energy of Stokes scattering light was greater than that of anti-Stokes scattering light at equivalent levels of scattered light. Moreover, in the same type of scattered light (Stokes scattering light or anti-Stokes scattering light), the energy of the scattered light decreases as the level increases. The results of these

measurements are extremely useful in interpreting the process and mechanisms of stimulated Raman scattering. Table 1 also shows that it is possible to use stimulated Raman scattering to obtain laser light at a specific wavelength and at rather high power. Thus, it is one feasible method for selecting the wavelength of laser light.

Table 1

	λ(Å)	E(mJ)	η(%)	P_s(kW)
S_1	9758.0	83.4	16.7	834
S_2	16412.3	8.4	1.67	84
S_{a1}	5388.5	1.4	0.28	14
S_{a2}	4402.8	1.2	0.24	12

Measurement error was caused mainly by poor coincidence between the positioning of the energy meter probe and the position of the light spot. To overcome error on this part, we made several measurements of each value (five times) and the values shown in the table are arithmetic averages. The error is less than 10 percent. The second cause of error was instability in laser energy output. Measurements indicated that laser energy output varied by about 2 percent.

3. Discussion

Figure 6 shows the molecular energy levels of the scattering medium. The i represents the ground state, while f, u, and w represent the vibration energy levels. If a laser of frequency v_p emits molecules at energy level u, and if there is an inverse particle count between u and f, then lasing action is created and scattered light at a frequency of v_{s1} is emitted. This emission is first-level Stokes scattering (S1). If the pump laser energy is sufficient, this process can be sustained.

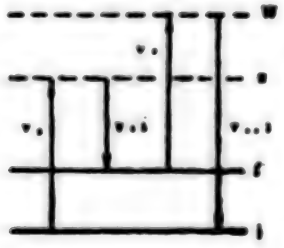

Figure 6. Molecular Energy Levels of the Scattering Medium

If a vibration energy level w exists in the molecules of the medium and if the difference between the w and f energy levels is hv_p, the incident laser light will pump the particles from f to w, after which the particles will be pushed to energy level i, and a photon hv_{as1} also is emitted. This light is first-level anti-Stokes scattering light and its frequency is v_{as1}. The interaction of these two incident light photons with a first-level Stokes

photon creates an anti-Stokes scattering photon. Next, the effects of the first-level Stokes light (v_{s1}) and first-level anti-Stokes light (v_{as1}) are similar to the pumped input light. They also create second-level Stokes light and second-level anti-Stokes light, and so on in succession. It is apparent that anti-Stokes scattering light is a prerequisite for the existence of Stokes scattering light at the same level. Higher-level scattered light (including Stokes scattering light and anti-Stokes scattering light) is conditioned on the existence of lower-level scattered light. If the pumped laser intensity is sufficient, the Stokes scattering light definitely is capable of creating anti-Stokes scattering light and thereby creating higher-level Stokes and anti-Stokes scattering light. This was the reason why the different types of scattered light either failed to appear or appeared concurrently in the experiment. It proves that the stimulated Raman scattering process is a parameter process of the interaction of multiple waves. The interdependence and mutual constraint of the different types of scattered light is determined by the quantum process of the medium molecules.

The quantum process shown in Figure 6 also can explain why the energy of Stokes scattering light is greater than the energy of anti-Stokes scattering light in scattered light of the same level and why the energy of higher level scattered light is less than the energy of lower level scattered light in the same type of scattered light. The reason is that only part of the Stokes scattered light can contribute to anti-Stokes scattering at the same level. In addition, only part of the anti-Stokes scattering light contributes to the next higher level of Stokes scattering light. This is determined by the absorption profile.

Comrades Fang Zichen [2455 5261 3819] and Mao Jianshan [3029 0494 0444], and Comrade Gao Guochang [7559 0948 2490] of the Optics and Fine Mechanics Institute of Anhui provided substantial assistance for this article and I would like to express my gratitude.

REFERENCES

1. G.T. Razdobrin, Nuclear Fusion, No 19, 1978, p 1439.

2. J. Roberto, Journal of Nuclear Materials, No 93/94, 1980, p 367.

3. K. Tsuchda, Plasma Physics, Vol 25, No 9, 1983, p 991.

12539/6091

STUDY OF LASER IMPLOSION DYNAMICS BY FOUR-FRAME X-RAY SHADOWGRAPHY, THEORETICAL SIMULATION

40090067b Beijing WULI XUEBAO [ACTA PHYSICA SINICA] in Chinese Vol 37 No 1, Jan 88 pp 20-28

[English abstract of article by Lin Zunqi [2651 1415 3825], et al., of Shanghai Institute of Optics and Fine Mechanics, Chinese Academy of Sciences; Li Jiaming [2621 1367 2494], et al., of the Institute of Physics, Chinese Academy of Sciences]

[Text] The authors present studies of laser-imploded glass microballoons using the newly-developed time-resolved four-frame X-ray shadowgraphy. The simulation results of their one-dimensional Lagrangian hydrodynamic computation code (WL code) are in good agreement with the diagnostic experiments. The joint effort of the diagnostic experiments and theoretical simulations is crucial for understanding laser implosion dynamics.

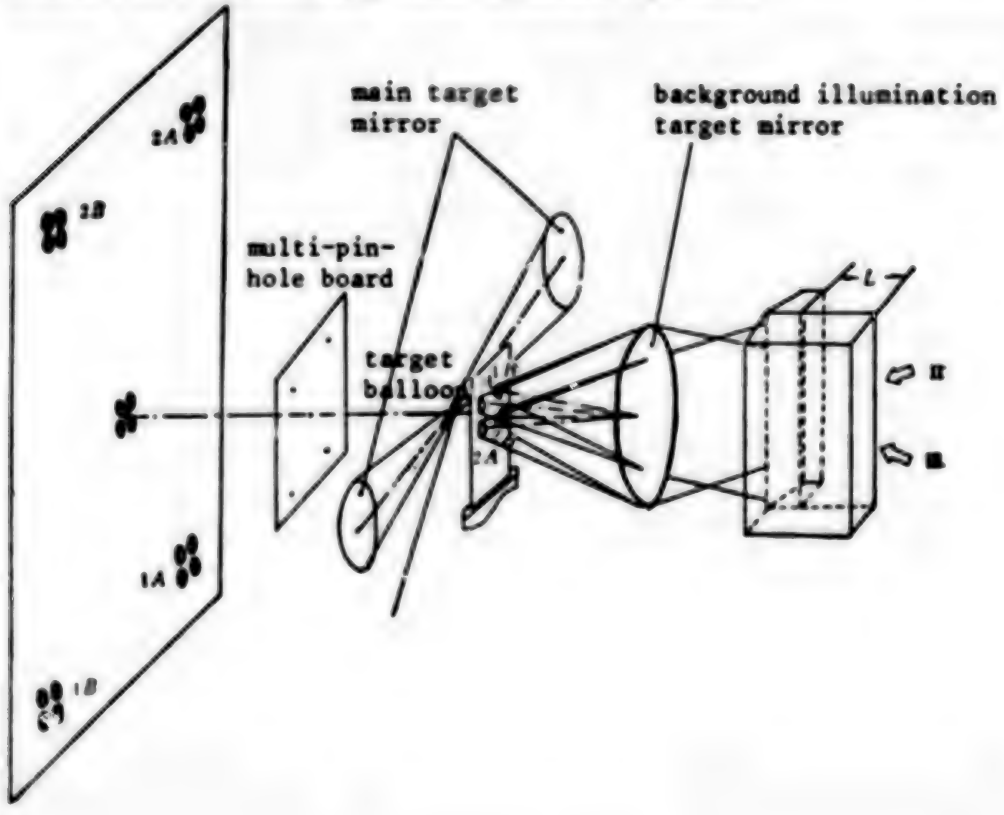

9717

SHANGHAI CALLED LEADER IN LASER DEVELOPMENTS

40080079b Beijing RENMIN RIBAO (OVERSEAS EDITION) in Chinese 2 Mar 88 p 4

[Article by Zhu Tianze [4376 1131 3419]: "Major Accomplishments in Laser Research in Shanghai"]

[Text] The Shanghai Institute of Laser Technology serves the economy with laser technology. In recent years, it has achieved over 30 major accomplishments. Some have filled voids in China while others have reached advanced world levels.

Laser technology research began in Shanghai a few years ago. The Shanghai Institute of Laser Technology, with a technical staff of over 200, has applied laser technology in production and obtained a number of important results. For instance, the 3d Laboratory successfully developed a testing apparatus for the mask of a VLSI circuit which greatly reduces defects. Each defect found on the mother board is worth 1,000 yuan. This is the first piece of equipment of its kind in China. Other equipment successfully developed include a vernier caliper line engraver, a laser letter engraver and a laser speedometer for water flow.

This institute is actively pursuing the use of lasers in medical applications. Recently, it developed a Doppler flowmeter for microscopic blood flow and a multi-functional portable laser treatment machine. The latter was successfully developed by the first laboratory. It works as a laser scalpel and a laser acupuncture needle. Surgically, it can remove tumors, warts, and moles. In obstetrics, it can be used to correct the position of a fetus. It also anesthetizes, stimulates, and reduces nerve inflammation. This product received a gold medal at the 15th international exposition in Zagreb.

In laser technology research, the Shanghai Institute of Laser Technology also developed a number of products for export. For example, their multi-purpose carbon dioxide lasers and helium-neon lasers for applications in medicine, measurement, holography, and laser processing are being exported to America, Europe, Australia, and Hong Kong.

12553/08309

STATUS OF PARTICLE ACCELERATOR DEVELOPMENT IN CHINA REVIEWED

40080034 Beijing WULI [PHYSICS] in Chinese Vol 16 No 9, Sep 87 pp 541-546, 556

[Article by Xie Jialin [6200 1367 7792] of the High Energy Physics Institute, Chinese Academy of Sciences [CAS]: "Outline of Chinese and Foreign Particle Accelerator Developments"]

[Excerpt] II. PRC Accelerator Development

Accelerator development and construction have surged in recent years in China. Three medium- and high-energy accelerator projects in China will be finished after 1988. Low-energy accelerators, with primary applications in the national economy, also have begun to play a role in important realms. A brief introduction to the situation in these two areas follows.

1. The 2.2 GeV Beijing Positron/Negatron Collider (BEPC)

Figure 5 illustrates the BEPC project. It includes five main components: 1) A positron/negatron linear accelerator, which generates and accelerates positrons and negatrons and is a storage ring injector. 2) A storage ring, which further accelerates and collides the positrons and negatrons. 3) A Beijing spectrographic detector, which examines other reaction particles for tracking, momentum, and energy losses. 4) A synchronous radiation experiment area, which uses synchronous radiation generated by the cycled electron beam for experiments in various fields. 5) A computing center, used for off-line analysis of the data obtained by the detectors in high-energy physics experiments.

The BEPC has an energy of 2.2/2.8 GeV, which is much less than the world's highest-energy colliders described previously, but its design luminance in this energy region is the highest among the world's positron/negatron colliders. This gives it clear physics goals involving precise physics research. Moreover, the high photon energy synchronous radiation produced by the BEPC also has applications in basic and applied research in many fields.

Design and pre-study for the BEPC project began in 1982 and it was approved as a key state project at the end of 1983. The achievement of collision is expected by the end of 1988. The stages of project design, component

pre-study, prototype manufacture, and batch production of non-standard equipment have been completed and civil engineering for the accelerator basically is under way. Moreover, some installation work was begun in mid-1986. The positron generator portion of the linear accelerator is being debugged. The 200-plus storage ring magnets produced by the CAS High Energy Physics Institute, CAS Hefei Plasma Institute, and the Shanghai Xianfeng Plant have been completed and magnetic surveys attained design indices. The power sources and vacuum pumps have been delivered and all eight 25 kW emitters have been installed and are being debugged. Most transport line magnets are in place and ring installation is starting. In the area of detectors, the processing of the drift chamber, shower detector, flying time detector, and magnetic devices has been completed and wire-drawing work on the more than 30,000 wires is under way. It has been estimated that overall installation and debugging can be done at the end of 1987.

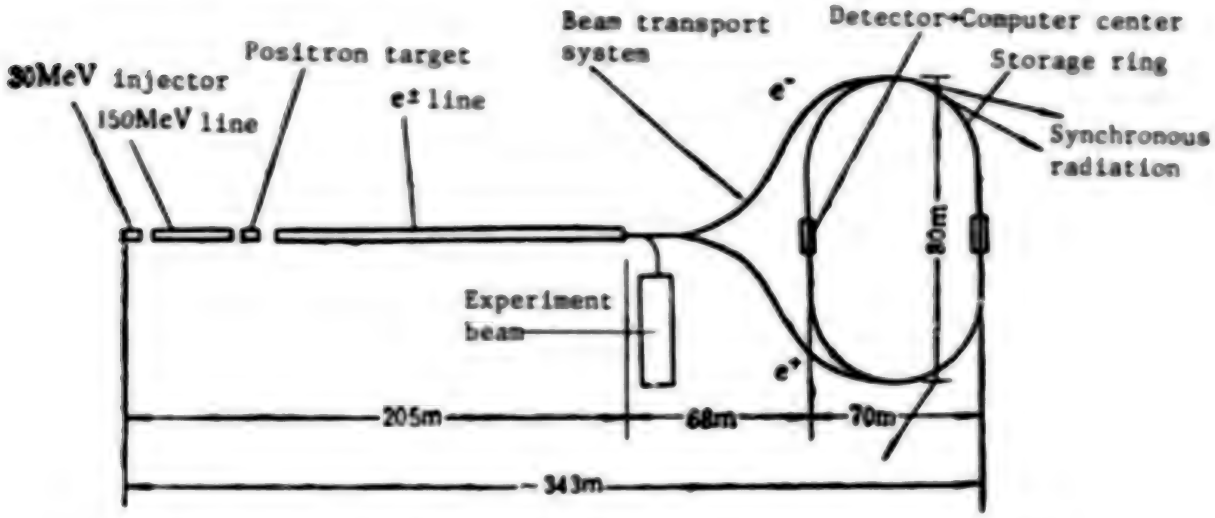

Figure 5. Diagram of the Beijing Positron/Negatron Collider (BEPC)

2. Lanzhou Heavy Ion Research Facility (HIRFL)

Figure 6 shows the Lanzhou Heavy Ion Research Facility. It is composed of an injector (SFC), main accelerator (SSC), eight experimental terminals, and pre- and post-beam transport lines. The injector is a rebuilt segmented focusing cyclotron. The main accelerator is a newly-built large-scale separation segmented cyclotron. This accelerator has four 52° segmented magnets, each weighing about 500 tons; two high-frequency acceleration chambers capable of producing a 100 to 250 kV acceleration voltage; and one large integral vacuum chamber with a volume of approximately 100 m^3 and a beam plane vacuum of better than 10^{-7} Torr.

The HIRFL is China's first large heavy ion accelerator facility. It is comparable to similar accelerator facilities in France and Japan. Its completion created the conditions for research on low- and medium-energy

heavy ion collision research and heavy ion beam applications in China. Although many of the world's accelerators are involved in work in this energy region, the far greater complexity of heavy ion nuclear reactions compared to light nuclear reactions means that China still has to do quite a bit of thorough and careful research work.

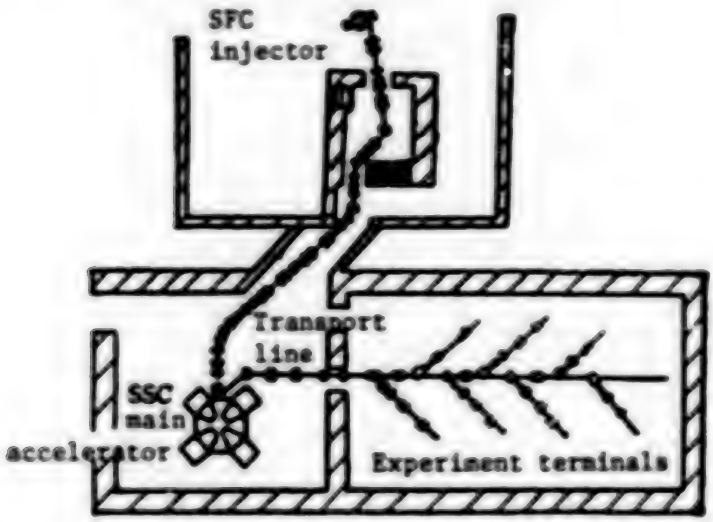

Figure 6. Diagram of the Lanzhou Heavy Ion Research Facility (HIRFL)

The State Planning Commission approved the start of development and construction of the HIRFL as a major S&T project in November 1976, so it also is known as the 7611 project. Construction of the synchronous accelerator building began in late 1984. The injector has been assembled and debugged and it is emitting beams. All of the main equipment basically has been received and it is of excellent quality. Installation of the main parts and subsystem debugging is under way. The high frequency chamber has been put through high-frequency tempering and the voltage at 8.5 MHz exceeds 100 kV. The first test sample of the vacuum chamber was successful. The vacuum was 6 x 10^{-8} Torr. Magnetic surveys of the four segmented magnets now are in progress. It is possible that the entire project will be completed and start emitting in 1988.

3. 800 MeV Hefei Synchronous Radiation Facility

Figure 7 shows the Hefei Synchronous Radiation Facility. It has four component parts: the electron linear accelerator, the transport line, the storage rings, and the experiment area. The electron linear accelerator has an energy of 200 MeV. Its beam can be injected into the storage ring or transported to the Electron Lab for Nuclear Physics Lab experiments or other purposes. The storage ring has an energy of 800 MeV. The synchronous radiation produced by the electrons cycling in it can be extracted at as many as 27 ports for work in the experiment area. Initially, a light beam line and a photoelectron energy spectrum experiment station will be built. Later, it

will be expanded gradually into research on photoetched--soft X light microscopy, time resolution spectrometry, photochemistry, and other areas.

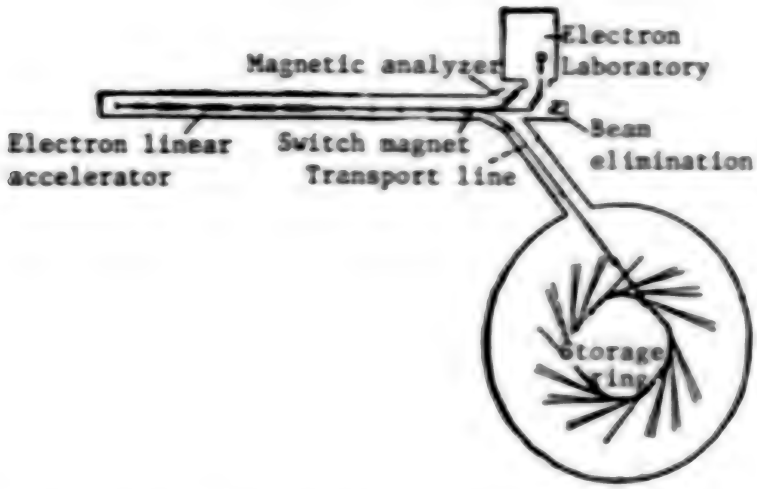

Figure 7. Diagram of the Hefei Synchronous Radiation Facility (HESYRL)

HESYRL is China's first special-purpose synchronous radiation facility. It will provide the conditions for research and application in many fields after it is completed. The strongest point in the synchronous radiation spectrum (near the critical wavelength λ_c) produced by its bias energy magnets is 24 Å. Its design also allows many types of components to be inserted into the linear joints. Examples include superconducting torsional pendulum magnets, permanent-magnet undulators, and so on, to shorten the critical wavelength and increase radiation intensity. The focusing structure of the storage ring has several working models to meet the needs of different experiments.

The HESYRL project was proposed in 1977 and approved by the State Planning Commission in April 1983. Construction began in 1984 and completion is expected in 1989. The present situation is that all the equipment in the linear accelerator has been processed, capital construction is finished, and installation is under way. The magnets, vacuum chamber, high frequency chamber, and other prototypes for the storage ring are finished and batch production is in progress. Full installation is expected to begin at the end of 1987.

4. Development of Low-Energy Accelerator Applications in China

Besides a few used for basic research, most of China's linear accelerators are used in the national economy and other realms. In the area of basic research, the most prominent equipment is two tandem accelerators. One, with a terminal voltage of 13 MV, was imported from the High-Voltage Engineering Company in the United States by the Chinese Academy of Atomic Energy Sciences. The other, with a terminal voltage of 6 MV, was developed by the CAS Shanghai Atomic and Nuclear Institute. When these two accelerators go into operation, they will play an important role in nuclear physics research, fast neutron

physics research, analytical applications, and other areas in China. The main areas of low-energy accelerator applications include radiation therapy, isotope production, materials modification, pharmaceutical product sterilization, food preservation, ion injection, non-destructive flaw detection, breeding improved agricultural varieties, nuclear analysis, processing the three wastes [waste gas, waste water, and industrial residue], and other uses. According to 1980 statistics from the United States, more than 3,000 of the world's accelerators have technical applications and there are 25 companies specializing in their production. The value of output was $2 billion in 1973. This shows the importance of low-energy accelerator applications in the national economy.

China has built almost 90 low-energy accelerators of more than 10 types since the nation was founded. We have a technical workforce of about 2,000 people and more than 20 units with development and production capabilities. Many achievements also have been made in development research (see Table 2). In summary, our current situation only corresponds to that internationally during the early 1970's. Several problems in development urgently require solutions to meet the needs of national economic construction.

III. New Acceleration Principles and Advances in Them

High-energy accelerators are restricted by technology and funds. The general feeling is that this limit has been reached in plans for the SSC and so on via existing acceleration methods. Additional increases in energy require that new paths be opened. Thus, exploration of new acceleration principles has become the order of the day and is receiving growing attention. In the United States, for example, conferences on new acceleration principles were held in 1982 and 1985. About 120 physicists and engineers participated in the second conference, a 100 percent increase over the first meeting. Moreover, the discussion was intense and the conference had to be extended from its original 5 days to 9 days. It is not hard to see that new acceleration principles are coming closer to actual utilization with each passing day.

The electrons and protons cycling in a super high-energy accelerator cannot avoid in-flow energy loss caused by synchronous radiation, so the focus has been placed on developing linear accelerator facilities to achieve new principles of ultrahigh-energy acceleration. There are two key performance demands. The first is high field strength to hold the length of acceleration within a reasonable range. The second is high luminance to adapt to several important inverse proportional relationships between high-energy reaction profiles and the square of energy.

The field strength of laser light can reach 10^{12} V/cm. One extremely attractive idea has been to use it to accelerate charged particles. However, a closer look shows that the electric field of laser light is perpendicular to the direction of transmission and the transmission speed is the speed of light, so it cannot be synchronized with particles, making direct acceleration impossible. There are two possible means at present for using the strong electric field of laser light for acceleration. One method is to use a grating, medium, or periodic metallic structure to reduce the relative

Table 2. Low-Energy Accelerator Applications in China

Type of accelerator	Total units	Chinese-made units	Imported units: Early	Imported units: Recent	Tumor therapy	Medical sterilization	Isotope production	Industrial flaw detection	Radiation processing: Applied research	Radiation processing: Experimental production	Analytical techniques	Ion injection	Basic research	Standard measurements	Other
Classical cyclotron	4	2	2										4		
Isochronous accelerator	1			1			1								
Electron cyclotron	2	2												2	
Proton electrostatic accelerator	8	6	1	1									8		
Electron electrostatic accelerator	14	14							11	1					2
High-voltage multivoltage accelerator	18	17	1								6	9	1		
Insulated core transformer-type	6	6							2	1+1*					2 shut down
High and medium frequency multivoltage type	4	1+1*		2						1					
Tandem electrostatic	15	1+2*		12							13		2		
Electron screen accelerator	2			2											
Betatron	20	14	4	2	8			12							
Electron linear accelerator	59	16+1*		42	41	1		10	2				1		
High-power beam electron accelerator	8	8													
Electrocyclic waveguide-following energy booster	1	1													
Neutron generator	8	5		3											
Ion injector	168	138		22+8*											
Proton linear accelerator	1	1													
Separation segment-following accel.	1*														
Edge and ring-coupled electron linear separation segment heavy ion accelerator	1*														
Synchronous radiation storage ring	1*														
Positron/negatron collider	1*														

* Represents those in the process of testing or installation

speed of the light and create an electric field component along the direction of transmission. However, the particles must move near these "materials" (wavelength energy level), so it is called near-field acceleration. The other method is based on anti-free electron laser light from the Compton effect which employs the interaction between waves of two different frequencies and particles. One wave is the electrostatic field of the torsional pendulum magnets and the other is the laser light field. In this acceleration method, particles move both vertically and horizontally. They can be distant from "structures" so it is called far-field acceleration. These two methods have been examined in principle. Field strengths can reach the GV/m energy level, but there are many technical problems and real applications are very far away.

Another way of creating strong electric fields is to use the space charge waves in plasma. Most interesting is the use of two lasers with a beat frequency equal to the resonant frequency of a plasma to excite plasma waves. This is called beat wave acceleration. The lasers change the plasma electron density and thereby create vertical charge waves. The acceleration field strength measured experimentally is 1 GV/m and theoretically could reach 10 GeV/m. Still, plasma is very unstable, so many problems must be solved before an actual beat wave accelerator can be built.

Because neither laser acceleration nor plasma acceleration are sufficiently mature, while considerable progress has been made in research on free electron lasers in the past year or two, most people favor a program using a classical spiral-charged waveguide acceleration structure and a free electron laser to provide a high frequency electromagnetic field to accelerate positrons and negatrons. They would build a positron/negatron collider with an energy of more than 1 TeV to enable mutually supplementary physics research on SSC hadron colliders.

This type of accelerator is called a dual-beam accelerator, and is shown in Figure 8 [not reproduced]. The facility in the lower part of the diagram is a free electron laser for creating a high frequency field. The upper part is a reduced-dimension spiral-charged waveguide. Researchers at the Livermore Laboratory in the United States have produced electromagnetic waves at a frequency of 35 GHz and a power of a few 100 MW. They also have developed accelerator tubes the thickness of a pencil which work at 35 GHz. The parallel resistance of the accelerator tubes is directly proportional to the square root of the frequency, so under identical conditions, higher frequencies would result in stronger acceleration fields. Model experiments with this type of accelerator are in progress. Another type of dual-beam accelerator has been developed by DESY in West Germany. It has a low-energy, high-current circular electron beam which uses the excitation trailing field passing through the outer edges of an accelerator tube to accelerate a high-energy, weak-current particle beam moving along its axis. This also is called a trailing field accelerator.

The acceleration gradient of these two dual-beam accelerators can reach 100 to 200 MeV/m, which is about one numerical level above existing gradients. Both are in the model experiment stage and clear results should be available soon.

In summary, these new acceleration principles also propose many new technical demands. New accelerators will have higher field strengths to reduce construction costs and higher efficiency to conserve energy. They will have weaker emissions and stronger focusing to increase luminance (the SLC uses microwave beams and the next step will use particle beams with Å energy levels!), and so on. The present situation is that experimental work remains far behind theory, which demands major efforts to realize high-energy accelerators.

Information concerning the Lanzhou Heavy Ion Research Facility was provided by Comrade Li Zhenzhong [2621 2182 0022]. That concerning the Hefei Synchronous Radiation Facility was provided by Comrade He Duohui [0149 1122 1979]. Information on low-energy accelerator applications was taken from the Accelerator Society research report WOGUO DINENG JIASUQI YU SHEXIAN JISHU YINGYONG DE FAZHAN, XIANZHUANG YU FENXI [The Development, Current Status, and Analysis of China's Low-Energy Accelerator and Ray Technology Applications] (written by Liang Xiuru [2722 1485 1172]).

REFERENCES

1. T. Weiland, The Generation of High Fields for Particle Acceleration to Very High Energies, CERN, Geneva, 1985, p 13.

2. American Institute of Physics, The State of High Energy Physics, AIP CONF. PROC., No 134, 1985.

3. American Institute of Physics, Laser Acceleration of Particles, AIP CONF. PROC., No 130, 1985.

4. Elementary Particle Physics, National Academy Press, 1986.

5. The Challenge of Ultra-High Energies, CERN, Geneva, ECFA-RAL meeting, 1982.

12539/6091

PROGRESS OF RESEARCH ON SHIP PROPELLERS IN 1980'S DETAILED

40080035 Shanghai CHUANBO GONGCHENG [SHIP ENGINEERING] in Chinese No 5, 1 Oct 87 pp 3-6, 29

[Article by Fang Wenjun [2455 2429 0971] of the China Ship Science Research Center: "Progress in Propeller Research in China During the 1980's"]

[Text] Abstract: In the realm of ship hydrodynamics, propeller research has been the most active and many technical achievements have been made. This article will review research achievements in propeller illustration, propeller theory, ducted propellers, ship-propeller matchup, cavitation propellers, and other areas.

I. Preface

In the area of ship hydrodynamics research in China, propeller research is the liveliest and technical levels are extremely gratifying. This is due to China's excellent experimental equipment and repeated sending of visiting scholars abroad for retraining in recent years. China organized the first international symposium on propellers and cavitation in April 1986, and this was the first review of propeller research in China. We were lauded by internationally known scholars. China now is a member of the ITTC Propeller Commission and we have a definite international status.

ZHONGGUO CHUANYONG LUOXUANJIANG XILIE SHIYAN TUPUJI [Atlas of Illustrations of Chinese Ship Propeller Series Experiments], published in 1983, was a major achievement in propeller research in China. China has made rich experimental achievements and received international attention in theoretical research.

A monograph summarizing progress in propeller research in China up to 1980 was prepared for the 30th anniversary of the founding of the PRC[1]. Now, we will review research achievements in propeller illustration, propeller theory, ducted propellers, ship-propeller matching, cavitation propellers, and other areas made during the 1980's.

II. Propeller Illustration

Over the past decade, the Chinese Ship Science Research Center, Shanghai Jiaotong University, and the Ministry of Communications Ship Transport

Science Institute have done a great deal of propeller research and compiled the one-volume ZHONGGUO CHUANYONG LUOXUANJIANG XILIE SHIYAN TUPUJI for use use in design. It includes: 1) Illustrations of cavitation propeller series experiments; 2) illustrations of dual-body ducted propeller series experiments; 3) illustrations of BD ducted + D-series propeller experiments; 4) illustrations of JDC three-blade adjustable pitch propeller series experiments; 5) illustrations of simple ducted propellers JD75 and JD7704 + Ka propeller series open water experiments; 6) illustrations of JD7704 ducted + JDC three-blade adjustable pitch propeller series open water experiments; 7) illustrations of open water experiments with simple ducted propeller JD8001 + Ka 4-70 series fitted with a stern rudder system; 8) illustrations of DSN ducted + B 3-50 propeller system experiments; 9) illustrations of barrier knife-type propeller open water system designs; 10) illustrations of tandem propeller systems[2-6].

Multivariate polynomial regression analysis was used to provide a mathematical expression form for the propeller design illustration $\sqrt{B_p}$-δ[7].

III. Propeller Theory

The main goal in propeller theory is derivation of the induced velocity component for a particular field point. There are two methods. One is based on velocity potential, with the propeller represented by an eddy distribution. Its disadvantage is that the required load distribution on the blades cannot be determined directly as a design condition. In addition, eddy distributions are extremely complex when dealing with problems of unsteadiness. The other, and better, method uses velocity potential as a basis to suggest a method based on non-linearized acceleration potential. It is expressed as the distribution of lift on the blade surfaces to calculate field point induced velocities. Based on this theory, a propeller design program was obtained. First, the lift line is calculated, and next the lifting surface is used for correction. It can be used for single and tandem propeller design[8].

The core question in applying lifting surface theory to analyze propeller performance is solution of eddy strength distribution differential equations. The vortex lattice method usually is employed. A finite elementary solution method is used to derive the eddy strength distribution of the attached eddy and free eddy. Simplified Van-Gent boundary conditions are used to establish a computation formula. With this as a basis, the effects of trim, tilt, propeller blade thickness, radially variable pitch, and variable side flow were entered, and the radial induced velocity was entered during the computations. Computations were made for MAU-type 4-, 5-, and 6-blade propellers[9].

On the basis of analyzing pattern functions, lifting surface theory suggested methods for computing the pressure distribution and performance of large tilt propeller blades. Based on Kerwin's research achievements, consideration was given to slip flow compression, eddy blade curling, and pitch angle circular variations in side flow to adapt them to a pattern function for deriving a geometric model of the trailing vortex trail. A program was written to compute the performance and pressure distribution of propeller blades under different conditions in a non-uniform flow field[10].

A method was proposed for estimating propeller and rudder interactions. The interaction between propellers and rudders was considered to be periodic. A harmonic modulation method was substituted for a time-domain iteration method. Thus, non-convergence can be eliminated. The singular point distribution on the rudder surface and the arch face of the propeller blades was treated as a characterization body. After dealing with each harmonic modulation component, hydrodynamic performance and propeller-rudder interaction can be computed[11].

The results of four open-water propeller model experiments and performance calculations showed that calculation of the thrust and torque coefficients of a propeller only required the use of lift line theory in conjunction with simple viscosity empirical corrections and lifting surface effect corrections. Rather good results can be obtained without making boundary layer computations. Computations of single blade thrust and torque pulsation in a side flow field showed that when using lift lines for calculations, the water flow curve created by side flow has obvious effects on thrust and torque pulsation and only a minor effect on thrust eccentricity. This was used to compile programs suitable for use in medium-sized computers to compute thrust and torque pulsation for calculating the external force of main drive twisting vibration and axle system vibration[12].

Simplified lifting surface theory was used to estimate propeller performance. A quasi-steady method was used to select and design a rational blade lateral angularity and to estimate the geometric shape of cavitation in a non-uniform flow field. Circular flow field changes along the length of the blade can use a weighted function to average the side flow so that it approximates an eddy distribution on a flat plate to improve its theoretical value and to compile a computing program[13].

A tip unloading and blade tilt propeller was designed for a 15,000-ton single propeller cargo vessel. Model experiments for several programs were carried out in cavitation water tubes. They confirmed that the tip could improve propeller cavitation performance. Pulsation pressure was reduced substantially. An increase in blade tilt further improved performance and pulsation pressure declined again. Changes in cavitation volume and cavity collapse are the source of the high frequency component of pulsation pressure[14].

Propellers which differ only slightly from standard systems are called quasi-standard propellers. Methods to estimate the performance of such quasi-standard propellers were proposed[15].

IV. Ducted Propellers

A theoretical method was proposed to compute unsteady performance of propellers in ducts of arbitrary shapes. Dipoles and source-sink single points were used to represent the body surface. Interaction was determined through iteration. To simplify steady analysis, it was treated as a rotating duct model. Time and cavitation iteration was used to deal with the more common unsteady interacting flow fields[16].

Based on the results of model experiments with symmetrical blade cross section propeller systems in an axial tube, the characteristics of lateral thrust equipment fitted with a SSPS-626 propeller system were derived. They were used to plot a curve of the relationship between propeller power, using trough pipe diameter and blade rotation velocity as parameters, and the lateral force which the lateral thruster is capable of producing. This curve can be used as a reference for ship lateral thrust equipment at several ten to several thousand horsepower and for diameters within a range of 0.25 to 2.25 meters[17].

Open water experiments were carried out on a CLAU3-30 system tandem propeller within a duct, and comparisons were made to tandem propellers not in ducts. It was discovered that the optimum efficiency rose and the optimum diameter decreased[18].

V. Ship-Propeller Matchup

The Landweber method for computing the flow around a rotating body was extended to compute the flow around a rotating body fitted with a propeller. This led to a first-order Fredholm integral equation for the body surface velocity distribution after being affected by an additional propeller. Iteration of this method was used to derive an acceleration iteration formula which was substituted for the usual Landweber iteration formula. The reduction in thrust can be obtained for the integral pressure differential between a rotating body fitted and not fitted with a propeller. A computer program was written to derive a numerical solution. It is divided into three parts: 1) Hull potential flow; 2) the field point velocity of the propeller; 3) analysis of mutual interference[19].

On the basis of analyzing hull shape parameters which affect the degree of non-uniformity in a single propeller hull and according to empirical hull data, a restricted optimization method was used to derive an empirical formula which uses hull stern shape parameters to estimate side flow characteristics. Stern shape parameters and the immersion depth of propeller blade tips were used to express the product of propeller rotation velocity and diameter as boundary values. If the product of propeller rotation velocity and diameter is greater than this boundary value, parameters of stern linear shape or propellers must be revised[20].

VI. Cavitation Propellers

Quasi-steady lift line theory was used to compute the hydrodynamic performance of a propeller rotating in a non-uniform flow field. Four common uses are: lift equivalent; dynamic similarity; linear cavitation flow theory; and estimating the geometrical shape of cavitation. Because of variations in the geometric volume of cavitation, pressure variations due to cavitation and blade thickness are derived under quasi-steady assumptions. A comparison of experiments and computations confirmed that linear cavitation flow was most satisfactory with a semi-open model and dynamic similarity method[21].

The characteristics of pressure pulsations on the inner surface of a duct caused by cavitation have been discussed. Five ducted propellers were tested in the 800 mm diameter water tube at the China Ship Science Research Center. During the experiment, side flow fields were simulated, and measurements were made of pressure pulsation, noise, and corrosion. It was discovered that peak pressure pulsation values corresponding to the blade frequency were due to intense cavitation activity at the blade tips. Moreover, there were large numbers of microcavities in the propeller wake. The largest second-order frequency pressure created by the weak tip eddy cavitation associated with pressure and cavitation can be considered to be due in part to eddy fracturing. Cavitation corrosion of the inner surface of the duct and the propeller blades is due to the fracturing of the blade tip cavitation mixed bodies into vaporous cavitation[22].

Tandem propellers refer to two common front and rear propellers. Mutual interference occurs when they are rotating in a non-uniform flow field. The theory of quasi-steady and related cavitation and excitation force in common propellers was used to suggest ways to compute cavitation and excitation vibration forces of tandem propellers in a non-uniform flow field. The effective average side flow suggested by Sasajima was used to compute hydrodynamic values. Consideration was given to the effects of slip flow compression, bearing force, surface force harmonic waves, thrust eccentricity, and cavitation length and surface area. It confirmed that the matchup of the angular distance and pitch of front and rear propellers has substantial effects on cavitation length[23].

The characteristics and mechanisms of propeller singing were analyzed in experiments on ship propeller noise and excitation vibration. Simulation conditions were prepared and simulation experiments were carried out in a cavitation water tube. Two methods were suggested to eliminate singing. The first was affixing several small semi-circular metallic protuberances near the trailing edge of the back of the propeller blades at equal intervals along the radius at a location equal to 1/15th of the cross-sectional chord length, or cutting two or three radial grooves near the trailing edge of the back of the blade. The second method is to give the trailing edge a sawtooth shape. The sawtooth shape is the equivalent of a turbulence generator[3,24,25].

A narrow-band noise spectrum sometimes appeared in the noise spectrum during propeller model experiments. Some felt that these peaks were tip-eddy cavitation noise due to invisible tip cavitation. Experiments confirmed that these narrow-band noise peaks were related to flow at the propeller tip. They could occur both in the presence and absence of visible tip-eddy cavitation[26].

The negative pressure on the upper part of the propeller disk surface was used in conjunction with natural ventilation in an experiment involving the opening of one, four, and eight holes in a duct to allow a small amount of ventilation toward the tips of the model propeller blades. Noise could be decreased by 4 to 12 db within a range 2 to 40 kHz. This was due to the slowing of cavity collapse by the increased air content in the cavities, which decreased the speed of collapse, radiated noise energy and sound pressure, and elimination time[27].

VII. Jet Propulsion and Sail-Assisted Navigation

Given the need for jet propulsion in vessels on inland waterways, model wind tunnel experiments were carried out for water jet propulsion intakes and ducts. They measured intake and duct velocity distributions and energy recovery, and computed accessory and intake resistance. Static pressure on the intake walls was measured to predict the probability of cavitation. Improvements were made by adopting boundary layer aspiration measures[28].

Japan has successfully developed six energy-saving boats using sail-assisted navigation which depend mainly on engines aided by sails. China already is involved in research in this area. Experiments were carried out concerning hydrodynamic qualities of circular arc-shaped sails to explore the effects of sail shape on their parameters and aerodynamic properties. Data was provided for computing thrust and horizontal force when designing sails, and for writing automatic sail control programs[29].

VIII. Experimental Techniques

Three geometrically-similar propeller models were tested in a cavitation tube with a working diameter of 0.8 m. A laser was used to measure the flow velocity distribution of different fore and aft cross-sections and the pressure distribution on the tube walls. No-cavitation, cavitation and supercavitation experiments were carried out in the water tube, and revisions for tube wall effects were suggested[30].

The results of open-air propeller model experiments in a cavitation water tube were converted into open-water experiments and revisions for the propulsion velocity coefficient J were derived[31].

A design program was proposed for a four-hole Biot tube used to measure three-dimensional flow fields[32].

REFERENCES

1. He Yousheng [0149 0645 5116], "Thirty Years of Development in Ship Hydrodynamics in China," QINGZHU JIANGUO SANSHI ZHOUNIAN ZHENGWENJI 1949-1979 [Articles Solicited To Commemorate the 30th Anniversary of the Founding of the PRC 1949-1979], ZHONGGUO ZAOCHUAN [China Shipbuilding] Editorial Department.

2. Sheng Zhenbang [4141 2182 6721], Yang Jiasheng [2799 1367 4141], and Chai Yangye [2693 2254 2814], ZHONGGUO CHUANYONG LUOXUANJIANG XILIE SHIYAN TUPUJI [Atlas of Illustrations of Chinese Ship Propeller Series Experiments], ZHONGGUO ZAOCHUAN Editorial Department, 1983.

3. Zhu Chao [2612 6389], Chen Zeliang [7115 3419 2733], and Shi Yongshan [2457 3938 1472], "The JDC3-50 Adjustable Pitch Propeller," ZHONGGUO ZAOCHUAN, No 3, 1979.

4. Ye Yuanpei [0673 0337 1014], Zhou Liandi [0719 6647 1717], and Zheng Yongmin [6774 3057 2404], "Ducted Propeller Cavitation Performance System Experiments," ZHONGGUO ZAOCHUAN, No 4, 1980.

5. Yang Huaishu [2799 2037 5771], Zhang Jialong [1728 1367 7893], and Qian Zongbao [6929 1350 0202], "Open-Water Series Design Illustrations for Barrier Knife-Type Propellers," ZHONGGUO ZAOCHUAN, No 3, 1980.

6. Sun Qin [1327 0530], Gu Yunde [7357 5686 1795], and Zheng Shuzhen [6774 3219 3791], "A Simplified Theoretical Design Method for Tandem Propellers," ZHONGGUO ZAOCHUAN, No 4, 1980.

7. Shen Yide [3088 6318 1795] and Zhou Liandi, "Mathematical Representation of Propeller Design Illustrations," ZHONGGUO ZAOCHUAN, No 1, 1981.

8. P.C. Pien, Chen Zuqing, and Yang Changpei, "A Propeller Theory Based on an Acceleration Potential," ISPC, Wuxi, China, April 1986.

9. Jiang Jibi [1203 7139 7103], Fang Guosheng [2455 0948 0581], and Cong Liangzi [0654 5328 3320], "Using Lift Surface Theory To Forecast Propeller Performance and Propeller Blade Surface Pressure Distribution," ZHONGGUO ZAOCHUAN, No 4, 1984. Also Jiang Jisheng, Lao Guosheng, and Cong Liangzi, "Prediction of Propeller Characteristics and Pressure Distribution on the Blade by Lifting Surface Theory," Annual of CSNAME, 1983.

10. Cong Liangzi, "Hydrodynamic Analysis for Highly Skewed Marine Propeller," ISPC, Wuxi, China, April 1986.

11. Zhu Zili and Dong Shitang, "A Theoretical Method for Predicting the Hydrodynamic Performance of Propeller-Rudder Interaction," ISPC, Wuxi, China, April 1986.

12. Ye Yongxing [0673 3057 5281] and Xing Wenping [6717 2429 5493], "Using Quasi-Steady Lift Line Theory To Predict Propeller Performance in a Non-Uniform Flow Field," ZHONGGUO ZAOCHUAN, No 1, 1985.

13. Yang Lianmin and Wang Guojiang, "Prediction of Propeller Performance in Non-Uniform Wake Field," ISPC, Wuxi, China, April 1986.

14. Xing Wenping and Wang Tiankui [3769 1131 1145], "The Role of Propeller Tip Load-Shedding and Blade Lateral Slant in Reducing Pulsation Pressure," ZHONGGUO ZAOCHUAN, No 2, 1983.

15. Chen Jiaqing [7115 0502 5464], "Estimates of Quasi-Standard Propeller Performance," ZHONGGUO ZAOCHUAN, No 2, 1983.

16. Feng Jinzhang and Dong Shitang, "Panel Method for the Prediction of Unsteady Hydrodynamic Performance of the Ducted Propeller With a Finite Number of Blades," ISPC, Wuxi, China, April 1986.

17. Shen Guojian [3088 0948 7003] and Shen Xinglong [3088 5887 7893], "Model Experiments of Radial Tubes for Symmetrical Blade Cross-Section Propeller Systems," ZHONGGUO ZAOCHUAN, No 2, 1982.

18. Xu Huimin, "Open Water Experimental Investigations of Tandem Propellers in Nozzle," Selected Papers of CSNAME, 1986.

19. Yuan Jiale [5913 1367 2867], "A Numerical Prediction Method for Thrust Reduction in a Rotary Body--Propeller Combined Body," ZHONGGUO ZAOCHUAN, No 4, 1984.

20. Shen Yide, "Selecting Ship-Propeller Combinations To Avoid Single Propeller Hull Stern Vibrations," ZHONGGUO ZAOCHUAN, No 3, 1982.

21. Wang Dazhang, Jia Dashen, and Zhang Zhongyi, "Study on Cavity Characteristics and Fluctuating Pressure Induced by Cavitating Propeller," ISPC, Wuxi, China, April 1986.

22. Ye Yuanpei, Zhang Youjing, and Ji Zhiye, "A Comparison of Suction and Pressure Side Cavitation Characteristics of Ducted Propeller Blades," ISPC, Wuxi, China, April 1986.

23. Sun Qin, Gu Yunde, and Zhang Jialang, "Analysis of Cavitation and Excitation Force of Tandem Propeller in Non-Uniform Flow Field," ISPC, Wuxi, China, April 1986.

24. Wei Yimai [7614 0110 6701], Zheng Yongmin, and Chen Yunfen [7115 7301 5358], "Research on Ship Propeller Singing," ZHONGGUO ZAOCHUAN, No 1, 1986.

25. Wei Yimai, "A Study of Simulation and Elimination of Propeller Singing," Shipboard Acoustics, Proceedings of the 2d International Symposium on Shipboard Acoustics, ISSA, The Hague, The Netherlands, 7-9 October 1986.

26. Qian Xiaonan [6929 2556 0589], Gu Qichang [7357 0366 2490], and Zhang Chengyi [1728 2110 2034], "Research on One Type of Propeller Noise Model Experiments," ZHONGGUO ZAOCHUAN, No 2, 1986.

27. Zhu Yuerui [2612 2588 6904] and Xi Deyin [1598 1795 5255], "Experiments and Theoretical Analysis Concerning Natural Aeration To Reduce Ducted Propeller Cavitation Noise," ZHONGGUO ZAOCHUAN, No 1, 1984.

28. Wu Minquan [0702 3046 2938], Ren Chaohai [0117 3390 3189], Ha Bilao [0761 1732 5071], and Liu Hai [0491 3189], "Wind Tunnel Experimental Research on Water Jet Propeller Intakes and Ducts," ZHONGGUO ZAOCHUAN, No 4, 1983.

29. Zhang Yuncai [1728 0061 1752] and Sheng Zhenbang, "Experimental Research on the Aerodynamic Performance of Circular Arc-Shaped Sails," ZHONGGUO ZAOCHUAN, No 4, 1983.

30. Huang Pingtao [7806 1627 3447] and Chu Yongquan [5969 3057 3123], "Tube Wall Corrections in Cavitation Tube Propeller Model Experiments," ZHONGGUO ZAOCHUAN, No 3, 1984.

31. Qian Xiaonan and Chen Liuxiang [7115 3966 4382], "Tube Wall Corrections in Propeller Modelling Cavitation Tube Experiments," ZHONGGUO ZAOCHUAN, No 3, 1983.

32. He Yousheng and Lu Chuanjing [7627 0278 2417], "Four-Hole Biot Tube Principles," ZHONGCUO ZAOCHUAN, No 4, 1981.

12539/6091

SHANGHAI JIAOTONG UNIVERSITY DEVELOPS LSI/VLSI DESIGN/VERIFICATION/TESTING SYSTEM

40080062b Shanghai DIANZI YU ZIDONGHUA in Chinese No 5, (Oct) 87 p 48

[Article by Xin [0207]: "Shanghai Jiaotong University Develops a LSI/VLSI Design, Verification and Testing System"]

[Text] The LSI Institute of Shanghai Jiaotong University developed a LSI/VLSI computer-aided-design, verification and testing system based on advanced theory and algorithm. It was evaluated by the Ministry of Electronics Industry on 28 April. Experts and users agreed that it is the first practical, highly automated system for the design, verification and testing of LSI/VLSI. It is a complete CAD tool for the design of MOS and bipolar ECL [emitter-coupled logic] LSI/VLSI wafers at various stages.

The system comprises an automatic design system, an automatic verification system and an automatic testing system. These systems are linked together by the CAD database to become an integrated VLSI-CAD system. The same data format is used in the system, so it is possible to perform design, verification and testing in the same system. The database contains the description of the logic function, the logic symbol the domain symbol and the domain itself of several dozens of common logic units. It also has 300-1000-gate CMOS and ECL gate-array templates. In the design mode, either graphics or descriptive input can be used. The system automatically performs circuit emulation, logic emulation, and gate pattern design, and permits automatic or semi-automatic circuit layout. The design system is independent of the rules associated with the technique. It can be adapted to prepare 3-micron and 5-micron circuit diagrams by modifying the rules.

The automatic verification system can retrieve patterns and circuits and check their geometric design, including logic, topologic and geometric operations of the pattern. In addition to orthogonal patterns, it can conveniently handle oblique patterns, and even patterns formed by circular arcs and simple curves.

The automatic testing system uses the exploration method and simulated simultaneous breakdown technique to perform the test. Its coverage is over 90 percent and it is a worldwide state-of-the-art system.

The hardware environment of the system is a VAX-11/750 or Applicon super minicomputer with associated peripheral equipment and workstations such as plotters, digital instruments, graphics terminals and magnetic tape drives.

The software environment is the VMS and RSX operating systems. All applications programs are written in C language. In order to promote the software, it has been transplanted to Apollo, HP and Zijin AT computers.

Since the successful development of the system, more than 20 integrated circuits have been analyzed, verified and designed. The largest one is equivalent to 13,000 transistors. Some of the circuits are already available as chips.

12553

ACHIEVEMENTS OF MINISTRY OF ASTRONAUTICS' RESEARCH INSTITUTE REVIEWED

40080062a Tianjin TIANJIN KEJI XIAOXI in Chinese No 11, (Nov) 87 pp 17-18

[Article by Xu Guichang [1776 6311 2490] et al.: "Brief Introduction to Achievements Made at Research Institute 8358 of Ministry of Astronautics"]

[Excerpts] Laser Fuse for Missiles

In order to catch up with other countries, Institute 8358 of the Ministry of Astronautics has successfully developed a non-contact short fuse for ground-to-air and air-to-air missiles. Field test results showed that all technical specifications have met design requirements.

This laser-fuse test solved the problem of detection and detonation around a 360-degree band in space. Logarithmic amplification and comparative technology are used to ensure the accuracy in range control. In addition, a way has been found to miniaturize it.

The laser missile fuse was evaluated by the Institute in February 1987. Experts believe that this fuse was the first of its kind in China.

Model ZLM-1 Laser Target Simulator

The laser target simulator developed by Institute 8358 of the Ministry of Astronautics is an electro-optical system. It is used to simulate the laser beam reflected from a moving target of a certain velocity and acceleration. The reliability of the system is good. It is an excellent piece of experimental equipment for laser tracking and it can be further developed to become a simulator with multiple functions.

The Model ZLM-1 laser target simulator was evaluated by the Institute in February 1987. The maximum angular velocity the system can simulate is 25.5 degrees/s. The maximum angular acceleration is 59 degrees/s squared and the angular variation data is continuously adjustable. The system emits a 260-mm-diameter parallel beam. There are special characteristics in optics. Experts believe that it is an advanced system in China.

Laser-Beam Guidance System

The laser-beam guidance system developed by Institute 8358 of the Ministry of Astronautics was evaluated by the ministry in February 1987. This advanced

guidance system for missile control in attacks on enemy targets may be used in an anti-tank missile or a ground-to-air missile. It is very accurate, has a high resistance to interference, and can launch an attack in all directions. The system on board is very simple; it is reliable, lightweight and compact.

Major Technical Specifications of the System

Effective Range: greater than 5 kilometers with visibility better than 12 kilometers.

Minimum Start-up Control Range: less than or equal to 9 meters.

Telescope Aiming Field of View: 9 degrees.

Magnification Factor: 7.

Variable Beam Range: 16-320 milli-radians.

Error Signal Curve: linear, non-linearity within 5 percent.

Zero-position Error Signal Fluctuation: less than 1 percent of maximum output error.

Error Signal Informational Rate: 20 Hz.

The system uses a single reception unit. It may be used on spinning and non-spinning warheads. The system employs a light distortion focussing technique with a combination of spherical and cylindrical lenses to form a light strip. The power utilization rate is high and the transmitter needs no cooling. It has a large effective range and a wide variable beam range. This not only makes sure that the beam is introduced when the missile is launched but also guarantees its control sensitivity at a distance. It has a unique coding/decoding technique.

It was recognized at the review meeting that the system was independently developed and correctly designed, with a simple structure, smooth operation, and high accuracy and reliability. The system is unique and is on the leading edge in China; it is a good foundation for the development of laser guidance systems in China.

12553

SILICON-TARGET OSCILLOSCOPE DEVELOPED

40080062c Beijing KEJI RIBAO in Chinese 19 Nov 87 p 1

[Article by Su Kuoshan [5685 2368 0810] and Wang Hanlin [3769 5060 2651]: "Silicon-Target Oscilloscope Developed"]

[Text] A high-technology item which has been monopolized by an economic superpower country, the BSC-100 digital wave-form processing system (silicon-target oscilloscope), was successfully developed by China with its own resources. Certain specifications are better than those associated with the product made abroad. On November 18, scientist Zhu Guangya [2612 0342 0068], on behalf of the Defense Science and Engineering Committee, presented two silk banners to the responsible parties--Institute 10 of Division 9 of the Ministry of Nuclear Industry [MNI] and Institute 55 of the Ministry of Electronics Industry [MEI]. The banners were embroidered with the words "overcome technical difficulty, exceed world standard."

As nuclear technology and high technology continue to advance in China, we are desperately in need of a test instrument for fast processes. However, a certain superpower imposed an embargo against China. After several years of hard work, the technical staff at MNI and MEI successfully developed the core component of a silicon-target oscilloscope--a high-speed dual-gun silicon-target scanning converter tube, and the first prototype. In early 1986, the design of the silicon-target oscilloscope was completed and small-scale production began.

This system can be connected to a computer so that observation, storage and processing can take place simultaneously. In areas such as bandwidth, linearity and automatic calibration, it is at a worldwide state-of-the-art level. It is not only suited for major defense engineering and nuclear technology projects but also capable of measuring an instantaneous signal wave form in research projects involving high-energy physics, accelerator and laser technology. Consequently, it fills the void in measurement of instantaneous nanosecond signals with digital technology.

In order to quickly move this achievement into production, an economic entity was formed by Institute 10 of Division 9 of MNI and Institute 55 of MEI to develop and manufacture this oscilloscope.

12553

DEVELOPMENTS IN SILICON CRYSTALLOGRAPHY REPORTED

Homoepitaxial Growth on Si Substrates

40080078 Shanghai FUDAN XUEBAO [JOURNAL OF FUDAN UNIVERSITY (NATURAL SCIENCE)] in Chinese Vol 26 No 4, 1987 p 389

[Article by Jiang Weidong [5592 4850 2767] (Department of Physics), born in 1960 and graduated (Master's degree) from Fudan University in 1985]

[Text] Because silicon is widely used in VLSI and micro-structure devices and the technology is fairly mature, molecular beam epitaxial materials on silicon substrates are receiving a great deal of attention. For instance, the epitaxial growth of a III-V semiconductor on silicon or silicon on a III-V semiconductor may integrate a microelectronic device and an opto-electronic device on the same chip. The growth of a structure involving silicon/insulator/silicon, and silicon/silicon compound/single-crystal silicon is an effective way to realize three-dimensional integration to enhance the degree of integration. Based on existing experimental results in the literature, in order to obtain a heterogeneous junction device with little defect at the interface and of superior electrical and optical characteristics, it is extremely important to clean the substrate surface and then grow a buffer layer by molecular beam homoepitaxy as the device is being fabricated. In this work, 39-mm-diameter n-type Si(100) and 34-mm-diameter p-type Si(111) single-crystal wafers are used as substrates to study the conditions for substrate cleaning and homoepitaxial growth.

Usually either ion erosion and annealing or high-temperature treatment (about 1200°C) is used to clean silicon. However, these processes are not suited for the fabrication of a device because the former can damage and roughen the surface and the high temperature in the latter process can cause the re-distribution of the dopant. For this reason, we chose the multiple oxidation etching method introduced by Shizaka. After etching several times in boiling HNO_3 and HF, a thin oxide layer (about 10-20 angstroms), which prevents carbon contamination and sublimes easily upon heating in vacuum, is formed by heating the silicon in a mixture of HCl, H_2O_2 and H_2O. It was experimentally demonstrated that under UHV (ultra high vacuum) conditions a clean surface could be obtained at temperatures of 800°C and 820°C for Si(100) and Si(111), respectively. The original O and C impurity levels dropped to below the detection limits of the AES (auger electron spectroscopy) probe.

The smoothness of the annealed silicon surface was tested by RHEED (reflected high-energy electron diffraction). The repeatability of the surface is (2x1) for Si(100) and (7x7) for Si(111), consistent with earlier results. It is especially significant that a clear stripe shows up in the diffraction pattern. In general, the sample surface is not smooth prior to epitaxial growth. The RHEED pattern should be a point distribution resulting from three-dimensional scattering. The surface becomes smooth on the atomic scale after the homoepitaxial growth of approximately 100 atomic layers. At this time, the RHEED pattern is a stripe. However, the surface we obtained was fairly smooth before the epitaxial growth. This has never been reported in the literature before. It also proves the effectiveness of the method used.

Homoepitaxial growth was performed on a clean and orderly silicon surface. The growth temperatures are 520°C and 700°C for Si(100) and Si(111), respectively. The rate of growth is 2.0 angstroms/second. The film is approximately 1000 angstroms thick. The epitaxial film was examined by RHEED. It was found that there was no change in the repeatability of the surface structure. The contrast is even better compared to that prior to epitaxy. The surface smoothness was further improved. Electrical tests such as the four-probe conductivity test, C-V diagram and Hall effect showed that the epitaxial film is n-type. The unintentional dopant level is approximately 5×10^{14} to 1×10^{15} cm^{-3}. The RBS technique was used to measure the epitaxial film and χ_{min} is about 5 percent, indicating good structural integrity of the film.

Molecular Beam Epitaxy on GaP

40080078 Shanghai FUDAN XUEBAO [JOURNAL OF FUDAN UNIVERSITY (NATURAL SCIENCE)] in Chinese Vol 26 No 4, 1987 p 390

[Article by Jiang Weidong [5592 4850 2767] (Department of Physics), born in 1960 and graduated (Master's degree) from Fudan University in 1985]

[Text] When a semiconductor hetero-junction is made using the molecular beam epitaxy (MBE) technique, the selection of materials with matching lattice constants is one of the key factors required to yield a high-quality epitaxial film. The lattice mismatch factor between Si and GaP is only 0.37 percent and their thermal expansion coefficients are very close. Hence, the Si/GaP system is suited for MBE. This paper is a preliminary study of the epitaxial growth characteristics of this system.

Epitaxial growth is performed in an ultra-high vacuum (UHV) electron-beam evaporator (EBE). It consists of a growth chamber, an analytical chamber and an entrance chamber which can be isolated from one another. The growth chamber was equipped with an 8-kW EBE, a quartz thickness monitor, a reflected high-energy electron diffractometer (RHEED), a liquid-nitrogen-cooled shield and a rotating sample rack. The ultimate vacuum limit of the growth chamber is 8×10^{-9} Pa. The operating pressure was maintained at 1×10^{-7} Pa. The Si evaporation rate was 0.4 angstroms/second and the total thickness of the growth layer was 1500 angstroms.

The substrate was single-crystal n-type GaP($\bar{1}\bar{1}\bar{1}$). After chemical and mechanical polishing, it was heated in a mixture of HCl and HNO_3 for several dozen minutes and then rinsed in de-ionized water. After it was blown dry, it was immediately placed in the vacuum system. The substrate was heated to 550°C in a UHV. A spot pattern corresponding to the (1x1) structure was observed by RHEED. Auger electron spectroscopy (AES) showed the complete removal of major contaminants such as oxygen and carbon from the surface. Energy-loss spectroscopy (ELS) measurements proved that there were no Ga islands on the surface. The GaP surface thus prepared is orderly, but not very smooth.

Epitaxial growth of Si was conducted when the substrate temperature was 450°C. Both AES and RHEED were used to monitor the process continuously. It was found that the AES signal for P varied differently from that for Ga as the thickness of the epitaxial Si layer increased. As the thickness of the epitaxial Si layer exceeded 100 angstroms, the signal for Ga was beyond resolution in the AES spectrum, while the signal for P persisted until it reached 1500 angstroms. This indicated that both Ga and P were diffused into the epitaxial layer and it was more apparent for P. In the initial stage, the (1x1) spot diffraction pattern obtained by RHEED remained almost unchanged. After the layer was grown to 50 angstroms in thickness, it changed to a stripe pattern, indicating that the surface was getting smooth. The surface structure also changed as the epitaxial thickness reached 500 angstroms, from (1x1) to (3x3). This (3x3) pattern remained until the film was 1500 angstroms thick. We believe that the reason for this surface structural repeatability change after the epitaxial Si layer reaches such thickness is due to the variation of P concentration in the surface of the epitaxial layer. The thicker the epitaxial Si becomes, the fewer the number of P atoms diffusing to the surface. When the concentration of P drops to below a certain level, the structural repeatability will vary. If the P concentration at the surface is raised again, it will go back to the (1x1) structure from the (3x3) structure. This point has already been experimentally verified.

Grain Quality in Polycrystalline Si

40080078 Shanghai FUDAN XUEBAO [JOURNAL OF FUDAN UNIVERSITY (NATURAL SCIENCE)] in Chinese Vol 26 No 4, 1987 p 459

[Article by Yu Xitong [0151 1119 0681], born in 1945 and graduated from Fudan in 1970, and Tang Houshun [0781 0624 5293], both of the Department of Materials Science]

[Text] In other countries polycrystalline and single-crystal silicon solar cells are running neck and neck. In China, polycrystalline silicon materials and cells are in production. Because of differences in the growth techniques and conditions, the quality of the product varies. This paper introduces a method to evaluate the quality of the grain. It is different from the method introduced by D. Leung et al. It is non-destructive and directly measures the photoelectric potential of the diffusion junction of the polycrystalline silicon to determine the quality of a grain or a small area.

The conventional method is used to wash and etch a p-type polycrystalline silicon wafer. An n^+ layer is formed by diffusion. The phosphosilicate glass is then removed. The back side of the wafer is brushed with an aluminum paste and then sintered. It is followed by sintering a layer of silver to form a good ohmic contact with the silicon. After removing the parasitic junctions along the edge of the silicon wafer, the measurement of the photoelectric voltage of the diffusion junction can proceed. One terminal of the digital multimeter is in contact with the back electrode of the cell. The other is pressed hard against the grain or small area to be measured under a standard light source. The quality of the grain may be judged by the photo-voltage distribution obtained by the meter.

The effective circuit of a solar cell is $V = IR = I_{Sh}R_{Sh} - IR_S$, $I_{Ph} = I + I_{Sh} + I_D$, where V is the measured photo-voltage, R is the internal resistance of the meter, I is the current passing through the meter, V_{Ph} is light-induced voltage, R_S is the serial resistance, I_{Sh} is the shunt current, R_{Sh} is the parallel resistance, I_{Ph} is the light-induced current and I_D is the dark current. Because a high-impedance meter is used, $I \to 0$. Thus, $V = (I_{Ph} - I_D)R_{Sh}$. Also because in normal conditions $I_D \ll I_{Ph}$, V approximately $= I_{Ph}R_{Sh}$. Obviously, the measured photo-voltage is primarily determined by the photo-current and the parallel resistance. I_{Ph} is primarily determined by the diffusion length of the minority carrier and the concentration of the carrier current. The diffusion length of the minority carrier is also closely related to the impurity levels, dislocation density and grain boundary of the polycrystalline silicon. R_{Sh} is mainly dependent upon the microscopic crack, impurity enrichment, degree of segregation, and high dislocation density. If the diffusion is normal and the parasitic junctions are eliminated, the magnitude of the photo-voltage basically reflects the quality of the grain.

Because the concentration in the n^+ layer is 10^{19}-$10^{20}/cm^3$, and due to tunnel effect, the contact between the terminal of the meter and the n^+ layer is essentially ohmic. This point was verified by measuring the I-V characteristics at the contact point. The forward and reverse resistance value is 10-20 ohms. The slope is different by 1-2 ohms. It may be considered that there is no rectifying effect. The photo-voltage thus measured is only 1 percent different from that obtained with a sintered silver point. Because the diffusion layer is a low-resistance layer, if photo-voltage of a certain grain is low, a voltage gradient will result around it. Experimentally, the range of this voltage gradient is approximately 3 mm. Therefore, it is very easy to locate the "bottom," i.e. the low-quality grain or area.

This method not only can be used as a quality control measure in growing polycrystalline silicon but also can serve as an intermediate test step in the production of polycrystalline solar cells.

12553/6091

FEATURES OF NEW LARGE-SCALE CLEAN ROOM REPORTED

40080083a Tianjin TIANJIN KEJI XIAOXI in Chinese No 12, (Dec) 87 pp 13-14

[Article by Gong Gao [0180 4473]: "Large-Scale 0.5-Micron No-10-Class Clean Room"]

[Text] The Chinese Academy of Sciences (CAS) Microelectronics Center (formerly Plant No 109) is a plant engaged in the production of integrated circuitry specifically for application in computers. Its technical equipment is imported from Japan and the United States, its spotless workshops are based upon the major research topics and extended key projects of "Mass trial production of large-scale integrated circuitry," during the period of the Sixth 5-Year Plan. Its principal workshops are constructed on an area of 17,440 square meters, with 5,500 square meters purified, of which 650 square meters are given over to a class-100 clean room. Technical requirements dictate that a clean room of this class must be divided in two parts, with 155 square meters devoted to manufacture of boards and 500 square meters to photoetching. There has not been a clean room of such size in China before. As semiconductor technical devices change more quickly, there will be an increased demand for purified workshops with enough flexibility and advanced characteristics to keep up with the changes. To overcome the technical obstacles to a large-scale superclean room, the CAS' Architectural Design Bureau and its Microelectronics Center worked with the Hebei Academy of Engineering and the Tianjin Municipal Purification Equipment Plant, in joint design and development. In their joint measurements, the standard was a 0.5-micron class-10 clean room.

Features of Clean-Room Construction

This clean room is divided into upper and lower static pressure chambers and is constructed on three levels. The upper static pressure chamber and the clean room walls are all constructed of a double layer of steel plate, with a 5-cm thickness of polyamide between the layers to maintain temperature. The lower static pressure chamber is of brick-wall construction. The inside of the room is ceramic tile, with a terrazzo floor. The clean room ceiling has gratings packed with cloth high-efficiency filters. The lower portion of the room is reinforced with plastic safety gratings and lamps. The flooring consists of anti-static electricity cast-aluminum panelling. The clean room is 2.7 meters high, with the upper static pressure chamber being 2.0 meters high and the lower static pressure chamber 3.8 meters high. In the clean

room's outer wall there is a non-airtight observation window. Outside the window there is an observer's passageway 1.5 meters wide; in addition to allowing observation by personnel, it can also provide for some supplementary technical equipment, such as vacuum pumps, etc., and can be of use in maintaining temperature and cleanliness in a class-100 clean room.

Selection of High-Efficiency Filters and Fluid Slot Sealing

The equipment adopted was unpartitioned high-efficiency filtering and fluid slot sealing equipment developed by the Ministry of Electronic Industry's No 11 Design Institute, the Hebei Academy of Engineering and Tianjin Municipal Purification Equipment Plant. When the unpartitioned high-efficiency filters were compared with other filters having comparable efficiency rates and amount of draft, it was found that the former were small in volume, lightweight, easily installed and only 8-cm thick, rather than the more common 22 cm. To decrease the number of high-efficiency filters as much as possible, they designed the largest composition size, 1,260 X 630 mm (conventional filters are 480 X 480 or 630 X 630 mm). Success or failure of clean-room equipment hinges upon the quality of the filter sealant. In the past, the common practice employed mechanical sealing methods: in this method of seal installation, sponge-rubber strips are bound at high pressure and each filter requires a minimum of eight binders before it is tight. Often, due to a lack of precision in machining of parts, the rubber pads change shape with age and do not seal tightly, which causes short circuits which can in turn affect the degree of cleanliness. Moreover, it is a highly labor-intensive process, and the filters are not easily replaced. If the model GB-03 high-efficiency filter had been selected for use in this class-100 system, 1300 binders would be required. One can readily see how much difficulty is involved in changing just one filter. But, the filters currently used only have 700 binders. The sealing installation selected utilizes a special non-Newtonian liquid (in past form) which is poured into 50 X 50 U-model metal grooves. This liquid must be non-volatile, non-sceping and odorless. Moreover the filter itself will act as its own tool carriage. After installation, one only needs to lift the filter from the lower to upper section, and then gently set it down; one can then rely upon the filter's own weight to insert the tool into the liquid, with excellent sealing results. In addition, replacement is convenient. To protect the filter from damage, the bottom of the filter is covered with a protective plastic grid, and the liquid slots are supplemented by illuminating lights.

The Airflow System and Control of Air Pressure

Because a clean room requires so much forced air, it is very difficult to evenly distribute the air drawn into and exhausted from the room. Therefore, the design divides the 500-square-meter clean room into two parts. Each part is then equipped with one exhaust static pressure chamber and one intake static pressure chamber. The exhaust operates at a steady pressure. The maximum amount of draft is forced through the widest possible area of the intake and exhaust ducts. There are safeguards against the occurrence of any dead space. In addition, an intake filter is installed below the intake

screen panel. The filter's thickness (resistance) can be adjusted to help maintain an even pressure and assure a vertical air flow. At the same time, this assures a constant temperature in the clean room.

To ensure correct pressure in the clean room, when designing the quantity and arrangement of the air, it was planned that there should be a 5-Pa difference in pressure between the clean room's different levels. Under the clean room's walls there are electrically operated valves for releasing excess pressure.

Use of Intake Static Pressure Chamber

In addition to keeping a steady intake pressure, the intake static pressure chamber functions as the installation for water, electricity and gas tubing, as well the tubing which patterns the air draft. Technical requirements mandate that the clean room must utilize a system which both cools and patterns pure water and has several types of gas tubing, plus electric-cable and plastic air-flow tubes. Not only must all of these be installed in certain places, there also must be sufficient space for maintenance. There must be provision for a port suitable for receiving replacement equipment, and the inner parts of the static filter must be immaculately clean. Although the static filter is a large item, it must thus be utilized to the fullest.

Noise Control

Due to the massive quantity of exhaust from a clean room, there is a great deal of noise produced by the duct machinery and the air drive. So the design calls for the engine housing to be separated from the clean room by a double-thick wall. In addition, both the exhaust and intake ducts are equipped with non-dust producing microbore metal noise suppressors.

The Regulator System and Control of Temperature and Humidity

The exhaust system is a single machine system. The entire system is designed to have six 55-kW No 16 centrifugal ventilators circulating the exhaust. There are also two 40,000-cubic-meters-per-hour metal regulators with peripheral equipment to replenish the fresh-air supply and maintain temperature and humidity. There is computer-controlled electronic regulation of the cold and hot water pipes which utilizes temperature and humidity sensors. The primary and secondary exhaust valves, the fresh-air valve, the humidifier, etc., all automatically control the temperature and humidity. Also part of the design are two lithium-chloride rotating dehumidifiers acting as standby dehumidification equipment, so that when there are variations in the temperature at which the refrigeration equipment supplies water, the efficiency of dehumidification will not be affected. The exhaust is regulated by three levels of filtration, the duct system is designed with an intake shutoff valve, and to prevent reversal of flow there is equipment for disposing of waste gases.

12625/12232

NEW METHOD FOR MEASURING SMALL PHASE DIFFERENCE--THREE-SLIT HOLOGRAPHIC INTERFERENCE DEVICE

40090066 Chongqing CHONGQING DAXUE XUEBAO in Chinese Vol 11 No 1, Jan 88 pp 10-22

[English abstract of article by Cheng Tangguo [4453 1016 6753], Wang Linyu [3769 2651 3254] and Kuang Shi [0562 1395] of the Applied Physics Department, Chongqing University]

[Text] This paper introduces a new method for measuring flatness of the optical plane and thickness of a thin film. Using three single slits displaced equidistantly, a hologram is exposed three times in order to record respectively the spectrum of each slit, which includes the phase modulation (into F_0) and no phase modulation (into F_1 and F_2). The spectrum of three-slit interference is reconstructed with a thin beam which is illuminated at the first order of the Fraunhofer diffraction of the hologram. The device is simple and gives a high resolution of the order of $\lambda/400$. (Received 4 July 1987.)

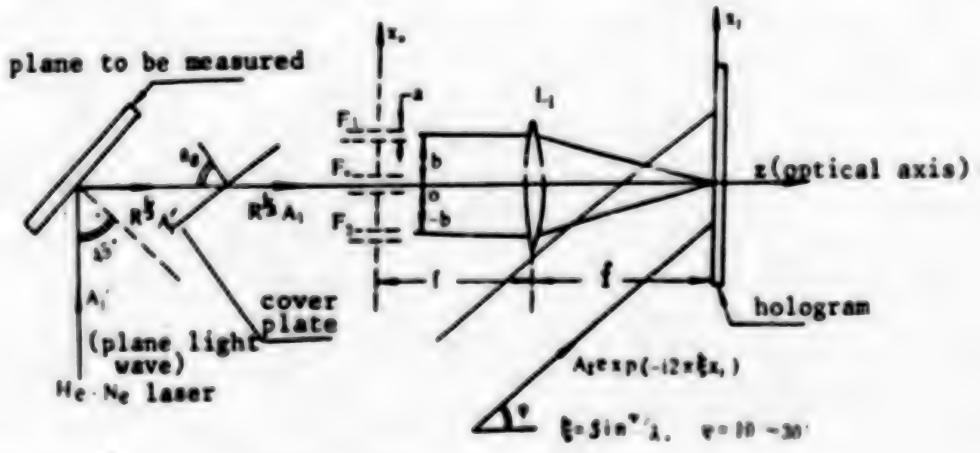

Figure 1. Experimental apparatus, first stage

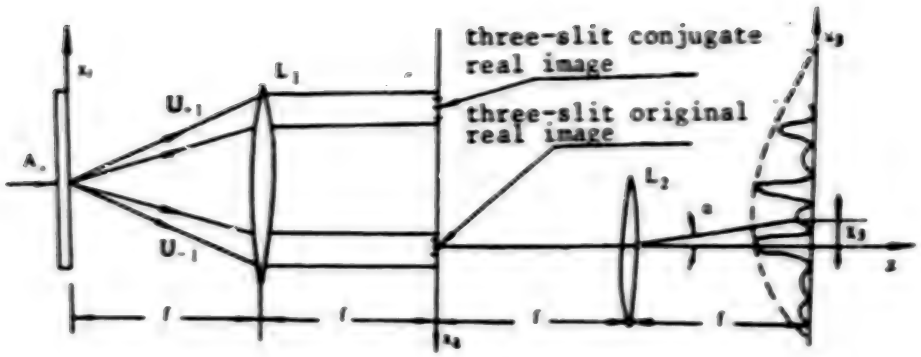

Figure 2. Experimental apparatus, second stage

REFERENCES

(1) Zhou Changxin [0719 7022 2450], "Applied Isochromatic Streak Ultraprecise Measurement for Polishing Rough Optical Surfaces," JILIANG XUEBAO Vol 7 No 3, July 1986.
(2) Yi Tengjin [0122 4696 6651], "Ultraprecise Optical Flatness Measurement Techniques," GUANGXUE, No 10, 1981 p 465.
(3) G. Binning, PHY. REV. LETT. No 56, 1986 p 930.
(4) Jing Ao Sun, Anni Dai and Glen Wade, "Profile Measurement on Ic Wafers by Holographic Interference," ICHA CONFERENCE DIGEST, 2-4 July 1986, Beijing.
(5) A.A. Husain, J. PHY. E. SCI. INSTRUM., No 7, 1985 pp 574-576.
(6) Yu Meiwen [0060 5019 2429], et al., "Optical Holography and Information Processing, pp 49-51, 59-60.
(7) A.P. Ovechkin, SOC. J. OPT. TECHNOL., 43, 1976, pp 258-261.
(8) A.B.S. Van Heel, "Advanced Optical Technique," pp 437-438.
(9) E.E. Bergmann, REV. SCI. INSTRUM., 44, 1973, p 1134.

9717

SUBBANDS, OPTICAL TRANSITIONS OF SUPERLATTICES IN ELECTRIC FIELD

40090067a Beijing WULI XUEBAO [ACTA PHYSICA SINICA] in Chinese Vol 37 No 1, Jan 88 pp 1-10

[English abstract of article by Xia Jianbai [1115 1696 4101], et al., of the Institute of Semiconductors, Chinese Academy of Sciences]

[Text] Assuming stationary states, the effective mass theory is extended to the case of superlattices in the electric field. When the tunnel penetration factors are small, the calculation results are in agreement with those of the tunnel resonance method. Subbands, wave functions and optical matrix elements are calculated. It is found that the shifts of particle densities and energies of the second excited states are opposite those of the ground states. In the electric field, the overall shape of the subbands is close to that of those not in an electric field, but the double degeneracy is removed. With the increase of the electric field, the selection rule $\Delta n = 0$ transforms to $\Delta n = \pm 1$ gradually. This changeover occurs at a moderate electric field.

9717

ACOUSTIC PROPERTIES OF AMORPHOUS SUPERIONIC CONDUCTOR $(AgI)_x(Ag_4P_2O_7)_{1-x}$

40090067d Beijing WULI XUEBAO [ACTA PHYSICA SINICA] in Chinese Vol 37 No 1, Jan 88 pp 57-63

[English abstract of article by Wu Kunyu [0702 2492 5940], et al., of the Department of Radio and Electronics, University of Science and Technology of China, and the Laboratory of Internal Friction and Solid Defects, Institute of Solid State Physics, Chinese Academy of Sciences, Hefei; Yu Wenhai [0205 2429 3189] of the Department of Physics, University of Science and Technology of China, Hefei]

[Text] An amorphous superionic conductor $(AgI)_x(Ag_4P_2O_7)_{1-x}$ system has been obtained through the liquid nitrogen rapid quenching technique. The ultrasonic attenuation and velocity of longitudinal and transverse sound waves in the samples for AgI with mol concentration x = 0.50, 0.60, 0.67, 0.75 and 0.80 were measured in the temperature range of 77-300 K at the frequency of 2, 5, 10 and 15 MHz. An anomalous strong ultrasonic absorption peak is observed at temperatures around 200-240 K, with evident characteristics of relaxation attenuation. The attenuation peak was found to shift with lower temperatures, while the peak attenuation value increased with increasing AgI content. In the experimental temperature region the internal friction Q_M^{-1} of longitudinal and transverse waves in the samples was almost equivalent. During attenuation measurements, the sound velocity, elastic moduli at room temperature and the dependence of the sound velocity on the AgI content were also measured.

The experimental data satisfactorily fit the unified theory of low frequency fluctuation, dissipation and relaxation processes (i.e., infrared divergence response theory, of IDR) proposed by Ngai. The apparent activation energy and infrared divergence exponent of the samples are presented.

9717

CONCENTRATED SUSPENSION THEORY OF SOUND ATTENUATION IN GRANULAR MEDIA, APPLICATIONS

40090067e Beijing WULI XUEBAO [ACTA PHYSICA SINICA] in Chinese Vol 37 No 1, Jan 88 pp 64-70

[English abstract of article by Qian Zuwen [0929 4371 2429] of the Institute of Acoustics, Chinese Academy of Sciences]

[Text] The concentrated suspension theory in granular media set up by the author is presented concisely in this paper. By comparing its numerical results with the relevant data published, a satisfactory consistency can be obtained. As far as the relationship of the attenuation coefficients in marine sediments to the frequency is concerned, a controversy among some authors has existed for a long time, i.e., it appears to be a linear dependence upon frequency in the high-frequency range (higher than several kilohertz) and to deviate somewhat from first power dependence in the low-frequency range (lower than 1 kilohertz). However, according to the author's theory, reasonable unity can be achieved. Through an investigation of the measurement of the granular media by means of the acoustic method, the author believes that, in addition to the mean diameter, the second granular parameter, such as the sorting coefficient, is necessary to enable a full characterization of the granular media.

This theory may offer a theoretical basis for designing new equipment to measure granular parameters.

9717

TOPOLOGICAL CLASSIFICATION OF MAGNETIC DOMAIN WALLS OF TUBE-, ENVELOPE-TYPE

40090067f Beijing WULI XUEBAO [ACTA PHYSICA SINICA] in Chinese Vol 37 No 1, Jan 88 pp 95-104

[English abstract of article by Yan Fengli [7051 7364 0448] of the Department of Physics, Hebei Normal University, Shijiazhuang; Li Bozang [2621 0130 5258] of the Institute of Physics, Chinese Academy of Sciences]

[Text] The classification of the static magnetic domain wall structures of the tube- and envelope-type is made in a unified way using the homotopy theory. The sets of topological classes for these two kinds of magnetic domain walls, $G_w^{(n)}$ and $\bar{G}_w^{(n)}$, correspond respectively, one-by-one, to the sets of homotopy classes relative to n+1 base points for the $S^2 \to S^2$ and $S^3 \to S^2$ continuous maps. Either $G_w^{(n)}$ or $\bar{G}_w^{(n)}$, therefore, can be constructed into a group isomorphic to Z, the additive group of integers. We call them the tube-wall group and envelope-wall group of type n, respectively. The "winding number" introduced by Slonczewski, et al., is considered anew. The sufficient and necessary conditions under which the "winding number" is allowed to be taken as the tube-wall class index are obtained. Finally, the topological classification of the magnetization states with M tube-walls and N envelope-walls coexisting is discussed. It is shown that the set of the corresponding topological classes, $G_w^{(M,N)}$, can be constructed into a group isomorphic to Z^{M+N}, the M+N dimensional lattice vector group. It is then referred to as the mix-wall group of type [M,N].

9717

THEORY OF POLARITONS IN DISORDERED MATERIALS, RAYLEIGH SCATTERING IN SiO_2, GeO_2 GLASSES

40090070a Shanghai GUANGXUE XUEBAO [ACTA OPTICA SINICA] in Chinese Vol 8 No 2, Feb 88 pp 97-104

[English abstract of article by Sun Hong [1327 1738], et al., of the Department of Physics, Shanghai Jiaotong University]

[Text] A theory of polaritons in disordered materials is proposed with the help of Green functions and diagrammatic methods. Rayleigh scattering in SiO_2 and GeO_2 glasses is calculated and the magnitudes of contributions to Rayleigh scattering from different disorder mechanisms are analyzed based on the theory, verifying the assumption in the fictive temperature approximation that Rayleigh scattering in glasses comes mainly from the density fluctuations in the glass solutions. The Rayleigh scatterings, as well as the effects of the polariton dispersions on the losses, are calculated for SiO_2 and GeO_2 glasses. The results show that, at the minimum loss wavelengths, the relative deviations of the Rayleigh scattering losses caused by the dispersion effects from the λ^{-4} law are 20 and 11 percent for SiO_2 and GeO_2 glasses, respectively.

9717

MAGNETO-OPTIC EFFECTS OF SOLIDS, THEIR PROPERTIES INVOLVING STRESS, TEMPERATURE, DISPERSION

40090070b Shanghai GUANGXUE XUEBAO [ACTA OPTICA SINICA] in Chinese Vol 8 No 2, Feb 88 pp 105-115

[English abstract of article by Liu Gongqiang [0491 0361 1730], et al., of the Department of Applied Physics, Shanghai Jiaotong University]

[Text] Fundamental formulas of magneto-optical effects are deduced according to classical theories concerning electro-magnetic fields. Obvious expressions of the Faraday rotation θ that are applicable to various magneto-optic media are obtained by using the concepts of effective fields. It is proved that θ is proportional to the effective field H_i and has a strong dispersion nature. θ is obviously affected by the external stress in the weakly magnetic media. The Verdet constant V of diamagnetic media is independent of temperature T. The ratio of the Verdet constant V_p of some paramagnetic media and their susceptibility χ satisfies the relationship $V_p/\chi = G(1+RT)$. In the antiferromagnetic and ferromagnetic media, θ is related to magnetization M_i of the various sublattices, and the temperature property of θ is dependent not only on M_i of the sublattices, but also on the temperature dependence of the magneto-optic coefficients. The experimental results conform closely to the deduced expressions. It has also been proved that, when the direction of light propagation is perpendicular to that of the effective field H_i, the linearly polarized light entering the magneto-optic medium would be resolved into an elliptical polarized light and a linearly polarized light, and the real and imaginary parts of the phase retardation ratio of this type of magnetic birefringence would be proportional to H_i^2.

9717

STUDY OF ENERGY DEPOSITION PROPERTIES OF XeCl EXCIMER LASER PUMPED BY C-C TRANSFERRED DISCHARGE

40090070c Shanghai GUANGXUE XUEBAO [ACTA OPTICA SINICA] in Chinese Vol 8 No 2, Feb 88 pp 125-131

[English abstract of article by Wang Shaoying [3769 4801 5391], et al., of Anhui Institute of Optics and Fine Mechanics, Chinese Academy of Sciences]

[Text] Based on the measured current and voltage oscillograms in laser discharge, laser output signals and an analysis of the pumping circuit, the authors have analyzed in detail the energy deposition process of the XeCl laser pumped by a C-C transferred discharge. Some results, useful for the design of similar lasers, are presented.

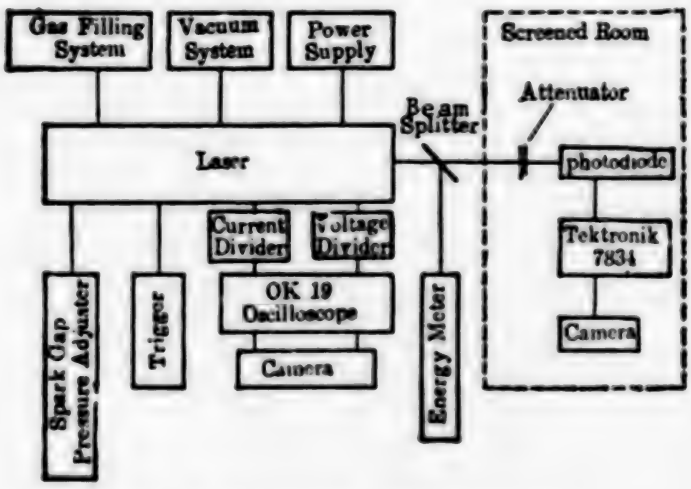

Block diagram of the experimental arrangement.

9717

OPTICAL MULTI-STABILITY, INSTABILITY FOR CO_2 LASER WITH FEEDBACK Q-SWITCHING

40090070d Shanghai GUANGXUE XUEBAO [ACTA OPTICA SINICA] in Chinese Vol 8 No 2, Feb 88 pp 132-139

[English abstract of article by Chen Lixue [7115 2980 1331], et al., of the Department of Applied Physics, Harbin Institute of Polytechnology]

[Text] It has been determined that the optical bistability and multi-stability of the CO_2 laser can be realized when an electro-optical modulator is inserted into the laser cavity, changing the Q-value of the laser by the opto-electric signal proportional to the output intensity of the laser. The mathematical model for the laser, described by three nonlinear first-order differential equations, has been set up. Its steady state model exhibits the characteristics of bistability and multi-stability, which have been confirmed by theoretical analysis and numerical calculation.

9717

BRIEFS

MILITARY DOCUMENT RETRIEVAL NETWORK--The "Chinese-language Military Document Retrieval and Service Network System" developed over a three-year period by the Academy of Military Scienc -China's first such microcomputer network system--has been officially placed into operation. Over 24,000 military periodical documents and over 6,000 book catalogs and abstracts have already been entered into the system. Using the variable-length data format--which can store three times as much data as the fixed-length format--data is entered in eight ways, including by class number, topic name, translator, topic word, publisher, and date. Network service is provided to libraries and intra-Academy offices so that laboratory researchers can conveniently consult the database. [Summary] [Beijing GUANGMING RIBAO in Chinese 15 Feb 88 p 2] 08309

JINGYUE COMPUTER'S RAPID DEVELOPMENT--The Beijing/Guangdong ["Jingyue" 0079 4727] Chinese-character Computer Development Research Center has now expanded its product line of Chinese computer systems to 14 models in 5 categories. Jingyue products, which in the last few years have won 8 awards at the provincial level and higher, were used at the 13th Communist Party Congress and at the Sixth National Games. In comparison with similar microcomputers widely available in China and overseas, these products demonstrate advanced concepts, almost twice the operational speed, greater overall storage, and better display performance. They come with a large number of applications software packages, including "complete form" [quan xing 0356 1748] Chinese-character processing and system-level high-quality Chinese-character printing, and can accommodate several Chinese-character inputting techniques. [Summary] [Beijing GUANGMING RIBAO in Chinese 16 Feb 88 p 1] 08309

CAS SINICIZES UNIX OPERATING SYSTEM--The Chinese Academy of Sciences' (CAS) Software Institute has announced that its Sinicized UNIX Operating System, incorporated into the Chinese-made Zijin 0530, the Langchao 0530, and similar compatible computers, has resulted in tangible economic and social benefits. Over many years, CAS achieved this transformation of UNIX by first examining its kernel, then moving on to its shell command interpretation system, its file and 10-record management system, its electronic mail function, its logic system, its high-level language, its DBMS, and its network communications software. The two now-Sinicized systems--UNIX System V and XENIX--can work in

complete compatibility with the original systems, not only providing the user with a low-priced practical Chinese-character output system, but also completely retaining the original systems' functional style and utility. [Summary] [Beijing GHANGMING RIBAO in Chinese 19 Feb 88 p 1] 08309

NEW FIBER-OPTIC SENSOR--A new fiber-optic sensor--a pyrometric-cone-style wavelength-division-multiplexer--developed by Shanghai University of Science & Technology underwent evaluation a few days ago. Technical specialists unanimously agreed that this product fills a domestic gap and that its quality has reached that of internationally famous firms' products as of 1987. [Text] [Beijing GUANGMING RIBAO in Chinese 21 Feb 88 p 1] 08309

NEW PHOTOELECTRIC SWITCH--A new photoelectric energy-saving switch developed by the Zhaoyang [2600 7122] Scientific Instrument Factory of Beijing recently underwent municipal-level technical appraisal. This dry-reed-relay-style microswitch not only fills a domestic void but also can save on foreign exchange; its performance is even better than that of similar foreign products. It is estimated that its installation in a room can save approximately 45% on electric energy. [Summary] [Beijing RENMIN RIBAO [PEOPLE'S DAILY] (Overseas Edition) in Chinese 12 Mar 88 p 1] 08309

ROCKET ENGINE COMBUSTION COMPUTATIONAL MODEL--Changsha (Xinhua), 12 Mar--The liquid-fuel rocket engine combustion chamber computational model developed by the National Defense Science & Technology University underwent technical evaluation a few days ago by a panel of nationally known astronautics specialists. This worldwide state-of-the-art technology will open a new stage in China's R&D of liquid-fuel rocket engines. The model uses several advanced techniques such as an ultramicropump fuel system and laser ignition. The unit is designed for detailed quantitative analysis of the combustion course and various structural parameters, operational parameters, and propellant characteristics, as well as for fault analysis of jet richness degradation [rao shi 7437 5793] and improvement thereof. It has broad applications in computer simulation of power sets for heavy launch vehicles and space-shuttle systems. [Text] [Beijing RENMIN RIBAO [PEOPLE'S DAILY] (Overseas Edition) in Chinese 14 Mar 88 p 1] 08309

NEW ZIJIN MICROCOMPUTER MODEL--The Zijin IIA microcomputer system, a new model in the 0300 optimum series and a key state project in the Seventh 5-Year Plan, was recently developed by the Nanjing Wire Electric [Youxiandian] Factory, and underwent design finalization accreditation in Nanjing in mid-January. Compatible with the Apple IIe, the Zijin IIA has a 6502 CPU, 64 KB RAM in a dual-chip 50464 IC, 16 KB ROM from a 27128/27256 IC and a two-chip 2732 IC. It can handle not only Zijin and Apple IIe high-capacity system software and selected expansion software, but also the newly developed utility software for Chinese word processing and report processing, and the newly developed high-resolution Chinese graphics display card. The Zijin IIA is 90% domestically made, with an improved cost performance. It has applications not only in elementary and middle-school computer literacy courses and as a teaching side, but also in the areas of business management, industrial control, and small-scale word processing. [Summary] [Beijing JISUANJI SHIJIE [CHINA COMPUTERWORLD] in Chinese 10 Feb 88 p 1] 08309

FIBER-OPTIC COMMUNICATIONS PRODUCTS--Five scientific achievements of the Beijing Glass Institute--an optical terminal for fiber-optic closed-circuit color TV transmission, a digital TTL level terminal, a 32-channel time-division-multiplexing fiber-optic digital transmission installation, an infrared tachometer using a fiber-optic sensor, and an apparatus for manufacturing cable from optical fiber--recently underwent municipal-level evaluation in Beijing. The circuit design for these products is reasonable, performance is good, and practicality is high. The recently inaugurated "Eastern Beijing Traffic-Signal Control System"--China's first such worldwide state-of-the-art system--completely utilized these optical cable and optical terminal products for its image signal transmission. These five scientific achievements have contributed to China's development of fiber-optic communications technology. [Text] [Beijing WUXIANDIAN [RADIO] in Chinese No 1, (Jan) 88 p 24] 08309

FIRST INSTALLATION OF C-1 MINISUPERCOMPUTER--China has installed its first model C-1 minisupercomputer at the Chinese Academy of Sciences' Atmospheric Physics Institute. This computer's word length is 64 bits, vector speed is 40 MFOB, scalar speed is 4Mips, internal storage is 32MB, and disk system storage is 2800 MB, making it the strongest imported system in computational capacity. Also provided is a dual-CPU Pyramid 98X reduced-instruction-set computer which permits the user to access the C-1's kilomega-capacity disk drive through an Ethernet linkup. Including the C-1 and the 98X, the system's domestic price is US$1.1 million. [Text] [Beijing JISUANJI SHIJIE [CHINA COMPUTERWORLD] in Chinese 3 Feb 88 p 1] 08309

BROADBAND SOLID-STATE OSCILLATOR, SIGNAL-SOURCE SERIES--The "40-120GHz broadband solid-state harmodotron [i.e., millimeter-wave oscillator] and signal-source series" developed by the Applied Physics Department of the Chengdu Institute of Telecommunications Engineering has undergone technical appraisal by the Ministry of Electronics Industry. This achievement fills a gap in domestic broadband millimeter-wave sources. Several of the main technical indicators have reached or exceeded the international state-of-the-art as of 1986, while others have reached the domestic state-of-the-art. This first [domestic] manufacture of a broadband millimeter-wave solid-state source provides the necessary conditions for further domestic development of millimeter-wave resources, and meets the urgent need for millimeter-wave technological development in the research, production, and education sectors. This product's superior cost performance hopefully will enable it to be introduced into the world market. [Text] [Beijing WUXIANDIAN [RADIO] in Chinese No 1, (Jan) 88 p 24] 08309

CSO: 40080094

PROPAGATION OF ACOUSTIC GRAVITY WAVE SPECTRUM THROUGH VERTICAL WIND SHEAR REGION

40090068a Beijing DIQIU WULI XUEBAO [ACTA GEOPHYSICA SINICA] in Chinese Vol 31 No 1, Jan 88 pp 1-9

[English abstract of article by Yi Fan [2496 1581] and Liang Baixian [2733 4102 0341] of the Department of Space Physics, Wuhan University; Li Jun [2621 6874] of Wuhan Institute of Physics, Chinese Academy of Sciences]

[Text] In this paper, the variation in spectral structures of acoustic gravity waves (AGWs) propagating through a vertical wind shear region is investigated. Using the compressible hydrodynamic equations, a spectral equation describing the propagation of AGWs in a vertical wind shear region is derived. It is pointed out that the spectral equation is a generalized form of the Taylor-Goldstein equation for the case of compressible medium and arbitrary vertical wavelength. Starting from the spectral equation, considering an AGW force with a two-dimensional Gaussian spectrum at its lower boundary and by using a differential method, the AGW spectrum at a higher level is calculated. It is shown that under the influence of the vertical wind shear, the AGW's spectral structure is considerable changed as follows: 1. Some spectral components in the forcing spectrum are filtered off and, therefore, several sharp spectral peaks occur. 2. The main peak moves in a frequency-wave number space. 3. The spectrum at a higher level becomes narrower. These calculated results may explain some of the phenomena observed in the ionosphere.

9717

EXPERIMENTAL STUDY OF EXCITATION FACTOR FOR TE MODE OF VLG RADIOWAVES OVER EAST-WEST PATHS

40090068b Beijing DIQIU WULI XUEBAO [ACTA GEOPHYSICA SINICA] in Chinese
Vol 31 No 1, Jan 88 pp 21-26

[English abstract of article by Liu Wantong [0491 8001 6639] of the China Research Institute of Radiowave Propagation, Henan, Xinxiang]

[Text] In this paper, phase changes in signals from the H and C stations of the Omega system are analyzed, with the signals being received simultaneously at Xinxiang and Lingtong. The existence and characteristics of the TE modes are determined from the measured data for the four possible propagation paths.

The excitation factor of the TE mode is obtained through solving a set of leading equations using the regression method. However, the value of the factor deduced from the experimental results seems to be larger than the theoretical one when using the propagation of VLF radiowaves over east-west paths at night.

9717

ISOLATION, IDENTIFICATION OF MARINE LUMINOUS BACTERIA FROM WATERS OF SOUTH CHINA SEA

40091044a Beijing HAIYANG YU HUZHAO [OCEANOLOGIA ET LIMNOLOGIA SINICA] in Chinese Vol 19 No 1 Jan 88 p 80

[Abstract by Shen Jianwei (now in "Institute of Biotechnicology, Shanghai Jiao Tong University, China", Zhu Wenjie, Wu Zirong, Qian Lingmei, Liang Peiqing, and Yang Yikang with East China Normal University, Shanghai]

[Abstract] One hundred and nineteen strains of marine luminous bacteria from the waters of the South China Sea were submitted to an extensive characterization. A numerical analysis of the results by computer grouped these strains and other typical strains into two clusters which were formed with the overall phenotypic similarity and single linkage. These two clusters include the typical strains of Photobacterium leiognathi and Vibrio harveyi. According to this analysis and the description of these two species in "Bergey's Manual of Systematic Bacteriology", the strains of these two clusters are readily identified as Photobacterium leiognathi and Vibrio harveyi respectively.

/9274

REVIEW OF MARINE ENVIRONMENTAL CHEMISTRY

40091044b Beijing HAIYANG YU HUZHAO [OCEANOLOGIA ET LIMNOLOGIA SINICA] in Chinese Vol 19 No 1,Jan 88 p 100

[By Li Xu and Gu Hongkan, of the Institute of Oceanology, Academia Sinica, Qingdao]

[Abstract] A review of marine environmental Chemistry is given in four aspects, i.e. pollutants and their sources, transfer and exchange, laboratory modelling and enclosed ocean experiments, and environment analytical chemistry.

The environmental capacity of the ocean and atmosphere is almost without limit, so obvious pollution is just within the limits near pollution source. The pollutants from human activities is not so great as to affect the vast ocean and atmosphere. Therefore, the increasing temperature of earth and the El Nino are mainly the natural rules, not the greenhouse effect etc. from human. Thus city water without treatment can directly discharge into the offshore ocean current through the pipe. However, industry sewage area are not suitable for fishery because of long term effects on ecosystem.

The free ions Zn^{2+} and Cu^{2+} are highly toxic to shrimps, but the Zn and Cu in suspended particle are not. The free ions Zn^{2+} and Cu^{2+} of natural seawater can be analyzed by "Anti-adsorption physically coated mercury film electrode system" without any reagent. If the seawater is acidified, the Zn and Cu in suspended particle will be dissolved into free ions and highly analytical results which has no meaning to toxicity will be obtained. Because of this, the national environment standards of Zn^{2+} and Cu^{2+} concentrations are rather too high.

The fine particles from car and factory can pass through the air filter, so the analytical results of trace metal ions in clean laboratory in polluted city has not much reliability. There is no real clean laboratory in air polluted city, especially use the analytical method with acidified water sample and AAS that has big influence from fine particles.

Moving clean laboratory and its research vessel, underwater concentrator, and underwater probe has to be developed for analysis on shipboard and sea in situ.

/9274

BRIEFS

DEEP SUBMERSIBLE SUIT DEVELOPED--Guangzhou has developed an "armored man" to be used in deep-dive seabed operations. The KZF-1 armored type normal-pressure submersible is the first in the world to be made of titanium. The device was developed in 1987 by the Guangzhou Marine Salvage and Rescue Equipment Institute and a dozen or so other units in a joint research effort. This recently developed submersible device is on a par with similar units in the world. Nicknamed "armored man", the suit can maintain a pressure of 1 atmosphere, enabling its single operator to descend to depths of 300 meters and carry out work for fairly long periods of time. It will be used in work to develop offshore coastal resources, marine engineering, and in missions for the Navy. [Text] [Guangzhou NANFANG RIBAO in Chinese 20 Feb 88 p 2] /9738

CSO: 40081059

ISOLATION, CHARACTERISTICS OF PHENOL-DEGRADING, Hg-RESISTANT BACTERIA

40091042 Guangzhou ZHONGSHAN DAXUE XUEBAO [ACTA SCIENTIARUM NATURALIUM UNIVERSITATIS SUNYATSENI] (NATURAL SCIENCES EDITION) in Chinese No 4, Oct 87 pp 111-114

[English abstract of article by Zhou Shining [0719 0013 1337] of the Department of Biology]

[Text] A Pseudomonas species designated as S7 was isolated from a polluted environment using a minimal medium containing salicylate as the sole carbon source and a rich medium containing $HgCl_2$. The organism could degrade and utilize phenol, salicylate, benzoic acid or catechal as the sole carbon source and was resistant to $HgCl_2$ when it was grown in a rich medium. The minimal inhibitory concentration of phenol for the bacterium was 7.4 mM. The degradation of phenol and salicylate by S7 was inducible and regulated by catechal or its catabolites as a repressor. S7 is a promising environmental cleaning bacterium.

9717

WIDER COAL ASH UTILIZATION

40081055 Beijing ZHONGGUO HUANJING BAO in Chinese 1 Dec 87 p 1

[Article by reporter Liu Xiaojie (0491 2556 2212)]

[Summary] The State Economic Commission has decided to establish a coal ash utilization coordination group to expand the use of the waste material and has posted the target of using 2.5 million tons of coal ash in 1988. Since 6 million tons of coal ash is discharged each year by thermal power plants, how to treat and how to utilize this waste material become serious problems of the electrical engineering groups. Although a dozen methods have been tested, still no progress has been made. The utilization rate still stays around 20 percent. Coal ash can be used as ballast for road building if it is first made to react with water and them mixed with concrete. After being tested in Beijing, Shanghai, and Tianjin, coal ash proved capable of bearing heavy loads without subsidence. This characteristic of coal ash provides not only a sound way to control environmental pollution caused by rising production of the ash, but saves funds for road construction due to its remarkable economic benefit. Today urgent attention should be paid to using 100,000 tons of ash to construct 1 mile of superhighway and reducing construction cost.

/9738

NEW ADVANCES IN ULTRASOUND THERAPY BEING MADE

40081030 Beijing YINGYONG SHENGXUE [APPLIED ACOUSTICS] in Chinese Vol 6 No 4, Oct 87 pp 6-9

[Article by Zhou Wansong [0719 8001 2646] of the Department of Physiotherapy, Beijing Central Army Hospital: "New Advances in Ultrasound Therapy in China"]

[Text] Abstract: Ultrasound therapy is an effective treatment method which has a broad range of clinical applications. On the basis of using ultrasound therapy in China to treat hemiparalysis caused by cerebrovascular disease, sciatica, bronchitis, coronary heart disease, pain in the soft tissue of the neck, shoulders, lumbus, and legs, injury to joints and soft tissues, peripheral omarthritis, upper urinary tract calculus, central retinitis, herpes zoster, carpopedal tinea, neurodermatitis, acute and chronic maxilliary sinusitis, and other diseases[1], advances also have been made in other areas. They will be summarized and evaluated here.

I. Clinical Applications

1. Internal diseases

On the basis of previous applications of ultrasound therapy to treat hemiparalysis caused by cerebrovascular accidents,[1] advances have been made in the use of ultrasound "intensification" treatment methods. These methods combine affected projection region therapy with cerebral cortex functional location region therapy. The functional location regions of the cerebral cortex are the speech intensification region, the movement intensification region, the intelligence intensification region, the central blindness intensification region, and the pelvic and visceral intensification region. This method was used to treat 110 cases. They included 52 cases of encephalitis B in the recovery stage and sequela. Among these cases, it was effective in 36 cases with paralysis, including 28 recovered and improved cases. In 49 cases of aphasia, it was effective in 34 cases, including 16 recovered and improved cases. The results were rather good in all 48 cases of cerebrovascular accidents and hemiparalysis. The results also were rather apparent in 12 cases of toxic encephelopathy. Overall, the efficacy of the treatment was greater for paralysis than for aphasia, and there was even restoration to varying degrees of limb function in cases of post-encephalitis B sequela which had existed for more than 10 years. The author[2] felt that the

mental disorders, limb paralysis, and aphasia disorders manifested in the above disorders as well as certain cases of blindness, urinary and fecal incontinence, and so on, were functional disorders with a specific cortex function site on the cerebral cortex. Practice has proven that "intensification" therapy for projection sites of the cortex function sites plays a definite role in improved treatment. Another author has reported[3] that comprehensive treatment of hemiparalysis caused by cerebrovascular diseases focused on ultrasound therapy provided rather good results, with a 98 percent overall rate of effectiveness and a rate of recovery and obvious improvement as high as 93.1 percent. Frequent passive movement of the paralyzed limbs is necessary. The use of ultrasonics and point low frequency electricity to treat hemiparalysis caused by cerebrovascular thrombus has the advantages of being very effective, providing quick results, causing no pain to the patient, and so on. This treatment can promote the physiological functions of the central nervous system, peripheral nervous system, and muscles, and it also improves and restores them.[4] Other authors have reported that rather good results have been obtained in the use of ultrasound therapy for injury to the central nervous system suffered during battle.[5]

The results of using ultrasound therapy to treat severe carbon monoxide toxic encephelopathy were obvious. After one or two ultrasound therapy treatments, consciousness is clear, speech is restored, and muscle functions are restored.[6] In another case of carbon monoxide toxic encephalopathy, the patient could sit up after one ultrasound therapy treatment, and could nod, cry, and answer questions after three treatments. Restoration of speech functions began after six treatments, and the patient could stand by himself after 13 treatments and walk by himself, carry on a conversation, and be dismissed from the hospital after 17 treatments.[7]

Retesting regarding these craniocerebral diseases showed that ultrasound therapy is an effective treatment method which has definite value in clinical applications.

Ultrasound point therapy for nervous headaches was effective in 92 percent of 50 cases.[8] Ultrasound and iodine ions also were used to treat one case of right-side phrenic paralysis.[9]

In 110 cases of peripheral surface phrenic paralysis treated with ultrasound therapy, symptoms disappeared and facial expression was restored in 58 recovered cases. The symptoms were basically eliminated and rather obvious improvements were seen in 29 patients, so it was effective in 99.1 percent of all the cases. The effects of the treatment in 57 cases were confirmed by tracking for 1 year. During ultrasound therapy, intensified treatment focused on the nerve outlet holes at the lower surface of the margin of the ears can play a role in improving the function of nerve cell membranes, reducing nerve swelling and edema, and other things.[10]

Results also were obtained in ultrasound treatment of coronary heart disease.[1] The effectiveness in treating patients with simple coronary artery blood supply inadequacies was rather good, but it should be used cautiously in coronary heart patients with cardiac slowness and heart blockage to avoid making the disease

more serious.[11] The use of ultrasound on eight points including the umbilicus, antidiarrheal, front-Mu point of the large intestine (St 25), Shui-fen (Ren-9), and others was effective in treating 97 percent of 100 cases of diarrhea caused by acute and chronic bacterial dysentery, acute and chronic gastroenteritis and other diseases, so the results were excellent.[12] There also are reports of excellent results in the use of ultrasound points to treat diseases caused by bowel function disorders, acute and chronic enteritis, poor digestion in children, and other disorders.[13]

Ultrasound therapy was effective in 97.8 percent of 78 cases of bronchial pneumonia, while the rate of effectiveness in a comparison group treated pharmacologically was 87.5 percent. The effectiveness of the treatment in the ultrasound therapy group obviously was superior to that in the pharmacologically-treated comparison group ($P < 0.01$). At the time of treatment, the sound head was attached closely to the back in the Rale apparent site using small circular movements for treatment.[14]

Obvious results have been obtained in the use of ultrasound, sound frequency electrotherapy, and electromagnetic massage to treat one case of gastroliths. After 15 treatments, X-ray re-examination showed that the stones in the stomach had disappeared.[15]

2. External diseases

Rather good results were obtained in the use of ultrasound to treat Raynaud's disease. In treating seven cases, there were four cases in which a blood flow chart and re-examination with a thin arterioscope showed an increase in pulse blood flow.[16]

The use of ultrasound therapy to treat the epididymidis accumulations which occur after vasoligation had good results, produced results quickly, and had a short course of treatment.[17]

Ultrasonic waves superimposed on pulsed electric current were effective treatment in all of 64 cases of sciatica, acute sprains and contusions, stiff necks, hypertrophic rachitis, and neck and shoulder syndrome.[18] Another author reported that ultrasound-intermittent electric current was effective in treating 105 of 113 cases of lower abdominal pain disorders and peripheral omitis.[19] Ultrasound also has been used in conjunction with equal amplitude intermediate frequency sinusoidal current to treat peripheral omitis, musculus piriformis syndrome, etc.[20] Ultrasound-sinusoidal modulated intermediate frequency electrotherapy has been used to treat peripheral omitis, strain, chronic pelvic inflamation, and so on.[21] Ultrasound and intermittent current has been used to treat peripheral omitis.[22] Ultrasound point therapy devices also have been used to treat sciatica and peripheral omitis.[40] The results in all of these applications have been rather good. Ultrasound therapy is quite effective in treating costal chondritis.[24] There were obvious benefits to post-injection induration from ultrasound therapy.[27]

Scar induration or hemotoma organization are extremely common in healing wounds. Ultrasound in conjunction with iodine ion DC injection treatments was completely effective.[28]

The results have been excellent in ultrasound therapy for mammary gland disorders, including treatment of mammary gland enlargement[29] and acute mastitis.[30] Obvious results have been achieved in treatment of slowed or delayed formation of crust on broken bones in adult femurs and trunk bones.[31] The use of ultrasound therapy to treat six cases of warts also has been reported.[33]

3. Other diseases

The results were excellent in the use of ultrasound to treat temporomandikular joint syndrome.[34] The shorter the course of treatment in ultrasonic drug injection to treat chronic pharyngitis, the better the results.[35]

Rather good results were obtained in potassium iodide ultrasonic injection therapy for 40 cases of fundulus oculi diseases, including central retinitis, optic nerve atrophy, macula lutea hemorrhage, uveitis and meningitis, retinal pre-papillary membranes, and retinal peripheral phlebitis.[36] Ultrasound therapy also has been used to treat central retinitis[37] and traumatic anterior hemorrhagic secondary glaucoma, with rather good results in both.

II. Experimental Research

To learn if ultrasound superimposed on modulated intermediate frequency electric current could increase its effectiveness, we observed its role in analgesia, promoting blood circulation, improving vein and lymph backflow, and softening scars and lysing adhesions. Its role in analgesia was studied in a group of 120 healthy adults. The results were that the pain threshold in a group receiving ultrasound combined with modulated intermediate frequency current was quite obviously higher than that in a group which received only ultrasound and a group which received only modulated intermediate frequency current. By measuring the skin temperature of the subjects, it was discovered that the skin temperature of a group which received ultrasound combined with modulated intermediate frequency was higher than that of a group which received only ultrasound and a group which received only intermediate frequency current. The group which received ultrasound in conjunction with modulated intermediate frequency current also showed superior results to the groups receiving only ultrasound or only modulated intermediate frequency current in improving vein backflow, lymph backflow, and in softening scars and lysing adhesions. This shows that the two factors have coordinative effects when used simultaneously, which can increase their effectiveness.[25]

To observe analgesia following ultrasound-intermittent current therapy on the human body, some authors carried out comparative experimental research before and after a single treatment. The results of the experiment with 50 subjects showed that after the subjects had received the effects for 6 minutes, a photothermal method used to measure the pain threshold and compare the before-and-after effects showed an obvious differential ($P < 0.01$) in pain threshold variation. It was 48.99 ± 16.79 seconds before treatment and 58.52 ± 16.70 seconds after treatment, indicating obvious analgesic effects.[26]

Isotopic radioactive iodine[3] was used to observe the effects of sinusoidal modulated ultrasound combined with synchronized superimposition of intermediate frequency current on drug uptake. Uptake was compared using ultrasound injection alone, modulated intermediate frequency current, and direct current. The results showed no apparent interaction between modulated intermediate frequency current and ultrasound.[23]

Some authors have carried out fluorescein sodium semi-transparent membrane uptake experiments to determine if it might be possible to increase drug uptake by combining ultrasound with pulsed current. The results showed that the uptake with combined application of ultrasound and pulsed current was obviously higher than uptake in a single instance of pulsed current ($P < 0.01$). The results of experiments on uptake of fluorescein sodium fanshu [5603 5620] stem tuber drug were that when examining the tissue slice under a fluorescent microscope, besides the strongest fluorescence appearing with the ultrasound-pulsed current cathode group, the pulsed current cathode group was stronger than the DC current electrode group. The results of fluorescein sodium rabbit skin drug experiments were basically the same as those in the fluorescein sodium fanshu stem tuber drug uptake experiments, in that the intensity of fluorescence was most apparent in the ultrasound-pulsed cathode group, indicating that uptake was the greatest. The results of the experimental research showed that drug uptake via ultrasound-pulsed current not only exceeded that of pulsed current alone but also that the tissue penetration of uptake was deeper. Under the effects of electric current, the ions follow the path of least electrical resistance, meaning that they migrate from the deep interstices between the cells, but the electrical resistance of the cell membranes is great, which prevents the drug from being taken into the cells. Under the effects of ultrasound, however, the transparency of the cell membranes is increased and the ions move from the cell interstices and easily pass into the cells. As a result, the joint application of ultrasound and pulsed current can be effective in injecting drugs.[32]

Human experimental observations were carried out to explore the effects of point ultrasound on gastric function. Ten minutes after an intramuscular injection of 18 healthy subjects in Group A with paspertin, peristalsis was speeded up in 16 subjects, and the sound of gurgling and hyperfunction grew louder and increased in frequency, averaging 47.3 times per minute. After He-Sea Point (S+36) ultrasound point therapy, the gurgling sounds of hyperfunction were reduced and their frequency decreased until they gradually returned to pre-injection levels. Compared with after the injection of paspertin, there was an obvious reduction in the number of gurgling sounds ($P < 0.01$). Group B was composed of 15 patients suffering from diarrhea and gastric function disorders. Gastric gurgling sounds decreased after treatment. Group C had 13 healthy individuals for systematic comparison. A non-emitting sound head was placed at the same points for 2 minutes, and there was no obvious difference in gastric gurgling sounds after the treatment ($P > 0.05$). These experimental results show that the use of ultrasound at the He-Sea Point (S+36) creates a gastric function readjustment effect which proves the intrinsic relationship between this point and the viscera. The anti-diarrheal actions of point ultrasound first of all involve control of hyperfunctioning peristalsis and readjustment of gastric function, aiding in the reabsorption of water and inorganic salts, which have anti-diarrheal effects. Moreover, the He-Sea and other

points also strengthen the immunity and anti-inflammation functions of organisms and increases organism resistance, which may be one of the main reasons for its efficacy.[12]

Some authors have studied ultrasound needles (ultrasound effect points) and their effects on skin temperature. Experimental measurements were made using ultrasound at 152 points on 23 people. The results were that the electrical resistance of the skin decreased following ultrasound therapy, with the current strength rising by an average of 1.59 to 3.28 μA. There were obvious differences before and after the effect ($P < 0.05$ to 0.01), and it also had certain effects on skin temperature. Measurements were made of 155 points on 32 subjects and a total of 42 points were measured for pulse ultrasound emission therapy. There were no obvious changes in skin teperature. Continuous ultrasound emission therapy on a total of 113 points, however, raised skin temperatures by an average of 1.375° to 2.05°C, and there was an obvious difference before and after treatment ($P < 0.01$). The length of time in which the rise in skin temperature from continuous ultrasound is sustained also was observed at 30 points. The result was no obvious difference from the skin temperature of a comparison group, while the skin temperature of the treated group rose an average of 1.5°C and continued to be 0.4°C higher after 2 hours.[39]

III. Development Trends and Prospects

The range of ultrasound therapy applications has broadened considerably in recent years and many diseases now are suited to ultrasound therapy appli ations. There have been some additional developments from previous diseases for ultrasound therapy applications. New explorations have been made in therapeutic methods to gain even better treatment results like "intensification" therapy for cerebrovascular and brain diseases.

In the area of experimental research, explorations into the mechanisms of action have attracted attention and valuable results have been obtained. It deserves mention that the action of ultrasound therapy on certain points improves certain functions in organisms. This was the first time that these research results have been suggested. They also aided in research and exploration on the mechanisms of acupuncture.

To improve the effectiveness of ultrasound therapy, many scholars in China have carried out rather thorough research on the combined application of ultrasound and other physical therapies, which in turn has led to new developments in treatment methods. Besides improvements in conventional methods, ultrasonic drug injection, ultrasound point methods, ultrasound vaporization and absorption treatment methods, ultrasound intermittent electrotherapy, and ultrasound weak DC electrotherapy,[1] improvements made in recent years have included ultrasound superimposed pulsed electrotherapy, ultrasound pulsed electrotherapy, ultrasound and equal-amplitude intermediate frequency sinusoidal electrotherapy, ultrasound-sinusoidal modulated electrotherapy, and so on. These new therapies have been proven in experimental research, and some of them have improved the effectiveness of treatment through clinical practice. Examples include authors who applied ultrasound-pulsed current drug ion injection therapies to treat 68 cases with waist sprains and strains. The results were obvious, with one patient being cured

after a single treatment.[32] These new treatment methods have a definite theoretical foundation. Ultrasound is a therapeutic factor, and other treatment methods also are physical therapy factors, so the organic integration of two types of physical therapy factors for combined use in the human body can permit them to play a coordinating role which increases therapeutic effectiveness. For this reason, besides traditional treatment methods, integrated utilization with other physical factors will be a future development trend.

Further exploration and research concerning clinical applications of ultrasound therapy and the mechanisms of therapeutic action will promote development and deepening of ultrasound therapy and gain even more achievements.

References

1. Zhou Wansong [0719 8001 2646], YINGYONG SHENGXUE [Applied Acoustics], Vol 2 No 2, 1983 p 29.
2. Jiang Luquan [1203 7773 5425], ZHONGHUA LILIAO ZAZHI [China Physiotherapy Journal], Vol 5 No 3, 1982 p 150.
3. Tao Ruijuan [7118 3843 1227], et al., ZHONGHUA LILIAO ZAZHI, Vol 5 No 4, 1982 p 223.
4. Cheng Mantang [2052 3341 1016], ZHONGHUA LILIAO ZAZHI, Vol 9 No 1, 1986 p 27.
5. Jin Wancheng, [6855 1346 2052], writer, RENMINJUN YI [PLA Medicine], No 9, 1983 p 16.
6. Yu Shixun [0205 0013 8113] et al., ZHONGHUA LILIAO ZAZHI, Vol 8 No 1, 1985 p 59.
7. Jiang Feilong [3068 7378 7893], ZHONGHUA LILIAO ZAZHI, Vol 8 No 2, 1985 p 115.
8. Li Yingqi [2621 5391 1142], ZHONGHUA LILIAO ZAZHI, Vol 9 No 1, 1986 p 33.
9. Yue Jiaxin [2867 0857 7451], ZHONGHUA LILIAO ZAZHI, Vol 6 No 1, 1983 p 53.
10. Yuan Mingxin [5913 2494 2450], ZHONGHUA LILIAO ZAZHI, Vol 5 No 4, 1982 p 220.
11. Wang Shuying [3769 3219 5391] et al., ZHONGHUA LILIAO ZAZHI, Vol 6 No 1, 1983 p 24.
12. Guo Zhiying [6753 1807 5391] et al., ZHONGHUA LILIAO ZAZHI, Vol 7 No 3, 1984 p 192.
13. Jin Wancheng et al., ZHONGHUA LILIAO ZAZHI, Vol 8 No 3, 1985 p 147.
14. Qu Jingyu [2575 7234 1342] et al., ZHONGHUA LILIAO ZAZHI, Vol 6 No 4, 1983 p 225.
15. Zhang Qinglin [1728 7230 2651], ZHONGHUA LILIAO ZAZHI, Vol 7 No 3, 1984 p 183.

16. Wu Zeyi [0702 0463 0308], ZHONGHUA LILIAO ZAZHI, Vol 6 No 2, 1983 p 99.

17. Liu Chaofan [0491 6389 0416] et al., ZHONGHUA LILIAO ZAZHI, Vol 6 No 1, 1983 p 26.

18. Wang Debin [3769 1795 1755] et al., ZHONGHUA LILIAO ZAZHI, Vol 6 No 12, 1983 p 60.

19. Sun Xingjiong [1327 2502 3518], ZHONGHUA LILIAO ZAZHI, Vol 7 No 2, 1984 p 94.

20. Chen Wenbin [7115 2429 1755] et al., ZHONGHUA LILIAO ZAZHI, Vol 8 No 1, 1985 p 40.

21. Zhang Zhen [1728 3791] et al., ZHONGHUA LILIAO ZAZHI, Vol 8 No 2, 1985 p 82.

22. Zhang Zhen et al., RENMINJUN YI, No 10, 1985 p 52.

23. Du Baocong [2629 1405 3827] et al., ZHONGHUA LILIAO ZAZHI, Vol 8 No 1, 1985 p 36.

24. Xiao Zhaoxiang [5135 0340 4382] et al., ZHONGHUA LILIAO ZAZHI, Vol 8 No 2, 1985 p 94.

25. Du Baocong et al., ZHONGHUA LILIAO ZAZHI, Vol 7 No 1, 1984 p 18.

26. Wang Tongjiang [3769 0681 3068] et al., ZHONGHUA LILIAO ZAZHI, Vol 7 No 4, 1984 p 219.

27. Hou Guihua [0186 2710 5478] et al., ZHONGHUA LILIAO ZAZHI, Vol 7 No 3, 1984 p 181.

28. Guo Dezhi [6753 1795 5365] et al., ZHONGHUA LILIAO ZAZHI, Vol 8 No 1, 1985 p 42.

29. Su Zhanfu [5685 0594 4395] et al., ZHONGHUA LILIAO ZAZHI, Vol 8 No 1, 1985 p 55.

30. Wei Zixiang [7614 3320 4382], ZHONGHUA LILIAO ZAZHI, Vol 8 No 1, 1985 p 48.

31. Chen Xiao [7115 2556], ZHONGHUA LILIAO ZAZHI, Vol 8 No 1, 1985 p 59.

32. Hong Xiu'e [3163 0208 6759], ZHONGHUA LILIAO ZAZHI, Vol 8 No 4, 1985 p 210.

33. Li Zhaobang [2621 0340 2831], ZHONGHUA LILIAO ZAZHI, Vol 5 No 3, 1982 p 163.

34. Chen Zuohua [7115 0146 5478] et al., ZHONGHUA LILIAO ZAZHI, Vol 6 No 1, 1983 p 60.

35. Zhou Jufen [0719 0547 5358] et al., ZHONGHUA LILIAO ZAZHI, Vol 6 No 2, 1983 p 91.

36. Liu Fengyun [0491 7364 0061] et al., ZHONGHUA LILIAO ZAZHI, Vol 6 No 2, 1983 p 93.

37. Xu Mingrui [6079 2494 3843] et al., ZHONGHUA LILIAO ZAZHI, Vol 5 No 4, 1982 p 34.

38. Wang Dongchu [3769 2639 0443] et al., RENMINJUN YI, No 6, 1984 p 50.

39. Jin Wancheng et al., ZHONGGUO ZHENJIU [Chinese Acupuncture and Moxibustion], Vol 4 No 5, 1984 p 1.

40. Guo Zhiying et al., ZHONGHUA LILIAO ZAZHI, Vol 6 No 1, 1983 p 47.

12539/08309

EFFECT OF MONOCLONAL ANTIBODIES ON PLATELET FUNCTION EXPLORED

40081052a Beijing KEXUE TONGBAO in Chinese Vol 32 No 24, Dec 87 pp 1902-1905

[Article by Chen Zhang [7115 3864], Bao Chengxin [0545 2110 9515], Yu Shouxin [0060 1947 2450], Jin Xueqin [6855 1331 0530], Wu Xiaowei [2976 2556 0251], Shen Decheng [3088 1795 6134], Li Jiazeng [2621 1367 1073], Tang Meihua [3282 5019 5478], Yang Xifeng [2799 1585 1496], Chen Guanzhen [7115 7070 3791], Qi Shuling [7871 3219 3781], and Ai Xuewen [0755 1331 2429], Hematology Institute, Chinese Academy of Medical Sciences, Tianjin: "A Group of Anti-Human Platelet Monoclonal Antibodies Having Different Functions"]

[Text] Anti-human platelet monoclonal antibodies obtained through the use of hybridoma techniques provide an important means for studying the relationship between blood platelet membrane structure and function. We discovered anti-platelet monoclonal antibodies to have different effects on platelet function: stimulating, inhibiting, or having no effect at all. Monoclonal antibodies having different functions can provide even richer data about blood platelet function and structure. This article describes a group of differently functioning types of monoclonal antibodies (inhibiting and stimulating) that we obtained.

I. Materials and Methods

We used immunofluorescence techniques[1] and ABC enzyme-linked immunization techniques on four monoclonal antibodies HIP_1, HIP_2, HI_{20}, and HI_{21} that we obtained through the use of hybridoma techniques for the study of the traits of monoclonal antibody tissue. We used competitive inhibition assays to study differences and similarities in monoclonal antibody identification of antigens; we used a group of standard rabbit-anti-rat Ig subgroup antisera to assay monoclonal antibody immunoglobin Ig types; we used protein A agarose CL-4B gel to purify monoclonal antibodies Ig; we used SDS-polyacrylamide gel electrophoresis to verify purity; and we used the iodine marker blood platelet solution immunoprecipitate method (completed with assistance from Dr Berndt of Westmead, Australia) to assay the antigenic determinants in monoclonal antibody identification. Please see references number 3 and 4 for the assay method used for blood platelet adherence and concentration. Blood clot retraction was assayed using the conventional method.

Table 1. Biological Traits of Four Different Antigens

Monoclonal Antibody	Type	Identified Antigen	Tissue Specificity						Function		
			Blood Platelet	Megakaryocyte	Granulocyte	Monocyte	Red Cell	Other Tissue	Aggregation	Adhesion	Blood Clot Retraction
SIP_1	G_1	GP Ib	+++	+++	-	-	-	-	-	-	-
SIP_2	G_3	GP IIb	+++	+++	-	-	-	-	+	-	+*
SI_{20}	G_1	ND	+++	+++	+	+	-	ND	+	-	-
SI_{21}	G_{20}	ND	+++	+++	+	+	-	ND	+	-	-

ND not done, * retraction not good

II. Results and Discussion

1. Biological Traits of the Four Different Monoclonal Antibodies. (See Table 1) The four antibodies belong to different types of Ig. HIP_1 belongs to IgG_1; HIP_2 belongs to IgG_3; HI_{20} belongs to IgG_1; and HI_{21} belongs to IgG_{2a}. Assay using the immunofluorescence method showed the HIP_1 and the HIP_2 to react only with the blood platelets and megakaryocytes, while the HI_{20} and HI_{21} reacted not only with the blood platelets, but also had a cross reaction with other cells. Results from the use of the immunoprecipitation method to analyze antigens identified in the HIP_1 and the HIP_2 showed the HIP_1 identification location to be the 35,000 peptide chain on the GP Ib alpha chain. Further analysis following trypsin digestion of GP Ib showed the HIP_1 site at the end of the GP Ib alpha chain. Now it has been verified that the 35,000 peptide chain at the end of the GP Ib alpha chain is the functional site for Ristocetin induction platelets, and that the HIP_2 identified antigen to be GP IIb. (See Figure 1)

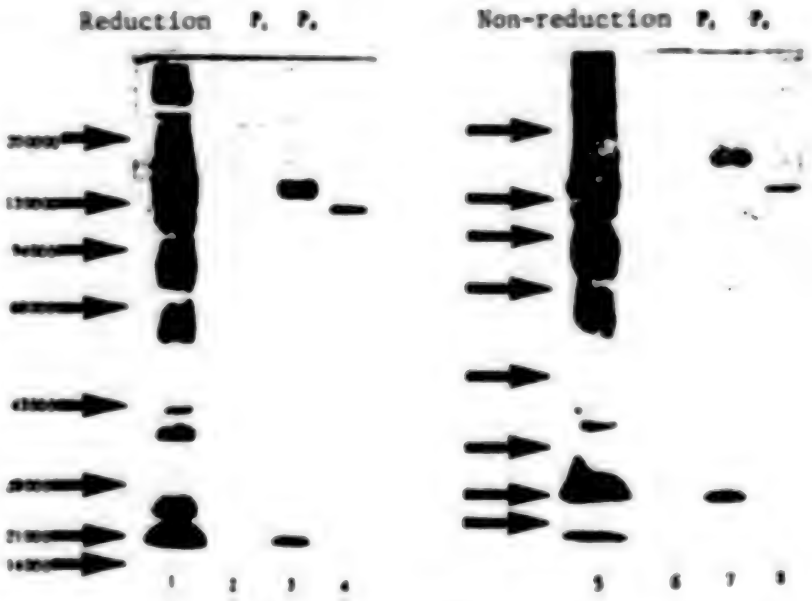

Figure 1. Figure Showing 5-15 Percent SDS Polyacrylamide Gel Electrophoresis of HIP_1 and HIP_2 Immunoprecipitate Marked Blood Platelets

2. Antigenetic Determinants Identified in the Four Kinds of Antigens. Table 2 shows a marked crossclosing in the fluorescent marked antigen HIP_1(HIP_1-FITC) and the international first anti-platelet GP Ib monoclonal antibody AN_{51}[5], but without competitive inhibition with other anti GP Ib monoclonal antibodies. There were no cross reactions between the marked monoclonal antibodies HIP_2(HIP_2-FITC) and the other monoclonal antibodies assayed in the table. Nor was there any cross reaction with the four monoclonal antibodies we prepared. Therefore, the HIP_1 is the first monoclonal antibody similar to the AN_{51} to be reported inside China. Their identical or extremely similar identified antigen site differs from that of the Chinese reported anti GP Ib monoclonal antibody SZ-2.

Table 2. Expression of Platelet Monoclonal Antibodies in Competitive Inhibition Assay

	HIP_1-FITC	HIP_2-FITC
HIP_1	--	++
HIP_2	++	--
HI_{20}	++	++
HI_{21}	++	++
SZ-2	++	++
AN_{51}	--	++
SZ-21	++	++

-- Platelets without fluorescent dye
++ Platelets showing fluorescent dye positive

3. Effects on Platelet Function

(1) HIP_1 is an inhibiting monoclonal antibody capable of blocking the platelet clumping reaction induced by Ristocetin (Figure 2) but without adversely affecting platelet adherence to the glass surface, which shows inability to block the combining of VWF and GP Ib.

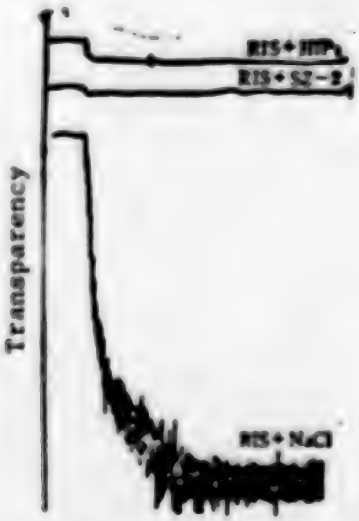

Figure 2. HIP_1 Inhibiting RIS Induction Platelet Coagulation

Figure 3. Four Curves for Anti Induction Platelet Calculation

(2) The three monoclonal antibodies HIP_2, HI_{20} and HI_{21} are all of the stimulating type, meaning that they can directly give rise to a clumping of platelets (Figure 3) without adversely affecting platelet adherence. Among these three monoclonal antibodies, the HIP_2 also is able to block clot retraction. Electron microscopy showed that when HIP_2 was present, fibrin formation was reduced (Figure 4 [not reproduced]). When non-anti-platelet

IgG_3 was used as a control, this did not happen. Neither the HI_{20} nor the HI_{21} has an adverse effect on clot retraction, showing that the HIP_2 had a role in fibrin formation.

Research on the mechanism whereby HIP_2 induces platelet clumping showed no clumping of platelets by HIP_2 in seven patients suffering from blood platelet anergy. Use of epoxidase inhibiting aspirin or ADP receptor competitive agent ADP, and ATP scavenger agent Apyrase inhibited in varying degrees the action of HIP_2 in inducing blood platelet clumping. HIP_2 can cause the clumping of washed blood platelets suspended in blood plasma or in blood serum; however, it cannot cause washed blood platelets to clump in a medium containing fibrinogen or blood serum that has been deactivated at 56°C for 30 minutes, or in EDTA-PRP (Table 3). The foregoing results suggest that the ability of HIP_2 to induce blood platelet clumping is through activated platelet membranes GP IIb or GP IIIa compounds. There has to be not only an alexine in the reaction medium, but metabolism by arachidonic acid, ADP dilution and calcium flow have to be relied on as well, the monoclonal antibodies of HIP_2 that has been purified by staphylococcus protein and the Fab from the digestion of its papain unite with the platelets to produce the clumping effect. HIP_2 and rabbit F(ab)' anti-rat F(ab) were used in the fluorescent marking of antibodies to carry out an indirect immunofluorescence assay of blood platelets, which exhibited a marked fluorescent positive reaction showing that the action of the HIP_2 on the platelets is not caused by Fc acceptors.

Table 3. Effect of Media Components on HIP_2 Induction Coagulation

Platelet type	Coagulation reaction
EDTA-PRP	-
WP + NP	+
WP + F	-
WP + NS	+
WP + killed NS	-

Note: PRP plasma rich in platelets, NP normal plasma, NS normal serum, F fibrinogen

References to stimulated monoclonal antibodies began to show up in foreign references in 1983, a total of seven reports having been seen to date[6-12] on 16 different monoclonal antibodies. In China, our first report was on three different monoclonal antibodies. We also did a fairly comprehensive and thoroughgoing study of HIP_2, finding it to be a new monoclonal antibody that differs from those reported in foreign journals.[13] Further research on another two stimulating monoclonal antibodies is currently under way.

REFERENCES

1. Chen, Z. et al., Cell. Immuno., 85 (1984), 297-308.

2. Hsu-Sm, et al., J. Histo. Chem. Cytochem., 30 (1982), 1079-1082.

3. Bao Chengxin et al., CHONGHUA XUEYEXUE ZAZHI [CHINESE HEMATOLOGY MAGAZINE], 1 (1980), 225-228.

4. Li Jiazeng et al., TIANJIN YIXUE ZAZHI [TIANJIN MEDICAL MAGAZINE], Blood Transfusion and Hematology Supplement, 1 (1963), 213-216.

5. Kuan, C., et al., Blood, 62 (1983), 800-807.

6. Thigarajin, P., et al., Am. J. Hematol., 14 (1983), 255-269.

7. Boucheix, C., et al., FEBS Lett., 161 (1983), 289-295.

8. Jennings, L.K., et al., Blood, 62 (1983). 258a (abstr).

9. Higashihara, M., et al., Blood, 65 (1985), 382-391.

10. Corman, D.J., et al., Nour. Rew. Fr. Hematol., 27 (1985), 255-259.

11. Modderman, P., et al., Throm. Haemost., 54 (1985), 197.

12. Miller, J.L., et al., Blood, 68 (1986), 743-761.

13. Bao Chengxin et al., CHONGHUA XUEYEXUE ZAZHI [CHINESE HEMATOLOGY MAGAZINE], 8 (1987), 65-69.

9432/6091

CORNEAL LESIONS INDUCED BY CO_2 LASER

40081052b Beijing ZHONGHUA YANKE ZAZHI [CHINESE JOURNAL OF OPHTHALMOLOGY] in Chinese Vol 23 No 6, Nov 87 pp 344-345

[Article by Xu Jiemin [1776 4309 2404], Xiao Lu [5135 7215], Zhou Shuying [0719 3219 5391], and Cao Weiqun [2580 4850 5028], Institute of Radiation Medicine, Chinese PLA Academy of Military Medicine: "Scanning Electron Microscopy of Corneal Lesions Induced by CO_2 Laser." Assistance was given by the Electron Microscope Unit of the Instruments Center and by the Institute's Instrument Measuring Unit, for which gratitude is hereby expressed.]

[Text] Abstract: This article reports scanning electron microscope observations of 31 normal and CO_2 irradiated rabbit corneas. The surface of a normal corneal epithelium is full of microvilli and microplicae, and shows up in scanning electron microscopy as light, medium and dark cells depending on their densities. Coagulation, depressions, edematious lesions, and nodule-like diverse surface changes may be observed on the cornea after CO_2 laser irradiation at dosage levels of 4-13 W/cm^2 for 0.12 seconds or 1.02 seconds.

Far infrared laser from a CO_2 laser at a wave length of 10.6 μm can be absorbed by non-metallic material, and the CO_2 laser absorption rate for moisture contained in biological tissue is very high. The moisture content of the cornea is approximately 70 percent. As a result, when irradiated by a CO_2 laser, more than 99 percent of the energy is absorbed by the cornea.[1] The extent to which a CO_2 laser damages a cornea varies with the irradiation dosage and the irradiation time. Large dosages of irradiation can create coagulation, edema, gasification and even puncturing of the cornea. This article reports scanning electron microscope observations of cornea damage caused by low dosage CO_2 irradiation for use in framing pertinent laser safety standards.

Assay Methods

The irradiation equipment used in the assay was a Model JGD-1 CO_2 laser device with 5 percent constant emission stability, a light intensity pattern of distribution close to single transverse [0830 2897 2875], and a 2.6 mrad light beam angle of divergence. Measurement of irradiation dosage was done with a Model NJ-J 1 laser energy measuring device, and a light distribution point reflecting type galvanometer. Monitoring was done with a pass

through [6639 6665 1709] dynamometer. Duration of irradiation was controlled with an electromechanical shutter, and real time monitoring was done, time measuring accuracy being within 2 percent. Before animals were irradiated, dosage tests were conducted to derive the cornea average incident power density.

The animals used in the assay were purplish blue-gray rabbits weighing approximately 2 kg each. Slit-lamp examination showed their corneas to be normal. During irradiation, the rabbits were placed in a three-dimensional adjustable frame, and an He-Ne laser of the same optical path was used for aiming. A diaphragm (ϕ 1 mm) was placed in front of the eyes to define the beam. The surface of each cornea was irradiated at five different points. Following irradiation, they were examined with a slit-lamp, and histopathology was examined under a scanning electron microscope.

Scanning electron microscopy was performed using conventional methods of preparation, a 4 percent solution of glutaric dialdehyde being used first to fix the corneas for between 12 and 24 hours. Then they were fixed for 2 hours in a 1 percent osmic acid solution after which an ethanol gradient was used to remove water, which was replaced with isoamyl acetate and dried to the CO_2 critical point. They were coated by ion sputtering and observed under a PHILIP Model 505 scanning electron microscope. A total of 31 rabbit corneas were observed in this assay.

Assay Results

1. Scanning Electron Microscope Imagery of Normal Cornea Epithelium

When observed under a scanning electron microscope, normal corneas are by no means smooth "mirror surfaces." There are countless microvilli and microplicae on the epithelium of the mosaic-like polygonal cornea. When enlarged slightly, the epithelium appears granular, coarse, and uneven, and the cells may be divided into dark, medium, and light. The cells show a random arrangement; however, the dark cells are usually clumped in piles, the cell nuclei being somewhat swollen. When enlarged more than 2,000 times, large numbers of microplicae and microvilli can be seen on the surface of the cornea, intersecting in a transverse direction, rising on the surface of the epithelium like ridges or fingers. Among some "senile" cells, newer small round "gaps" may be seen, between four and five "gaps" per one or several cells. The "gaps" range in size from less than 0.1 to more than 10 μm, and the cell rises all around the "gaps." Within the "gaps," microvilli and microplicae are frequently visible on the surface of the new cornea epithelial cells below.

2. Low Dosage CO_2 Laser Damage to Corneas Observed by a Slit-Lamp

This experiment used low dosage CO_2 laser irradiation, the cornea average incident power density being between 4 and 13 W/cm^2, and duration being 1.02 and 0.12 seconds. Damage was slight and superficial, being limited to the cornea epithelium. Slit-lamp observation revealed only small circular, light gray or grayish-white spots with clear edges. When injury was

extremely light, the shape was like a new moon, with a grayish-white spot in the center and an ill-defined edge. Fluorescein dyeing showed positive for some damaged areas.

3. Scanning Electron Microscopy of CO_2 Laser Damage to Corneas

Slit-lamp examination of corneas damaged by close-to-threshold dosage of irradiation showed small graying-white or light gray spots. Under the scanning electron microscope, classic foci showed coagulated depressions and edematous lesions. The coagulated depression type of damage was characterized by a sunken middle surrounded by a raised area resembling a "caldera," or the surrounding area being a "cauliflower" shape. The edematous foci were raised above the surface of the cornea, and were round, half moon shaped or new moon shaped.

Since the surface of the damaged corneas had received different amounts of heat, the extent of injury varied and showed up in four main ways as follows: Coagulated epithelial tissue and edematous spaces crisscrossed to form a mesh pattern. Necrotic cornea epithelial cells curled and peeled away like detached "leaves." When magnified more than 1,000 times, the corneal epithelium microvilli and microplicae showed up as being edematous and pyknotic, the burned surface being covered with pearl-like nodules of different sizes. Some of the burned surface appeared uneven and honeycomb shaped.

One point worth noting is that slit-lamp examination did not show damage in some cases where a close-to-threshold or a sub-threshold irradiation dosage had been given, but the injury was visible under the scanning electron microscope. In tissue irradiated at 1.02 seconds, for example, when the cornea average incident power dropped to 4.17 W/cm^2, the damage occurrence rate was only 1.96 percent. No damage was seen when corneas had been irradiated five times at this rate, but small circular shaped damaged places could be seen with the electron microscope. In tissue irradiated at 0.12 second, when the cornea average incident power was 6.79 W/cm^2, no damage was seen using the slit-lamp on 72 irradiated spots. For rabbit eyes given an irradiation dosage close to this (6.62 W/cm^2), when the scanning electron microscope magnification was increased 1,250 times, small circular injury foci could be seen.

Discussion

Scanning electron microscopy shows normal cornea epithelial cells may be categorized as being dark, medium, or light. This may be related to the dispersal and length of the microvilli and microplicae, darkness resulting where they are dense and long. Pfister[2] calculated 26 microvilli per μm^2 of dark cornea epithelial cells, and 13 microvilli per μm^2 of light cells. The existence of corneal microvilli and microplicae increases the serous membrane surface area of the epithelial cells, and increases storage of mucin, which helps moisture absorption and maintenance of lacrimal layer stability, thereby helping keep the cornea wet.

Normal cornea epithelial cells are in a constant process of renewal, reports showing the epithelial cells of rabbit corneas being replaced approximately every 4 days. The gaps seen in "senile" cells of normal corneas under the scanning electron microscope were the beginning of cell renewal. It is generally believed that the light cells are relatively young cells on the cornea epithelium, while the dark cells are relatively old. As the cells become steadily older, the gaps gradually expand; the amount of surrounding degenerated serous tissue increases, and the edges of the gaps thicken. Then a new second layer of epithelial cell microvilli and microplicae appears. As a result of their absorption of mucine, the replacement cells gradually change from hydrophobic to hydrophilic corneal epithelial cells. The peeling away of these cells as a means of renewal may also be regarded as a periodic process of autolysis, which is very apparent under the scanning electron microscope.

Damage to the retina caused by far infrared CO_2 lasers comes mostly from heat. The temperature rises to approximately 35°C at the time of threshold injury to the cornea. The basic affection is the edema reaction and the protein coagulation, degeneration and necrosis caused by the heat damage. Using a slit-lamp to look at damage from a threshold value dosage shows only small, round, light gray or grayish-white spots. Under the scanning electron microscope, however, it is possible to see many kinds of surface injury from heat such as nodular, mesh-like, honeycomb shape, and curled "leaf" shape necrotic tissue. This shows that when irradiation is done for a long period of time using such low dosages, though the injury to the cornea from the CO_2 laser beams is limited to the surface layer, the extent of heat damage to the cornea focus area differs, both edema and coagulation and edema alternating, and coagulation and necrosis occurring at the same time. The focus shape is manifested by sinking in coagulation, and by swelling in edema. However, these changes do not markedly differ with incident dosage. This may be related to differences in the CO_2 laser beam intensity over time and space, the "hot spot" not remaining fixed.

The threshold value for CO_2 laser damage to the cornea usually occurs within 10 minutes after irradiation. Slit-lamp examination shows an irradiation dosage of (ED_{50}) as needed to cause a 50 percent injury rate. The 1.02 s CO_2 laser irradiation used in this assay was lower than the injury threshold value dosage (4.17 W/cm^2), and when the injury rate was 1.96 percent, injury to the cornea was not visible using the slit-lamp. However, the injury could be seen under the scanning electron microscope, demonstrating that the injury rate changes as the observation method changes. Dosages were low though the observed injury rate was high when the scanning electron microscope was used. This should be taken into consideration when inspection is done with a slit-lamp to set injury threshold values.

REFERENCES

1. Peppers, N.A. et al., Corneal Damage Threshold for CO_2 Laser, Appl. Optics, 1969; 8.37.

2. Pfister, R.R., The Normal Surface of Corneal Epithelium: A Scanning Electron Microscopic Study. Invest. Ophthalmol. Vis. Sci. 1973; 12:654.

9432/6091

BIOLOGICAL RESEARCH PROVING FRUITFUL

40101006a Beijing XINHUA in English 1216 GMT 15 Mar 88

[Text] Beijing, March 15 (XINHUA)--Chinese scientists have for the first time identified a genetically-engineered bacteria, marking a great step in the study of the human growth hormone, according to the Chinese Academy of Sciences.

The achievement on gene engineering was made by scientists at the academy's Shanghai Institute of Cell Biology.

This is one of the 34 major achievements in biological research to be made during China's Seventh 5-Year Plan (1986-1990).

A Shanghai medical institute and a north China medicine factory have obtained good results in researching another genetically-engineered bacteria able to produce penicillin acylase.

By the end of last year, Chinese biologists had succeeded in achieving the regeneration of whole plants from protoplast, genetically-engineered varieties of plants resistant to cauliflower mosaic virus and herbicides.

In addition, scientists from the agricultural academy and the genetics institute developed more than 100 new types of paddy rice and wheat by the methods of haploid breeding and chromosome engineering.

Last year China also made great strides in research into high temperature-resistant yeast and membranous separation techniques.

/6091

SCIENTISTS DISCOVER NEW HEPATITIS B VACCINE

40101006b Beijing XINHUA in English 1305 GMT 29 Mar 88

[Text] Shanghai, March 29 (XINHUA)--Scientists here have developed a new vaccine for hepatitis B, XINHUA learned today.

The vaccine, called recombinant hepatitis B vaccine, is more effective than two other vaccines now in use in China, said Wang Yuan, associate professor at the Shanghai Institute of Biochemistry under the Chinese Academy of Sciences.

The vaccine contains pre "s" and major "s" peptides, three elements in all, making up the hepatitis B surface antigen.

The other two vaccines contain only one of the elements--the major "s" protein. They have been shown ineffective in nearly 10 percent of the population.

The new vaccine neutralizes the hepatitis antibody more readily, thus enhancing protection.

The development is significant for China, which has a high incidence of the disease, Wang said.

/6091

TRANSFORMATION OF BACILLUS SUBTILIS WITH PLASMID pCJ3 FROM BACILLUS PUMILUS

40091041 Guangzhou ZHONGSHAN DAXUE XUEBAO [ACTA SCIENTIARUM NATURALIUM UNIVERSITATIS SUNYATSENI (NATURAL SCIENCES EDITION)] in Chinese No 4, Oct 87 pp 74-79

[English abstract of article by Luo Jinxian [5012 6651 6343] of the Department of Biology]

[Text] The Tc^R plasmid pCJ3 from Bacillus pumilus was used to transform competent cells of different B. subtilis mutants. It was shown that B. subtilis BR151, SB202, 168, QB1130 and QB1133 are suitable as recipients for plasmid pCJ3, with a transformation efficiency of 10^3 transformants/μg DNA. Plasmids isolated from different transformants and their BamHI fragments have the same electrophoresis patterns as the plasmid pCJ3 and its BamHI fragment, and have the same Tc^R activity as pCJ3. The relegated plasmid from the BamHI fragment of pCJ3 has a transformation efficiency one to two magnitudes higher than the original plasmid. The effect of divalent cations, pH and medium composition on the transformation has been investigated. Ca^{++} promotes the transformation, while Cu^{++} and Zn^{++} inhibit it. The optimal pH for transformation is between 7.2 and 7.5, while a rich medium can increase the transformation efficiency.

9717

RESEARCH REPORT CITES S&T BACKWARDNESS

40080089 Beijing ZHONGGUO XINWENSHE in Chinese 1321 GMT 29 Feb 88

[Report by correspondent Qin Lang (4440 2597): "Experts Maintain That Scientific and Technological Backwardness Has Become a Serious Obstacle to the Take-off of China's Economy"]

[Text] Beijing, 29 Feb (ZHONGGUO XINWENSHE)--The input of funds and manpower in scientific research is now lagging far behind the demands of economic construction. Scientific and technological backwardness has become a serious obstacle to the future take-off of China's economy.

This is the view put forward in a research report entitled "Appraisal of China's Scientific and Technological Development." The research report was discussed and approved by experts today. It contains a total of 500,000 words and is an important consultative document the state organs at the central level can refer to when making macroscopic plans.

The research report said that although China now has more than 15 million various types of professional and technological cadres, less than 10 percent of these cadres are currently engaged in scientific research activities. The forefront of scientific research now obviously lacks a technological backbone. Moreover, the structure and distribution of the scientific and technological personnel should be rationalized. In terms of the funds spent on scientific research, the amount of funds, the proportion of the funds in the GNP, and the per capita funds all lag behind those of Japan, the United States, the Federal Republic of Germany, and Eastern European countries.

Thus, the experts suggested that greater efforts be made to further the reform of the structure of scientific and technological cadres. At the same time, the state should properly increase the proportion of input in research on basic sciences and applied sciences and use legal measures to manage the distribution, utilization, and supervision of the funds earmarked for scientific research.

The report, which was jointly compiled by the Institute of Machinery Science of the State Machinery Commission and the Hefei Polytechnical University has become the major topic for state soft science. Over the past 18 months, the experts have collected, sorted, and analyzed more than 400,000 pieces of data, consulted more than 4,500 scholars, ans used computers to carry out calculations. They have analyzed and appraised the overall situation in China's scientific and technological field and have put forward relevant proposals.

/9738 END

END OF

FICHE

DATE FILMED

25 May 1988